NASA TECHNICAL MEMORANDUM NASA TM 75320

INTEGRAL METHOD FOR THE CALCULATION OF THREE-DIMENSIONAL, LAMINAR AND TURBULENT BOUNDARY LAYERS

H. W. Stock

Translation of "Integralverfahren Zur Berechnung Dreidimensionaler, Laminarer Und Turbulenter Grenzschichten," Dornier GMBH, Friedrichshafen, West Germany, Report 77/51 B, BMVG-Vertrag Nr. T/RF 410/51 154, October 1977, 129 pages

NATIONAL AERONAUTICS AND SPACE ADMINISTRATION
WASHINGTON, D.C. 20546 JULY 1978

STANDARD TITLE PAGE

1. Report No. NASA TM 75320	2. Government Accession No.	3. Recipient's Catalog No.
4. Title and Subtitle INTEGRAL METHOD FOR THE CALCULATION OF THREE-DIMENSIONAL, LAMINAR AND TURBULENT BOUNDARY LAYERS		5. Report Date July 1978 6. Performing Organization Code
7. Author(s) H. W. Stock, Dornier, Inc.		8. Performing Organization Report No. 10. Work Unit No. 11. Contract or Grant No.
9. Performing Organization Name and Address Leo Kanner Associates, Redwood City, California 94063		13. Type of Report and Period Covered Final Report
12. Sponsoring Agency Name and Address National Aeronautics and Space Administration, Washington, D.C. 20546		14. Sponsoring Agency Code.

15. Supplementary Notes

Translation of "Integralverfahren zur Berechnung Dreidimensionaler, Laminarer und Turbulenter Grenzschichten," Dornier GMBH, Friedrichshafen, West Germany, Report, 77/51 B, EMVG-Vertrag Nr. T/RF 410/51 154, October 1977, 129 pages

16. Abstract

Integral methods for the calculation of three-dimensional, laminar and turbulent boundary layers are presented. The method for turbulent flows is a further development of an existing method; profile families with two parameters and a "lag-entrainment method" replace the simple "entrainment" method and power profiles with one parameter. The method for laminar flows is a new development. The "moment of momentum" equations are used for the solution of the problem, the profile families were derived from similar solutions of boundary layer equations. Laminar and turbulent flows at the wings are calculated. The influence of wing tapering on the boundary layer development is shown. The turbulent boundary layer for a revolution ellipsoid has been calculated for 0° and 10° incidence angle.

17. Key Words (Selected by Author(s))	18. Distribution Statement
Integral Method for Three-dimensional, laminar and turbulent boundary layers, boundary layers at wings and bodies.	

19. Security Classif. (of this report)	20. Security Classif. (of this page)	21. No. of Pages	22. Price
No	No	129	

Table of Contents

	Page
Designations	v
1. Introduction	1
2. General Fundamentals	1
2.1 Choice of Coordinates	2
2.2 The Metric Coefficients of the Coordinate System	3
2.3 Basic Equations	4
3. An Integral Method for the Calculation of Three-dimensional Turbulent, Incompressible Boundary Layers	9
3.1 Empirical Statements	10
3.1.1 Velocity Profiles	10
3.1.1.1 Direction of Main Flow	10
3.1.1.2 Direction of Crossflow	11
3.1.2 Wallfriction Equation	13
3.1.3 Entrainment Coefficient F	13
3.2 Final Form of the Differential Equations	16
3.3 Numerical Integration	17
3.4 Comparison with Experiments	19
3.4.1 van den Berg and Elsenaar [11]	19
3.4.2 Johnston [14]	21
3.4.3 Vermeulen [16]	21
3.5 Discussion	22

Page

4. An Integral Method for the Calculation of Three-dimensional, Adiabatic Laminar, Compressible Boundary Layers 23

4.1 Velocity Profiles 23

4.1.1 Similitude Solutions for the Two-dimensional Incompressible Boundary Layer 23

4.1.2 Direction of Main Flow 25

4.1.3 Direction of Crossflow 25

4.2 Determination of Integral Functions 26

4.3 Numerical Integration 31

4.4 Comparison with the Calculated Results of a Difference Method 32

4.5 Discussion 34

5. Boundary Layers on Wings 34

5.1 The Influence of Wing Tapering on the Development of a Three-dimensional, Turbulent Boundary Layer on a Transsonic Wing 34

5.1.1 The Metric Coefficients 35

5.1.2 Descriptions of the Various Types of Calculations 37

5.1.3 Discussion of Results 38

5.2 The Development of the Laminar Boundary Layer on a Transsonic Wing 38

6. Turbulent Boundary Layers on Bodies (Revolution Ellipsoid) 39

6.1 The Metric Coefficients 39

6.2 Results 41

7. Summary 42

		Page
References		44
Appendix A.	Definition of functions a_i and b_i	47
Appendix B.	The integral functions in the x,y,z coordinate system	48
Appendix C.	Relation between the integral functions in the x,y,z and t,n,z coordinate system	50
Appendix D.	(Turbulent Boundary Layer) Calculation of the integral functions of the boundary layer in the t,n,z coordinate system	55
Appendix E.	(Turbulent Boundary Layers) The integral functions of the boundary layer in the x,y,z coordinate system	58
Appendix F.	(Turbulent Boundary Layer) The right-hand sides of equations (31)-(36)	61
Appendix G.	(Turbulent Boundary Layer) Calculation of the initial condition	64
Appendix H.	(Laminar Boundary Layer) The transformed and physical integral functions	66
Appendix I.	(Laminar Boundary Layer) The right-hand sides of the equations (62)-(66)	74

Designations

A	function defined in eq. (19)
a	velocity of sound
a	variable function, eq. (54)
a	main axis of revolution ellipsoid
a_i	functions defined in appendix A, i=1.5
B	constant in eq. (14)
b	variable function, eq. (55)
b	main axis of revolution ellipsoid
b_i	functions defined in appendix A, i=1.5
c	variable function, eq. (59)
c	wing chord
c_f	wallfriction coefficient
$c_{fx}, c_{fy}, c_{ft}, c_{fn}$	components of the wallfriction coefficient in the x,y,t, resp. n-direction
D_i	functions defined in appendix I, i=1.5
f	current function
f'	defined as $\frac{df}{d\eta} = \frac{U}{U_e}$
f'', f'''	higher derivations of f after η
f''_w	velocity gradient of the main flow direction at the wall $f''_w = \left[\frac{\partial \cdot (\frac{v}{U_e})^x}{\partial \eta}\right]_w$
h_1, h_2	metric coefficients
H	shape factor $H = \frac{\delta_1^x}{\theta_{11}}$
$\bar{H}$	shape factor $\bar{H} = \frac{1}{\quad} \int_0^\delta \frac{\rho}{\rho_e} (1 - \frac{U}{U_e})\, dz$

H_1	shape factor $H = \frac{\delta - \delta_1^x}{\theta_{11}}$
I_i	functions defined in appendix F, i=1.6
k	von Kárman constant
M	Mach number
m	exponent in eq. (41)
n	crossflow direction
L_{11}, L_{12}, L_{22}	transformed dissipation integrals, appendix H
$K_1, K_2, K_{12}, K_{22}, K_{111}, K_{112}, K_{221}, K_{222}$	transformed integral functions, appendix H
p	static pressure
q	function defined in appendix A
s_x, s_y	dissipation integrals of the profiles in the directions of main current and crossflow current, appendix C
t	main flow direction
U_e	resultant velocity at the outer edge of the boundary layer
U,V	components of the velocity in the directions of main flow and crossflow
u,v,w	components of the velocity in the x,y,z direction
u_1, v_1	components of the velocity U_e in x and y direction
W	universal wake function
X,Y,Z	Cartesian coordinates
x,y,z	curvilinear, nonorthogonal coordinates
y_T	length defined in Fig. 29
α	angle between the projection of the flow line at the outer edge of the boundary layer onto the body surface and the x-direction

α^x	angle of attack
β	pressure gradient factor
β	wallcurrent line angle
$\delta_1 \delta_i$	boundary layer thickness in the physical, resp. transformed plane
δ^x	displacement thickness of the three-dimensional boundary layer
$\delta_1^x \delta_2^x$	displacement thicknesses of the profiles in the main flow and crossflow directions, appendix C
Δ_1^x, Δ_2^x	displacement thicknesses of the profiles in the x-, resp. y-direction, appendix B
Δ_1^x, Δ_2^x	displacement thickness, appendix B
η	similitude variable
η_δ	value of the similitude variables for which $\frac{U}{U_e} = 0.99$
$\textcircled{H}_{11}, \textcircled{H}_{12}, \textcircled{H}_{21}, \textcircled{H}_{22}$	moment loss thickness of the profiles in the x- and y-directions, appendix B
$\theta_{11}, \theta_{12}, \theta_{21}, \theta_{22}$	moment loss thicknesses of the profiles in the directions of main flow and crossflow, appendix C
$\textcircled{H}_{111}, \textcircled{H}_{112}, \textcircled{H}_{221}, \textcircled{H}_{222}$	energy loss thicknesses of the profiles in the x- and y-direction, appendix B
$\theta_{111}, \theta_{112}, \theta_{221}, \theta_{222}$	energy loss thicknesses of the profiles in main flow and crossflow directions, appendix C
λ	angle between the x- and y-directions
λ_0	angle between the x- and y-directions at the origin of the coordinates
μ	coefficient of viscosity
ν	kinematic viscosity
π	pressure gradient factor

ρ	density
σ	wallfriction factor
τ_x, τ_y	shearstress in the x-, resp. y-direction
ϕ_V, ϕ_H	angle of sweepback of the leading, resp. trailing wing edge
$\phi_{i,j}$	functions defined in appendix E, i=1.2; j=0.2
	angle defined in Fig. 37
ϕ, ψ	coordinates of the revolution ellipsoids

LINEAR METHOD FOR THE CALCULATION OF THREE-DIMENSIONAL, LAMINAR AND TURBULENT BOUNDARY LAYERS

H. W. Stock
Dornier, Inc.

1. Introduction /1*

Methods of calculation for three-dimensional, laminar and turbulent boundary layers and their application for three-dimensional aircraft wings and bodies will be described in this study. The methods of calculation are based on integral methods which, when compared to difference methods, suffer a loss of accuracy and are less flexible with regard to the use of various turbulence models. On the other hand, they require much shorter calculation times and storage facilities.

The integral method for the calculation of turbulent flows is an improved version of an existing method, the method for laminar flows is a new development.

2. General Fundamentals

2.1 Choice of Coordinates

There are two directions marked for three-dimensional boundary layer currents, as shown in Fig. 1. One direction results from the projection of the flow line at the outer edge of the boundary layer onto the body surface and indicates the direction of the main flow t; the other one runs vertical to the main flow direction t and represents the crossflow direction n. The distribution of the three-dimensional velocity

---

*Numbers in the margin indicate pagination in the foreign text.

profile into main flow and crossflow directions is shown in Fig. 1.

Three-dimensional boundary layers in the flow line coordinates t and n were often calculated; where t and n are curvilinear, orthogonal coordinates. Significant drawbacks result from the use of flow line coordinates. 1. The course of the flow lines at the outer edge of the boundary layer must be calculated. 2. The flow line coordinates must be newly determined for the same body geometry when the flow situation changes (change of angle of attack for instance). The introduction of arbitrary, curvilinear nonorthogonal coordinates x and y removes these drawbacks. In Fig. 1 the distribution of the three-dimensional velocity profile into the x- and y-directions is shown. There are simple relations between the velocity profiles in the t-, resp. n- and x- resp. y-direction, in Fig. 2, through the angles α and λ: /2

$$
\begin{aligned}
u &= \frac{U\sin(\lambda-\alpha) - V\cos(\lambda-\alpha)}{\sin\lambda} \\
u_1 &= U_e \frac{\sin(\lambda-\alpha)}{\sin\lambda} \\
v &= \frac{U\sin\alpha + V\cos\alpha}{\sin\lambda} \\
v_1 &= U_e \frac{\sin\alpha}{\sin\lambda}
\end{aligned}
\qquad (1)
$$

U_e is in this case the resultant velocity at the outer edge of the boundary layer, u_1 and v_1 are its components in the x- and y- directions. U and V are the velocity components in the t- and n- directions, see Fig. 1.

λ is the angle between the x- and y- direction; α is the angle between the flow line projection at the outer edge of the boundary layer onto the body surface and the x-direction and $\alpha+\beta$ is the angle between the wallflow line and the x-direction. /3

2.2 The Metric Coefficients of the Coordinate System

When the body surface, for which the boundary layer is to be calculated, is given in Cartesian coordinates X,Y,Z, then a curvilinear coordinate system x,y, can be so chosen on the surface that each point x,y defines a single point X,Y,Z. The transformation of the Cartesian coordinate system into the curvilinear one can be written as

$$\begin{aligned} X &= X(x,y) \\ Y &= Y(x,y) \\ Z &= Z(x,y) \end{aligned} \qquad (2)$$

and the metric coefficients h_1, h_2 and g of the curvilinear system are given by

$$h_1^2 = \left(\frac{\partial X}{\partial x}\right)^2 + \left(\frac{\partial Y}{\partial x}\right)^2 + \left(\frac{\partial Z}{\partial x}\right)^2$$

$$h_2^2 = \left(\frac{\partial X}{\partial y}\right)^2 + \left(\frac{\partial Y}{\partial y}\right)^2 + \left(\frac{\partial Z}{\partial y}\right)^2$$

$$g = \frac{\partial X}{\partial x}\frac{\partial X}{\partial y} + \frac{\partial Y}{\partial x}\frac{\partial Y}{\partial y} + \frac{\partial z}{\partial x}\frac{\partial z}{\partial y} \qquad (3)$$

From eq. (2) one gets, after differentiation over x and y, /4

$$h_1 \frac{\partial h_1}{\partial x} = \frac{\partial X}{\partial x}\frac{\partial^2 X}{\partial x^2} + \frac{\partial Y}{\partial x}\frac{\partial^2 Y}{\partial x^2} + \frac{\partial z}{\partial x}\frac{\partial^2 z}{\partial x^2} \qquad (4)$$

and

$$h_1 \frac{\partial h_1}{\partial y} = \frac{\partial X}{\partial x}\frac{\partial^2 X}{\partial x \partial y} + \frac{\partial Y}{\partial x}\frac{\partial^2 Y}{\partial x \partial y} + \frac{\partial z}{\partial x}\frac{\partial^2 z}{\partial x \partial y}$$

with similar expressions for $\frac{\partial h_2}{\partial x}$, $\frac{\partial h_2}{\partial y}$, $\frac{\partial g}{\partial x}$ and $\frac{\partial g}{\partial y}$.

2.3 Basic Equations

It is sufficient for the derivation of integral equations to start with the equations of the laminar boundary layers, since the integral equations for laminar and turbulent boundary layers are identical.

In nonorthogonal cuvilinear coordinates the continuity equation and the x- and y- pulse equations are

continuity equation

$$\frac{\partial}{\partial x}\left(\frac{q}{h_1}\rho u\right) + \frac{\partial}{\partial y}\left(\frac{q}{h_2}\rho v\right) + q\frac{\partial}{\partial z}(\rho w) = 0 \qquad (5)$$

x-pulse equation /5

$$\rho\left(\frac{u}{h_1}\frac{\partial u}{\partial x} + \frac{v}{h_2}\frac{\partial u}{\partial y} + w\frac{\partial u}{\partial z} + a_1 u^2 + a_2 v^2 + a_3 uv\right) =$$

$$a_4\frac{\partial p}{\partial x} + a_5\frac{\partial p}{\partial y} + \frac{\partial \tau_x}{\partial z} \qquad (6)$$

y-pulse equation

$$\rho\left(\frac{u}{h_1}\frac{\partial v}{\partial x} + \frac{v}{h_2}\frac{\partial v}{\partial y} + w\frac{\partial v}{\partial z} + b_1 u^2 + b_2 v^2 + b_3 uv\right) =$$

$$b_4\frac{\partial p}{\partial x} + b_5\frac{\partial p}{\partial y} + \frac{\partial \tau_y}{\partial z} \qquad (7)$$

τ_x and τ_y are the shearstresses in the x- and y- directions, u,v, and w are the velocity components in the x,y and z direction, ρ is the density and p the static pressure. The functions a_i and b_i are functions of the metric coefficients, as per appendix A. After integrating equations (6) and (7) from z=0 to z=δ (where δ is the boundary layer thickness) and using equation (5) one gets for the

x-pulse integral equation /6

$$\frac{1}{h_1}\frac{\partial \Theta_{11}}{\partial x} + \Theta_{11}\left\{\frac{(2-M_e^2)}{h_1}\frac{1}{U_e}\frac{\partial U_e}{\partial x} + \frac{1}{q}\frac{\partial}{\partial x}\left(\frac{q}{h_1}\right) + a_1\right\} + \frac{1}{h_2}\frac{\partial \Theta_{12}}{\partial y} =$$

(8)

$$+\Theta_{12}\left\{\frac{(2-M_e^2)}{h_2}\frac{1}{U_e}\frac{\partial U_e}{\partial y}+\frac{1}{q}\frac{\partial}{\partial y}\left(\frac{q}{h_2}\right)+a_3\right\}+\Delta_1^x\left\{\frac{1}{h_1}\frac{1}{U_e}\frac{\partial u_1}{\partial x}+a_1\frac{u_1}{U_e}\right\}$$

$$+\Delta_2^x\left\{\frac{1}{h_2}\frac{1}{U_e}\frac{\partial u_1}{\partial y}+a_2\frac{v_1}{U_e}+a_3\frac{u_1}{U_e}\right\}+\Theta_{22}a_2=\frac{c_{fx}}{2}$$

y-pulse integral equation

$$\frac{1}{h_1}\frac{\partial\Theta_{21}}{\partial x}+\Theta_{21}\left\{\frac{(2-M_e^2)}{h_1}\frac{1}{U_e}\frac{\partial U_e}{\partial x}+\frac{1}{q}\frac{\partial}{\partial x}\left(\frac{q}{h_1}\right)+b_3\right\}+\frac{1}{h_2}\frac{\partial\Theta_{22}}{\partial y}$$

$$+\Theta_{22}\left\{\frac{(2-M_e^2)}{h_2}\frac{1}{U_e}\frac{\partial U_e}{\partial y}+\frac{1}{q}\frac{\partial}{\partial y}\left(\frac{q}{h_2}\right)+b_2\right\}+\Delta_1^x\left\{\frac{1}{h_1}\frac{1}{U_e}\frac{\partial v_1}{\partial x}+b_1\frac{u_1}{U_e}\right. \quad (9)$$

$$\left.+b_3\frac{v_1}{U_e}\right\}+\Delta_2^x\left\{\frac{1}{h_2}\frac{1}{U_e}\frac{\partial v_1}{\partial y}+b_2\frac{v_1}{U_e}\right\}+\Theta_{11}b_1=\frac{c_{fy}}{2}$$

M_e is the Mach number of the outer edge of the boundary layer in this case and c_{fx} and c_{fy} are the components of the wallfriction coefficient c_f in the x- and y- directions. /7

The equations employed here, which are known as "moment of momentum" equations in the English language literature and have so far been used only for the calculation of two-dimensional currents, are derived in the following manner. The x-pulse equation, which is multiplied by the velocity component u, is integrated from z=0 to z=δ and by using the continuity equation multiplied by $u^2/2$ one gets the

x- "moment of momentum" equation

$$\frac{1}{h_1}\frac{\partial\Theta_{111}}{\partial x}+\Theta_{111}\left\{\frac{(3-M_e^2)}{h_1}\frac{1}{U_e}\frac{\partial U_e}{\partial x}+\frac{1}{q}\frac{\partial}{\partial x}\left(\frac{q}{h_1}\right)+2a_1\right\}+\frac{1}{h_2}\frac{\partial\Theta_{112}}{\partial y}$$

$$+ \Theta_{112}\left\{\frac{(3-M_e^2)}{h_2}\frac{1}{U_e}\frac{\partial U_e}{\partial y} + \frac{1}{q}\frac{\partial}{\partial y}\left(\frac{q}{h_2}\right) + 2a_3\right\} + 2(\Delta_1^x - \Delta_{1i}^x)\left\{\frac{1}{h_1}\frac{u_1}{U_e^2}\frac{\partial u_1}{\partial x}\right.$$

$$\left. + a_1\frac{u_1^2}{U_e^2} + a_2\frac{v_1^2}{U_e^2}\right\} + 2(\Theta_{21i} - \Theta_{12})\left\{\frac{1}{h_2}\frac{1}{U_e}\frac{\partial u_1}{\partial y} + a_3\frac{u_1}{U_e}\right\}$$

$$+ 2a_2\Theta_{221} = 2S_x \qquad (10)$$

In the same way one gets the y- "moment of momentum" equation by integrating the y-pulse equation multiplied by the velocity component v from z=0 to z=δ and using the continuity equation multiplied by $v^2/2$.

y- "moment of momentum" equation /8

$$\frac{1}{h_1}\frac{\partial \Theta_{221}}{\partial x} + \Theta_{221}\left\{\frac{(3-M_e^2)}{h_1}\frac{1}{U_e}\frac{\partial U_e}{\partial x} + \frac{1}{q}\frac{\partial}{\partial x}\left(\frac{q}{h_1}\right) + 2b_3\right\} + \frac{1}{h_2}\frac{\partial \Theta_{222}}{\partial y}$$

$$+ \Theta_{222}\left\{\frac{(3-M_e^2)}{h_2}\frac{1}{U_e}\frac{\partial U_e}{\partial y} + \frac{1}{q}\frac{\partial}{\partial y}\left(\frac{q}{h_2}\right) + 2b_2\right\} + 2(\Delta_2^x - \Delta_{2i}^x)\left\{\frac{1}{h_2}\frac{v_1}{U_e^2}\frac{\partial v_1}{\partial y}\right.$$

$$\left. + b_1\frac{u_1^2}{U_e^2} + b_2\frac{v_1^2}{U_e^2}\right\} + 2(\Theta_{12i} - \Theta_{21})\left\{\frac{1}{h_1}\frac{1}{U_e}\frac{\partial v_1}{\partial x} + b_3\frac{v_1}{U_e}\right\}$$

$$+ 2b_1\Theta_{112} = 2S_y \qquad (11)$$

in addition the "entrainment" equation is used for calculation of turbulent flows since it describes the change of mass flow in the boundary layer.

"Entrainment equation"

$$\frac{1}{\varrho_e U_e q}\left[\frac{\partial}{\partial x}\left\{\frac{\varrho_e q}{h_1}\left(u_1\delta - U_e\Delta_1^x\right)\right.\right. + \left.\left.\frac{\partial}{\partial y}\left\{\frac{\varrho_e q}{h_2}\left(v_1\delta - U_e\Delta_2^x\right)\right\}\right] \doteq F \tag{12}$$

The displacement thickness δ^x of the three-dimensional boundary layer, which is often required as result of a boundary layer calculation, can be calculated from /9

$$\frac{\partial}{\partial x}\left(\frac{\varrho_e q u_1 \delta^x}{h_1}\right) + \frac{\partial}{\partial y}\left(\frac{\varrho_e q v_1 \delta^x}{h_2}\right) = \frac{\partial}{\partial x}\left(\frac{\varrho_e q U_e \Delta_1^x}{h_1}\right) + \frac{\partial}{\partial y}\left(\frac{\varrho_e q U_e \Delta_2^x}{h_2}\right) \tag{13}$$

Equation (13) has been derived by Myring [1] according to the concept of the equivalent sources by Lighthill [2]. Equation (13) can be solved as soon as the functions Δ_1^x and Δ_2^x are known. It should be mentioned that equation (13) is not required for determination of the boundary layer development; it is solved independently of the boundary layer equations and serves only for the determination of the displacement thickness δ^x.

The integral functions of the boundary layer in the x,y,z coordinate system, Fig. 1, which appear in equations (8)-(13), are listed in appendix B. The integral functions of the x,y,z coordinate system can be expressed by the appropriate integral functions of the t,n,z coordinate system, with the help of equation (1), as per appendix C.

Three-dimensional laminar and turbulent boundary layers in curvilinear nonorthogonal coordinates can now be calculated with the above listed basic equations. Velocity profiles for the main flow and crossflow directions (t,n,z coordinate system) and temperature profiles are required for that. If those are available, the integral functions in the x,y,z coordinate system can be calculated in a simple manner, as shown in appendices B and C.

3. An Integral Method for the Calculation of Three-dimensional Turbulent, Incompressible Boundary Layers /10

Cooke and Hall [3] have shown in their study that for three-dimensional boundary layers the flow in the direction of the main flow corresponds to a two-dimensional boundary layer flow. Myring [1] has accepted this assumption in his method for the calculation of three-dimensional, turbulent, incompressible boundary layers through nonorthogonal, curvilinear coordinates. He used the pulse equations (9) and (10) and the entrainment equation (13) for determination of the boundary layer development. The description of the entrainment coefficient F, equation (13), is based on the concepts by Head [4]. The differences between the present method and that of Myring are as follows:

1. Power profiles of a single parameter for description of the velocity distribution in the direction of the main flow

have been replaced by Coles' profiles of two parameters [5]. The wallfriction parameter describes the velocity distribution close to the wall and the pressure gradient parameter determines velocity distribution in the outer part of the boundary layer.

2. The additional empirical information required about the wallfriction coefficient, when power profiles are used, drops out in this case.

3. Instead of the entrainment method used by Myring, in which the entrainment coefficient is determined directly, a "lag-entrainment" method has been employed in the present method which considers the nonequilibrium effects of the boundary layer.

3.1 Empirical Statements

When calculating incompressible, adiabatic boundary layers /11
the need to provide temperature profiles for the determination of integral functions is eliminated. The static temperature does not change in the boundary layer along coordinate z.

3.1.1 Velocity Profiles

3.1.1.1 Direction of Main Flow

The velocity profiles with two parameters by Coles [5] are used, as described by the wall principle and the wake principle,

$$\frac{U}{U_e} = \frac{\sigma}{k} \ln \frac{z \sigma U_e}{\nu} + \frac{\sigma}{k} \Pi W\left(\frac{z}{\delta}\right) + \sigma B \qquad (14)$$

where k is the von Kármán constant, δ is the boundary layer thickness, π the pressure gradient parameter, W the universal wake function which can be approximated (6) through

$$W\left(\frac{z}{\delta}\right) = 1 - \cos\left(\pi \frac{z}{\delta}\right) \tag{15}$$

and $\sqrt{}$ the wallfriction parameter which stands in the following relation to the wallfriction coefficient c_{ft}

$$\sqrt{} = \left(\frac{c_{f_t}}{2}\right)^{1/2} \tag{16}$$

The velocity distribution can also be written in /12
a form such as is used here for determination of the integral functions, with the values for $z=\delta$, as determined from equation (14), entered into equation (14) with $U=U_e$

$$\frac{U_e - U}{U_e} = \frac{\sqrt{}}{k}\left\{\Pi\left[2 - W\left(\frac{z}{\delta}\right)\right] - \ln\frac{z}{\delta}\right\} \tag{17}$$

3.1.1.2 Direction of Crossflow

As in Myring's [1] study, the statement by Mager [7] and Johnston [8] describing the crossflow profiles as functions of those in the main flow direction are applied here.

Mager [7] suggested the following relation

$$\frac{V}{U_e} = \frac{U}{U_e} A\left(1 - \frac{z}{\delta}\right)^2 \tag{18}$$

where A has the following relation to the wall flow line angle β, as seen in Figs. 1 and 2, which is equal to the angle between the projection of the flow line at the outer edge of the boundary layer of the body surface and the wall flow line,

$$A = \tan \beta \tag{19}$$

Johnston [8] provides for the boundary layer flow next to the wall the correlation

$$\frac{V}{U_e} = \frac{U}{U_e} \tan \beta \tag{20}$$ /13

and for the remaining part of the boundary layer

$$\frac{V}{U_e} = A \left(1 - \frac{U}{U_e}\right) \tag{21}$$

Johnston has shown that it is sufficient to use equation (21) for the calculation of integral functions of the crossflow.

The relation between A and β is given by Johnston as

$$\tan \beta = A \left(0.1 \left[c_{ft} \cos \beta\right]^{-1/2} - 1\right) \tag{22}$$

with the aid of the profiles in the directions of main flow and crossflow the integral functions in the t,n,z coordinate system can be stated as functions of δ, π, σ and A, in appendix D, which, in that way, become variable functions in the proposed method of calculation.

Integral functions of the x,y,z coordinate system are listed as functions of $\alpha,\lambda,\delta,\pi,\sigma$ and A in appendix E.

The necessary derivations of the integral functions from $\alpha,\lambda,\delta,\pi,\sigma$ and A can easily be determined.

3.1.2 Wallfriction Equation

/14

So far only three equations are available for the calculation of four dependent variables δ,π,σ and A; two pulse equations and one entrainment equation. A differential equation which can be derived from the expression for the wallfriction parameter σ, will be used as the fourth. Inserting z=0 with $U=U_e$ in equation (14) results in an implicit equation for

$$\frac{1}{\sqrt{\sigma}} - \frac{1}{\kappa}\ln\sqrt{\sigma} = \ln\left(\frac{\delta U_e}{\nu}\right) + \frac{2\Pi}{\kappa} + B \qquad (23)$$

Equation (23), differentiated for x, represents the fourth differential equation that must be solved simultaneously with the pulse equations and the entrainment equation

$$\frac{1}{\delta}\frac{\partial\delta}{\partial x} + 2\frac{\partial\Pi}{\partial x} + \left(\frac{1}{\sqrt{\sigma}} + \frac{\kappa}{\sigma^2}\right)\frac{\partial\sigma}{\partial x} = -\frac{1}{U_e}\frac{\partial U_e}{\partial x} \qquad (24)$$

3.1.3 Entrainment Coefficient F

Myring [1] used in his study the relation between F and the form parameter H_1 as suggested by Head [4] for two-dimensional flows. This empirical relation is based on measurements in boundary layers at equilibrium. Another suggestion was made by Horton [9], which takes into consideration

the so-called "upstream history effects" on the coefficient F in boundary layers of nonequilibrium.

The entrainment coefficient F is not given as the function of the form parameter H_1, as by Head, but is calculated through a differential equation, which is solved simultaneously with the abovementioned four differential equations, /15

$$\frac{\partial F}{\partial x} = C \frac{F_G - F}{\delta_C} \tag{25}$$

and where F_G is the entrainment coefficient under conditions of equilibrium, δ_C is a characteristic boundary layer thickness and C is a constant.

Horton [9] assumes that entrainment is closely bound up with the average shearstress in the outer part of the boundary layer and showed that measurements in the boundary layers at equilibrium can be correlated with

$$F_G = \frac{0.122}{(H_1 - 2.3)^{1.38}} \tag{26}$$

where $\tau_{0.5}$ represents the shearstress for $z/\delta = 0.5$. A mixing method relation of the Prandtl type is used for conversion of equation (26) into a relation between F_G and $(\partial U/\partial z)_{0.5}$,

$$\frac{\tau_{0.5}}{\rho_e U_e^2} = \left(\frac{\partial \frac{U}{U_e}}{\partial \frac{z}{\delta}}\right)^2 \left(\frac{\ell}{\delta}\right)^2 \tag{27}$$

where $1/\lambda = 0.083$.

With the aid of Coles' profiles it can be shown that /16

$$\left(\frac{\partial \frac{U}{U_e}}{\partial \frac{z}{\delta}}\right)_{0.5} \simeq \frac{1.87}{H_1 - 2.3} \tag{28}$$

The equations (26)-(28) result in

$$F_G = 1.585 \left(\frac{\tau_{0.5}}{\rho_e U_e^2}\right)^{0.69} \tag{29}$$

with

$$H_1 = \frac{\delta - \delta_1^x}{\theta_{11}} \tag{30}$$

In Horton's study [9] the characteristic boundary layer thickness δ_c in equation (25) was equal to the pulse loss thickness θ_{11} and the corresponding value for C was C=0.012. It turned out, however, that boundary layer thickness δ represents a more suitable measure of the characteristic thickness since it fits better into the order of magnitude of the big "eddies" that produce entrainment. The corresponding value for C is C=0.1. This C value corresponds to a typical relaxation length of 10 and agrees with the value by Bradshaw [10] in the equation for scaling of the dissipation length, which takes on a form similar to equation (25).

Since entrainment occurs in the outer part of the boundary layer, where velocities of the crossflow are small, the two-dimensional view can be extended to three-dimensional flows when entrainment is coupled to the velocity profiles in the main flow direction.

3.2 Final Form of the Differential Equations

Equations (8), (9), (12), (13) and (25) can be written with the aid of the empirical statements

x-pulse equation

$$\phi_{11}\frac{\partial\delta}{\partial x} + \delta\phi_{11_\tau}\frac{\partial\tau}{\partial x} + \delta\phi_{11_\pi}\frac{\partial\pi}{\partial x} + \delta\phi_{11_A}\frac{\partial A}{\partial x} = J_1 \quad (31)$$

y-pulse equation

$$\phi_{21}\frac{\partial\delta}{\partial x} + \delta\phi_{21_\tau}\frac{\partial\tau}{\partial x} + \delta\phi_{21_\pi}\frac{\partial\pi}{\partial x} + \delta\phi_{21_A}\frac{\partial A}{\partial x} = J_2 \quad (32)$$

entrainment equation

$$\phi_3\frac{\partial\delta}{\partial x} + \delta\phi_{3_\tau}\frac{\partial\tau}{\partial x} + \delta\phi_{3_\pi}\frac{\partial\pi}{\partial x} + \delta\phi_{3_A}\frac{\partial A}{\partial x} = J_3 \quad (33)$$

Wallfriction equation

$$\frac{\partial\delta}{\partial x} + \delta\left(\frac{1}{\tau} + \frac{k}{\tau^2}\right)\frac{\partial\tau}{\partial x} + 2\delta\frac{\partial\pi}{\partial x} = J_4 \quad (34)$$

entrainment coefficient equation

$$\frac{\partial F}{\partial x} = J_5 \quad (35)$$

displacement area equation /18

$$\frac{\partial \delta^x}{\partial x} =]_6 \qquad (36)$$

The expressions I_i are listed in appendix F and the functions ϕ_{ij} are listed in appendix E.

3.3 Numerical Integration

Equations (31)-(35) are solved simultaneously. If desired, the displacement area of the three-dimensional boundary layer can be calculated with equation (36).

Myring [1] has pointed out that the differential equations (31)-(33) are of hyperbolic nature. Of the resultant three characteristic directions the two outer ones describe the areas of influence and dependence in a calculated point. These areas are limited by two straight lines that pass through the calculated point and form the angles α and $\alpha+\beta$ with the x-axis. When determining the y-derivations contained in the functions I_i, this situation is taken into account.

When both angles α and $\alpha+\beta$ are positive backward directed differences are used

$$\left(\frac{\partial Q}{\partial y}\right)_{m,n} = \frac{Q_{m,n} - Q_{m,n-1}}{\Delta y} \qquad (37)$$

when α and $\alpha+\beta$ are negative forward directed differences are used /19

$$\left(\frac{\partial Q}{\partial y}\right)_{m,n} = \frac{Q_{m,n+1} - Q_{m,n}}{\Delta y} \qquad (38)$$

and when α and $\alpha+\beta$ have different signs centered differences are used

$$\left(\frac{\partial Q}{\partial y}\right)_{m,n} = \frac{Q_{m,n+1} - Q_{m,n-1}}{2\Delta y} \tag{39}$$

Q is a dependent variable, m is the counter for integration in the x- direction and n the counter for integration in the y-direction.

When the y-derivations of the dependent variables along line x=constant are known integration in the x-direction can be accomplished through an explicit intermediary step method

$$Q_{m+1,n} = Q_{m,n} + \Delta x \left(\frac{\partial Q}{\partial x}\right)_{m+\frac{1}{2},n} \tag{40}$$

$(\frac{\partial Q}{\partial x})_{m+1/2,n}$ is found by extrapolation of the value $(Q)_{m+1/2,n}$ at a distance of $\Delta x/2$ from $(Q)_{m,n}$ with $(\frac{\partial Q}{\partial x})_{m,n}$

$(\frac{\partial Q}{\partial x})_{m+1/2,n}$ can then be calculated with $(Q)_{m+1/2,n}$.

Boundary conditions are required where characteristic directions run into the calculated area from the outside. For the three-dimensional boundary layer this corresponds to a situation in which the boundary layer flow enters the calculation area from outside. It also follows that boundary conditions are not required in places where the boundary layer flow leaves the calculation area. /20

For the initial conditions of the calculated results shown in 3.4 the measured values of θ_{11}, H and β are used and

converted into the dependent variables δ, π, ∇ and A, as per appendix G. The initial value for coefficient F was determined from the measured value of form parameter H_1 and the relation valid for flows in equilibrium, by Head [4].

3.4 Comparison with Experiments

3.4.1. van den Berg and Elsenaar [11]

Berg and Elsenaar's experiment is of special significance since it best simulates the flow conditions at sweptback wings of all known measurements of three-dimensional boundary layers. Berg and Elsenaar have measured the turbulent boundary layer on a yawed plate (angle of sweepback 35°) in the low velocity area. The wall of the wind channel above the panel was so constructed that the generated pressure increase was large enough to cause separation of the boundary layer. Beyond that it has been attempted to approach conditions for an infinitely long sweptback wing through shaping of the end plates of the panel measured.

A nonorthogonal, straight line coordinate system was used for the calculation in which the x-direction is identical with the approach flow direction and the y- direction is parallel with the leading edge of the panel.

In Fig. 3 the results for the moment loss thickness /21
θ_{11}, the form parameter H of the velocity profile in the main flow direction and the wall flow line angle β were compared with the measurements. In addition the results of calculations, according to the methods of Cousteix [12] and Smith [12], are shown. Cousteix used the pulse equations and the entrainment equation. He determined the velocity profiles from the similar solutions of the turbulent boundary layer.

Smith expanded Myring's [1] method to compressible flows and carried out the verifications shown here of experiments in the incompressible area. The results correspond, therefore, to Myring's method. The curves by Smith, shown in Fig. 3, correspond to the results shown at the Euromech 60. The letters M and J in Fig. 3, and in all subsequent figures, next to the present method and that of Myring, correspond to the results for crossflow profiles by Mager or Johnston. For the calculations in Fig. 3 the measured wall pressure distribution and the condition of infinitely long yawed wings was used as input. Up to a panel depth of $x \approx 0.9$ the present procedure shows better agreement with the measurement than that of Myring.

Small digressions in the distribution of the resultant velocity U_e and of angle α resulted from different interpretations of the data measured in Fig. 4. In Fig. 5 the results of calculations for crossflow profiles according to Mager are shown for input of different velocity data at the edge of the boundary layer. The curves /1/ correspond to the measured values of U_e and of α, the curves /2/ were determined from U_e and the condition of infinitely long yawed wings and curves /3/ from the wall pressure distribution measured and the condition of infintely long yawed wings. From the results it becomes clear that small disturbances in the velocity data of the friction-free flow for boundary layer flows close to detachment, can provide widely varying results. Fig. 6 shows the corresponding results, as in Fig. 5, for Johnston crossflow profiles. In Fig. 6a a comparison with difference methods (Schneider [12], Krause [12]) is demonstrated. Curves /1/ and /3/ correspond to the conditions mentioned before. No advantage can be seen in the more complicated difference method. The detachment of the boundary layer is not

/22

calculated by any difference method. For crossflow profiles, according to Mager and Johnston, the present method determines the point of separation in the area of the experimentally determined separation, after input of measured values for U_e and α.

3.4.2 Johnston [14]

Johnston [14] examined the development of the boundary layer in the area of low velocity, as shown in Fig. 7. Air comes out of a rectangular channel and flows between two test plates, the height of the channel corresponding to the distance between them. The rear end of the measured distance is formed by a wall that is placed at right angle to the test panels and to the channel axis. The velocity distribution in the plane that is imagined stretched in the middle between the test panels, corresponds to the distribution for a two-dimensional ray incident on a wall at right angle. Since too few values are given for the outer velocities to calculate the boundary layer at the lower test panel, such velocities are used as would result for such a configuration according to potential theory [15]. The calculation is carried out with orthogonal, linear coordinates, the results are shown in Figs. 8. The calculated results by Smith [13] are shown for comparison. (A continuous curve of Smith's results cannot be reproduced since his results were shown only for discrete points.) The differences between the results of the present method and that of Myring are only small.

3.4.3 Vermeulen [16] /23

Vermeulen [16] measured the development of the boundary layer at the bottom panel of a rectangular channel that

had a 60° curvature. Fig. 9 shows a sketch of the measured distance together with the flow lines at the edge of the boundary layer and the wall flow lines. A curvilinear coordinate system was used in which the x-direction followed the test stations in the flow direction, with the y-direction at right angle to it. The values measured on lines A and E were used for limit conditions. Figs. 10 show a comparison with measurements and results by Smith [13]. The digressions of the present method from the measurements are clearly smaller than those of Myring's method. In Figs. 11 and 12 the velocity profiles in main flow and crossflow directions, that were measured and calculated for Mager crossflow profiles, are shown along line C. For the test case of Vermeulen and for the tests (11), (14), Figs. 13-17, the calculated results from both methods show the expected differences. In the area close to the wall and in the outer part of the boundary layer, Coles' profiles show better agreement with the measurements for the main flow direction than the power profiles of Myring. Agreement with the crossflow profiles is bad in both cases, though measurements are reproduced slightly better by the present method.

3.5 Discussion /24

The two parameter profile family by Coles, for description of the velocity profile in the direction of the main flow, showed better results for three-dimensional boundary layers than the use of one parameter power profiles, something already known for the two-dimensional case. An attempt has been made to include conditions of nonequilibrium, that should be considered for the calculation of turbulent boundary layers, by means of the "lag-entrainment" method. Agreement between measurements and calculations is good considered the effort

invested in the method. The proposed integral method provides good results even when compared with difference methods.

4. An Integral Method for the Calculation of Three-dimensional, Adiabatic, Laminar, Compressible Boundary Layers /25

The pulse equations (8) and (9) and the "moment of momentum" equations (10) and (11) should be employed for the calculation of three-dimensional laminar boundary layers. As in the case of turbulent boundary layers, chapter 3, temperature and velocity profiles are required for determination of the integral functions appearing in equations (8)-(11).

4.1 Velocity Profiles

It is assumed that velocity profiles for the main flow and crossflow directions can be determined from similar solutions of two-dimensional laminar boundary layers. Since the flows in question are compressible but adiabatic, a solution of the Cohen-Reshotko equations (17) can be dispensed with. The solution of the Faulkner-Skan equation (18) for similar incompressible flows provides the foundation for the putting together of the profile families, together with the Stewartson (19) transformation which provides a correlation between the adiabatic, compressible and incompressible flows. The use of the Stewartson transformation also alleviates the need to generate a temperature profile.

4.1.1 Similitude Solutions for the Two-dimensional Incompressible Boundary Layer /26

A simple type of solution for the two-dimensional Prandtl boundary layer is the similitude solution. These are

solutions that are so constituted that velocity profiles at various distances X can be made to fit them through proper scaling of the velocity U and the distance at right angle to the wall, Z (Z is identical with the independent variable y used otherwise for two-dimensional problems). For this case the boundary layer equations are reduced from partial differential equations to regular ones.

Similitude solutions exist for when the velocity of the potential flow U_e is proportional to a power of the running length measured from the stagnation point

$$U_e(X) = \text{const } X^m \tag{41}$$

The similitude transformation of the independent variable Z, which then leads to an ordinary differential equation, is

$$\eta = Z\left(\frac{m+1}{2}\,\frac{U_e}{\nu_e X}\right)^{1/2} \tag{42}$$

The known Faulkner-Skan differential equation then becomes

$$f''' + ff'' + \beta(1-f'^2) = 0 \tag{43}$$

with limit conditions

$$\eta = 0: \quad f = f' = 0 \quad \text{and} \quad \eta = \infty: \quad f' = 1 \tag{44}$$ /27

where $f' = \frac{df}{d\eta} = \frac{U}{U_e}$ and β represents the pressure gradient parameter which stands in the following relation to the exponent in equation (44):

$$\beta = \frac{2m}{m + 1} \qquad (45)$$

Fig. 18 demonstrates the results for U/U_e for $2 \geq \beta \geq -0.199$. The curve for $\beta=0$ corresponds to the Blasius solution for a flat plate, $\beta=-0.199$ provides the velocity profile for retarded flow, which leads straight to separation, and $\beta=2$ is valid for highly accelerated flows.

4.1.2 Direction of Main Flow

It is assumed that the velocities shown in Fig. 18 can represent the velocities in the direction of the main flow.

4.1.3 Direction of Crossflow /28

It is assumed that the velocity profiles in the direction of the crossflow can be represented by

$$\frac{V}{U_e} = c\left(\frac{V}{U_e}\right)^x \qquad (46)$$

where $\left(\frac{V}{U_e}\right)^x$ describes a certain type of profile and c is an arbitrary constant. A possibility for generation of the various types of profiles in the crossflow direction is shown in Fig. 19. The sectioned line represents the reference profile $(U/U_e)^x$, which corresponds to the velocity distribution U/U_e for $\beta=2.0$ with a freely chosen value for $\eta^x\delta=6.75$. $\eta\delta$ is the transformed boundary layer thickness and is defined as the distance from the wall in the transformed plane, for $U/U_e=0.99$. The curves drawn correspond to velocity distributions U/U_e for values of $2.0 \leq \beta \leq -0.18$. The following relation provides the curves for $\left(\frac{V}{U_e}\right)^x$

$$\left(\frac{V}{U_e}\right)^x = \left(\frac{U}{U_e}\right)^x - \left(\frac{U}{U_e}\right) \qquad (47)$$

which includes also such profiles of the "cross-over" type where $\left(\frac{V}{U_e}\right)^x$ changes signs in the boundary layer. To maintain conditions of symmetry after the passage through "cross-over" profiles, curves III and IV correspond to the curves for $\beta=2.0$ and 1.0 with changed signs. Curves I and II result from interpolation between curve III and the curve for $\beta = -0.18$.

4.2 Determination of Integral Functions

/29

The example of the energy loss thickness at the main flow profile

$$\theta_{111} = \int_0^{\delta} \frac{\varrho U}{\varrho_e U_e}\left(1 - \frac{U^2}{U_e^2}\right) dz \qquad (48)$$

is to show how the integral functions of the profiles in the main flow and crossflow direction, see appendix C, can be determined with the aid of the velocity profiles in Figs. 18 and 19 and the Stewartson transformation [19]. The Stewartson transformation

$$dZ = \frac{\varrho\, a_e}{\varrho_0\, a_0}\, dz \qquad (49)$$

permits the recalculation of compressible integral functions into incompressible ones. (ϱ_0 and a_0 are the density and sound velocity in a reference state of the gas.) Equations (48) and (49) lead to

$$\theta_{111} = \frac{\rho_e a_e}{\rho_o a_o} \int_0^{\delta_i} \frac{U}{U_e}\left(1 - \frac{U^2}{U_e^2}\right) dz \qquad (50)$$

where δ_i is the transformed boundary layer thickness in the incompressible plane.

Velocity profiles are shown as function of the similitude variable η in Figs. 18 and 19. With the aid of equation (42), equation (50) can be redefined to

(51)

with

The moment loss thickness of the velocity profile in direction of the main flow, θ_{11}, is chosen as scaling function for the boundary layer.

As per equation (51)

$$\theta_{111} = \frac{\rho_e a_e}{\rho_o a_o} \frac{dz}{d\eta} K_{111} \qquad (52)$$

with

$$K_{111} = \int_0^{\eta_\delta} \frac{U}{U_e}\left(1 - \frac{U^2}{U_e^2}\right) d\eta$$

Equations (51) and (52) then show

$$\theta_{111} = \theta_{11}\frac{K_{111}}{K_{11}} \tag{53}$$

All physical integral functions (θ_{111}, δ_1^x, etc.) can therefore be expressed by the physical scaling function θ_{11} and by the relation of the corresponding transformed integral functions (K_{111}, K_1, etc.).

The transformed integral functions, which depend only on the profiles in the main flow direction, shown in Fig. 18, are demonstrated in Fig. 20 (see appendix H for definition of the functions), plotted over the parameter /31

$$a = f_w'' \; K_{11} \tag{54}$$

where

$$f_w'' = \left(\frac{d\frac{U}{U_e}}{d\eta}\right)_w$$

a=0 corresponds to the detachment profile $\beta = -0.199$ and a=0.38954 to the profile of the strongly accelerated flow $\beta=2.0$.

The transformed integral functions, which depend only on the profiles in the crossflow direction $\left(\frac{V}{U_e}\right)^x$, see Fig. 19, are demonstrated in Fig. 21 (for definition of the functions see appendix H) plotted over the parameter

$$b = K_2' = -\frac{1}{\eta\delta_1^x}\int_0^{\eta}\left(\frac{V}{U_e}\right)^x d\eta \tag{55}$$

K_2 is the transformed displacement thickness of the crossflow profile $(\frac{V}{U_e})^x$ for a transformed boundary layer thickness $\eta\delta=1$.

The transformed integral functions K_{112}, K_{221}, K_{12} and L_{12} (see appendix H for definitions), which depend on the profiles in the directions of main flow and crossflow, are shown in Figs. 22-25 plotted over b with a as parameter. For determination of these mixed functions the transformed boundary layer thickness of the crossflow profile has been set equal to the main stream profile.

The following approach is suggested for determination of the constant c in equation (46), which permits calculation of the desired crossflow velocity profile V/U_e from $(V/U_e)^x$. The physical displacement thickness in the crossflow direction is /32

$$\delta_2^x = -\int_0^\delta \frac{\varrho V}{\varrho_e U_e}\, dz \tag{56}$$

With equation (49) we get

$$\delta_2^x = -\frac{\Theta_{11}}{K_{11}} \int_0^{\eta_\delta} \frac{V}{U_e}\, d\eta = -\frac{\Theta_{11}}{K_{11}}\, c \int_0^{\eta_\delta} \left(\frac{V}{U_e}\right)^x d\eta \tag{57}$$

or

$$\delta_2^x = -\frac{\Theta_{11}}{K_{11}}\, c\, \eta_\delta \int_0^1 \left(\frac{V}{U_e}\right)^x d\left(\frac{\eta}{\eta_\delta}\right) = \frac{\Theta_{11}}{K_{11}}\, c\, \eta_\delta\, K_2 \tag{58}$$

Consequently constant c is

$$c = \frac{\delta_2^*}{\theta_{11}} \frac{K_{11}}{b} \frac{1}{\eta_\delta} \tag{59}$$

All physical integral functions in the t,n coordinate system can then be determined in the following manner.

$$Q(t,n) = f(\theta_{11})g(c)h(a;b) \tag{60}$$

where Q is an integral function. All the required physical integral functions have been listed in appendix H. θ_{11},a,b and c thus become the dependent variables in the method of calculation suggested here. /33

The physical integral functions in the x,y coordinate system, which appear in the pulse equations x and y used here and in the "moment of momentum" equations (8)-(11), can be calculated from the physical functions of the t,n coordinate system through the relations given in appendix C.

$$Q(x,y) = Q(\theta_{11},a,b,c,\alpha,\lambda) \tag{61}$$

The required derivations of functions Q after θ_{11},a,b,c,α and λ can easily be determined.

The following holds

$$\frac{\partial Q}{\partial x} = Q_{\theta_{11}} \frac{\partial \theta_{11}}{\partial x} + Q_a \frac{\partial a}{\partial x} + Q_b \frac{\partial b}{\partial x} + Q_c \frac{\partial c}{\partial x} + Q_\alpha \frac{\partial \alpha}{\partial x} + Q_\lambda \frac{\partial \lambda}{\partial x} \tag{62}$$

wherein $Q_{\theta_{11}} = \frac{\partial Q}{\partial \theta_{11}}$ for instance.

Equations (8)-(11) can then be written

$$\Theta_{111}\theta_{11}\frac{\partial\theta_{11}}{\partial x}+\Theta_{111a}\frac{\partial a}{\partial x}+\Theta_{111b}\frac{\partial b}{\partial x}+\Theta_{111c}\frac{\partial c}{\partial x}=D_1 \qquad (62)$$

$$\Theta_{211}\theta_{11}\frac{\partial\theta_{11}}{\partial x}+\Theta_{211a}\frac{\partial a}{\partial x}+\Theta_{211b}\frac{\partial b}{\partial x}+\Theta_{211c}\frac{\partial c}{\partial x}=D_2 \qquad (63)$$

$$\Theta_{111}\theta_{11}\frac{\partial\theta_{11}}{\partial x}+\Theta_{111a}\frac{\partial a}{\partial x}+\Theta_{111b}\frac{\partial b}{\partial x}+\Theta_{111c}\frac{\partial c}{\partial x}=D_3 \qquad (64)$$

$$\Theta_{221}\theta_{11}\frac{\partial\theta_{11}}{\partial x}+\Theta_{221a}\frac{\partial a}{\partial x}+\Theta_{221b}\frac{\partial b}{\partial x}+\Theta_{221b}\frac{\partial b}{\partial x}=D_4 \qquad (65)$$ /34

$$\frac{\partial\delta^x}{\partial x}=D \qquad (66)$$

The expressions D_i are listed in appendix I.

Equations (62)-(65) are solved simultaneously. If so desired, the displacement area of the three-dimensional boundary layer can be determined with equation (66).

4.3 Numerical Integration

Numerical integration is handled in the same way as explained in section 3.3. The functions θ_{11}, H, δ_2^x and the wall-flow line angle β are required as initial conditions. The transformed integral functions, which are given as functions of a or b, or a and b, are made available through polynomial fits.

For the start of the calculation at the stagnation point or stagnation line of a body, the sign of the wallflow line angle β decides the sign of the crossflow velocity $(\frac{V}{U_e})^x$, Fig. 19, for the first integration step.

At the start of the calculation only such profile types can be considered for which

$$\left[\frac{\partial^2\left(\frac{v}{U_e}\right)^x}{\partial\eta^2}\right]_w \operatorname{sign}(\beta) \leq 0$$

holds.

Once the crossflow has developed from the stagnation point, /35 or stagnation line, then the profile type of the crossflow changes through change of the sign of function $\frac{\partial^2\alpha}{\partial x^2}$, i.e., the flow line at the outer edge of the boundary layer has a turning point. "Cross-over" profiles appear and after passage through this type of profile, profile forms as shown in III and IV, Fig. 19, are reached. Should a renewed change occur in the sign of the function $\frac{\partial^2\alpha}{\partial x^2}$, then "cross-over" profiles will reappear. The profiles will in that case pass through in the same direction as during their first appearance.

4.4 Comparison with the Calculated Results of a Difference Method

The results of difference methods for laminar flows can be used for comparison in estimating the quality of approximation methods such as the integration procedure. The difference method was developed by Horton [20]. Three test cases were used for infinitely long yawed wings with 45° sweepback in the incompressible region. A rectangular coordinate system was used with the y-direction running parallel to the leading edge. The velocity component at the outer edge of the boundary layer in y-direction, v_1, is for all test cases.

$$\frac{v_1}{U_\infty} = 1 \qquad (67)$$

with U_∞ corresponding to the component of undisturbed initial flow velocity in the x-direction. The velocity component at the outer edge of the boundary layer in the x-direction, u_1, is

/36

Test case 1: $$\frac{u_1}{U_\infty} = 3\left(\frac{x}{c} - \frac{x^3}{c^3}\right) \quad \text{for } \frac{x}{c} > 0 \tag{68}$$

Test case 2: $$\frac{u_1}{U} = 1 \quad \text{for } \frac{x}{c} \leq 1.0 \tag{69}$$

$$\frac{u_1}{U_\infty} = 1 - 0.567\left(\frac{x}{c} - 1\right) \quad \text{for } \frac{x}{c} \geq 1 \tag{70}$$

Test case 3: $$\frac{u_1}{U_\infty} = 1 \quad \text{for } \frac{x}{c} \leq 1 \tag{71}$$

$$\frac{u_1}{U_\infty} = 1 - 0.1134\left(\frac{x}{c} - 1\right) \quad \text{for } \frac{x}{c} \geq 1 \tag{72}$$

c is a reference length. Test case 1 corresponds to a boundary flow that starts at a stagnation line. The test cases 2 and 3 are boundary layer flows which correspond at first to a plate boundary layer and are then suddenly exposed to an increase in pressure. The calculations were made for a Reynolds number

$$Re = \frac{U_\infty c}{\nu_\infty} = 10^6$$

The comparison of results from calculations is shown in Figs. 26-28. All calculations end with the detachment of the laminar boundary layer. In test case 1 the sign of the wallflow

line angle changes but the displacement thickness of the crossflow direction δ_2 remains positive, which means that there are "cross-over" types of crossflow profiles in the range $\frac{x}{c}$ for $\beta>0$. The present integral method gives a very satisfactory description of these complicated flow conditions. Beyond that the separation point is determined accurately. For test case 2 results are equally satisfactory, but small digressions occur in the determination of the separation point. During recalculation of test cases 1 and 2 agreement was looked for in the wallfriction coefficient c_f during establishment of the initial conditions and deviation in the form parameter /37

$$H = \frac{\delta_1^x}{\theta_{11}}$$

was permitted. For test case 3 two different results of calculation are shown in Fig. 28, with agreement of c_f and H for the initial conditions. Here, too, the agreement is satisfactory.

4.5 Discussion

The results show that the idea for using the concept of the "moment of momentum" equations in the three-dimensional case as well, leads to good results.

5. Boundary Layers on Wings /38

5.1 The Influence of Wing Tapering on the Development of a Three-dimensional, Turbulent Boundary Layer on a Transsonic Wing

The development of a three-dimensional boundary layer on a wing was often calculated to an approximation with methods that were based on the concept of the infinitely long yawed wing. In comparison to this quasi-two-dimensional way of looking at

it one aspect of three-dimensionality, the wing tapering, will be examined closer here.

5.1.1 The Metric Coefficients

To make the calculation simpler the boundary layer development will be developed here not for the given wing contour but for a flat plate with a top view corresponding to that of the wing on which the potential-theoretical pressure distribution is superposed. The calculation is carried out in a nonorthogonal linear coordinate system. The x-direction runs parallel to the direction of initial flow, the y-direction is identical with percentage lines on the wing.

Fig. 29 shows the Cartesian coordinates X,Y,Z and not the nonorthogonal, linear coordinates x,y for the infintely long yawed wing and the tapered wing with straight leading and trailing edges.

The following connection results /39

$$X = a(y) + x \frac{b(y)}{b(y=0)}$$

$$Y = y \sin \lambda_0 \qquad (73)$$

$$z = 0$$

The functions a(y) and b(y) are shown in Fig. 29.
From equations (3) and (4) we get the metric coefficients and their derivations to (also on Fig. 29)

$$h_1 = 1 - \frac{y}{y_T} \qquad (74)$$

$$\frac{\partial h_1}{\partial x} = 0 \qquad (75)$$

$$\frac{\partial h_1}{\partial y} = -\frac{1}{y_T} \tag{76}$$

$$h_2 = \frac{\sin\lambda_0}{\sin\lambda} \tag{77}$$

$$\frac{\partial h_2}{\partial x} = -\frac{\cos\lambda}{y_T} \tag{78}$$

$$\frac{\partial h_2}{\partial y} = 0 \tag{79}$$

$$g = \cot\lambda \sin\lambda_0 \left(1 - \frac{y}{y_T}\right) \tag{80}$$

/40

$$\frac{\partial g}{\partial x} = -\frac{1}{y_T}\left(1 - \frac{y}{y_T}\right) \tag{81}$$

$$\frac{\partial g}{\partial y} = -\frac{\cot\lambda \sin\lambda_0}{y_T} \tag{82}$$

The angle λ in a point x,y corresponds to the angle between the lines x=const. and y=const. at the point x,y. λ_0 is the angle between the coordinates x and y at the origin of the coordinates.

The following holds true

$$\lambda = \text{arc tg}\left[\frac{1}{\sin\lambda_0}\left(\cos\lambda_0 - \frac{x}{y_T}\right)\right] \tag{83}$$

$$\frac{\partial \lambda}{\partial x} = \frac{\sin^2 \lambda}{\sin \lambda_o} \frac{1}{y_T} \tag{84}$$

$$\frac{\partial \lambda}{\partial y} = 0 \tag{85}$$

y_T is the distance from the origin of the coordinates to the point where the extended leading and trailing edges of the wing touch. ($y_T=\infty$ for the infinitely long yawed wing.)

5.1.2 Description of the Various Types of Calculations /41

Fig. 30 shows the top view of the wing, the wing section examined and the sweepback of the leading and trailing edges in that wing section.

Fig. 31 shows the distribution of the resulting flow velocity for that wing at the outer edge of boundary layer U_e, dimensionless as the initial flow velocity U_{Ref}, over the wing chord at the suction side in the section examined; c is the wing chord of the wing section examined. In addition, the run of angle α is given. The leading edge sweepback of the wing in the section examined is $\phi_V=32°$, the trailing edge sweepback is $\phi H=16°$. The sectioned line for function α in Fig. 31 presents the run of α for an infinitely long yawed wing with a sweepback of $(\phi_V+\phi_H)/2=24°$ for identical velocity distribution U_e/U_{Ref}.

The same integral method is used for two boundary layer calculations (13). Case 1 corresponds to the results for an infinitely long yawed wing with 24° sweepback. The wing for case 2 is tapered with a constant leading edge taper of 32° and

a constant trailing edge taper of 16°, corresponding to the wing of the wing section examined. The distribution of U_e and α over the wing chord, by percentage, is identical with that on the wing of the section examined.

5.1.3 Discussion of Results /42

The results for Mager-crossflow profiles are shown in Figs. 32-34. The moment loss thickness θ_{11} increases slower in the trailing edge area, i.e., in the area of retarded external flow at the tapered wing, than at the infinitely long yawed wing. The same holds for the form parameter $\bar{H}$. Since the form parameter $\bar{H}$ increases with retarded external flow, the wing taper acts to weaken the retardation of the effective external flow.

The wallflow line angle β is an effective measure for the three-dimensionality of the flow ($\alpha+\beta>0$ means that the boundary layer material flows toward the wingtip). Fig. 34 shows clearly that tapering weakens the three-dimensionality of the flow.

5.2 The Development of the Laminar Boundary Layer on a Transsonic Wing

The development of a laminated boundary layer on an infinitely long yawed wing in the region of transsonic velocity is shown in Fig. 35. The velocity data at the outer edge of the boundary layer correspond to those that are also used for the turbulence calculation in section 5.1.2, Fig. 31. The calculation is carried out with a constant value c, equation (46). The turbulent values of θ_{11} and β are shown for comparison in Fig. 35. The moment loss thickness is significantly smaller in the

laminar case. This result becomes understandable when comparing the development of the boundary layer on a flat plate in the laminar and turbulent case. For laminar flow

$$\theta_{11} \sim x^{1/2}$$ /43

and for the turbulent case

$$\theta_{11} \sim x^{4/5}$$

The velocity decrease of the external flow for $x \approx 0.5$ is so great that laminar separation occurs. In the turbulent case no separation occurs here. It is known that turbulent boundary layers can tolerate greater pressure increases in the external flow before they separate. Results for the wallflow line angle β show clearly that the three-dimensionality of the flow is far more pronounced for laminar boundary layers than for turbulent ones. A similar result is also described in reference [22].

6. Turbulent Boundary Layers on Bodies (Revolution Ellipsoid)

The development of a turbulent boundary layer on a revolution ellipsoid (ratio of main axes 4:1) has been calculated for an attack angle of 0° and 10°.

6.1 The Metric Coefficients /44

The connection between the Cartesian coordinates X,Y,Z and the coordinates ϕ,Ψ of the revolution ellipsoid, as per Fig. 36 is

$$X = a \cos \psi$$

$$Y = b \sin \Psi$$
$$Z = b \sin \Psi \cos \phi \qquad (86)$$

In this case a and b are the main axes of the revolution ellipsoid.

Using equations (3) and (4) for the metric coefficients and their derivation we continue

$$h_1 = (a^2 \sin^2 \Psi + b^2 \cos^2 \Psi)^{1/2} \qquad (87)$$

$$\frac{\partial h_1}{\partial \Psi} = \frac{1}{h_1} \sin \Psi \cos \Psi (a^2 - b^2)$$

$$\frac{\partial h_1}{\partial \phi} = 0$$

$$h_2 = b \sin \Psi$$

$$\frac{\partial h_2}{\partial \Psi} = b \cos \Psi$$

$$\frac{\partial h_2}{\partial \phi} = 0$$

$$g = 0$$

$$\frac{\partial g}{\partial \Psi} = 0$$

$$\frac{\partial g}{\partial \phi} = 0$$

/45

6.2 Results

The data for the friction-free flow around the revolution ellipsoid were determined through the procedure by K. Maruhn [22]. Figs. 37 and 38 show the distribution of the resultant velocity of friction-free flow U_e and of angle α for an attack angle of $\alpha^X=1.0°$, plotted over φ and x/a. The distance x and the angle α are defined in Fig. 37. The angle φ in the tangential plane at a surface point P is defined as the angle between the vector U_e and the straight line that is generated by sectioning the tangential plane with a plane that stretches through the x-axis and the point P, as in Fig. 36.

The results of a boundary layer calculation for a Reynolds number

$$Re = \frac{U_{Ref}a}{\nu_{Ref}} = 5.2 \times 10^5$$

where the undisturbed initial flow is the reference condition, /46 are shown in Figs. 39-41. The functions θ_{11} and H are shown in comparison for an attack angle of $\alpha^X=0°$. θ_{11} and with it all boundary layer thicknesses increase for the incident ellipsoid not only in the x-direction but also in the direction of the circumference. The minimum values lie in the plane of symmetry on the side facing the wind. For values of x/a>0.5 the wall-flow line angle on the topside assumes negative values while being positive on the side facing the wind. In the plane of symmetry of top and bottom side there are no crossflows ($\beta=0$). The course of θ_{11} and particularly of H for values of x/a>0.5 is noteworthy. The maximum values of these functions do not lie in the plane of symmetry on the topside ($\varphi=180°$), but for

$\varphi \approx 150°$. This may be explained through the piling up of boundary layer material because of the crossflow, which changes its sign at the circumference. Geissler [23] has observed similar conditions in his study (development of the laminar boundary layer for an incident ellipsoid). The maximum increase of the form parameter H on the side of the ellipsoid may also indicate the free separation of the vorticity layer [24], which was examined closer by Wang [25] for an incident ellipsoid.

7. Summary

Methods have been introduced for the calculation of three-dimensional, turbulent and compressible, laminar flows. In the turbulent method the power profiles, which were used in Myring's work for the description of the velocity profiles in main stream direction, were replaced by Coles' profiles. Beyond that a "lag-entrainment" method was introduced instead of the simple "entrainment" concept. The quality of the results of the calculations, as compared to the experiments, could be improved even more if more suitable models were available for description of the cross-velocity profiles. The proposed integral method gives good results in comparison with difference methods.

The laminar method, which uses "moment of momentum" equations for the first time for three-dimensional flows, gives good results in comparison with an exact difference method.

Calculations for wings showed that tapering of wings reduces the three-dimensionality of the flow. For identical pressure distributions the laminar boundary layer separates earlier and shows a more pronounced three-dimensionality than turbulent flows.

The development of a turbulent boundary layer was calculated for an ellipsoid for 0° and 10° incidence. The boundary layer thicknesses for incident ellipsoids are smaller on the bottom side and greater on the topside than for an ellipsoid with 0° incidence. A noteworthy result is that the maximum values of boundary layer thicknesses and of the form parameter do not occur at the apex of the topside but on the side on the part of the revolution ellipsoid turned away from the wind.

REFERENCES /48

[1] D. F. MYRING
An Integral Prediction Method for Threedimensional Turbulent Boundary Layers in Incompressible Flow
RAE TR 70147 (1970)

[2] M. J. LIGHTHILL
On Displacement Thickness
J. Fluid Mech. Vol. 4, S. 383-392 (1958)

[3] J. C. COOKE, M. G. HALL
Boundary Layers in Three Dimensions
Progr. Aero. Sci. Vol. 2 (1962)

[4] M. R. HEAD
Entrainment in the Turbulent Boundary Layer
ARC, R & M 3152 (1958)

[5] D. COLES
The Law of the Wake in the Turbulent Boundary Layer
J. Fluid Mech. Vol. 1, Part 2, S. 191-226 (1956)

[6] J. O. HINZE
Turbulence
McGraw-Hill, New York (1959)

[7] A. MAGER
Generalization of Boundary Layer Momentum Integral Equations to Threedimensional Flows, Including those of Rotating Systems
NACA Rep. 1067 (1952)

[8] J. P. JOHNSTON /49
On the Threedimensional Turbulent Boundary Layer Generated by Secondary Flow
J. of Basic Eng. Vol. 82, S. 223-250 (1960)

[9] H. P. HORTON
Entrainment in Equilibrium and Non-Equilibrium Turbulent Boundary Layers
Hawker Siddeley Aviation Ltd., Hatfield, Rep. Nr. Research/ 1094/ HPH (1969)

[10] P. BRADSHAW
Effect of Streamline Curvature on Turbulent Flow
AGARD ograph Nr. 169 (1973)

[11] B. VAN DEN BERG, A. ELSENAAR
Measurements in a Threedimensional Incompressible Turbulent Boundary Layer in an Adverse Pressure Gradient under Infinite Swept Wing Conditions
NLR TR 72092 U (1972)

[12] Computation of Threedimensional Turbulent Boundary Layers
FFA TN AE-1211
Euromech 60, Trondheim 1975

[13] P. D. SMITH
An Integral Prediction Method for Threedimensional Compressible Turbulent Boundary Layers
ARC, R. & M. Nr. 3739 (1974)

[14] J. P. JOHNSTON
Threedimensional Turbulent Boundary Layers
M.I.T. Gas Turbine Lab. Rep. 39 (1957)

[15] S. PAI /50
Fluid Dynamics of Jets
D. van Nostrand Co., Inc., New York (1957)

[16] A. J. VERMEULEN
Measurements of Threedimensional Turbulent Boundary Layers
PH.D. Thesis, Cambridge University (1971)

[17] C. B. COHEN, E. RESHOTKO
Similar Solution for the Compressible Laminar Boundary Layer with Heat Transfer and Pressure Gradient
NACA R 1293, 1956

[18] V. M. FAULKNER, S. W. SKAN
Some Approximate Solutions of the Boundary Layer Equations
ARC R & M 1314, 1930

[19] K. STEWARTSON
Correlated Incompressible and Compressible Boundary Layers
Proc.Roy.Soc. (London) A 200 S. 84-100, 1949

[20] H. P. HORTON
Numerical Solution of Incompressible Laminar Boundary Layer Problems Using Invariant Imbedding
Wird veröffenlicht im AIAA Journal

[21] K. MARUHN
Druckverteilungsrechnungen an elliptischen Rümpfen und in ihrem Aussenraum [Calculations of Pressure Distribution on elliptic bodies and their surrounding space)
Jahrbuch der deutschen Luftfahrtforschung S. I 135 - I 147 (1941)

[22] T. K. FANNELÖP, D. A. HUMPHREYS /51
The Solution of the Laminar and Turbulent Threedimensional Boundary Layer Equations with a Simple Finite Difference Technique
FFA R 126, 1975

[23] W. GEISSLER
Berechnung der dreidimensionalen laminaren Grenzschicht an schrägangeströmten Rotationskörpern mit Ablösung [Calculation of the Threedimensional Laminar Boundary Layer on Revolution bodies with Separation for Flow Incidence at a Slant]
Ing.-Arch. Vol. 43, Nr. 6 (1973/74), S. 413-425.

[24] E. C. MASKELL
Flow Separation in Three-Dimensions
RAE R 2565, 1955

[25] K. C. WANG
Separation Patterns of Boundary Layer over an Inclined Body of Revolution
AIAA J., Vol. 10, Nr. 8, S. 1044-1050 (1972)

Appendix A

/52

Definition of functions a_i and b_i

$$q^2 = h_1^2 h_2^2 - g^2$$

$$a_1 = \frac{h_1 g}{q^2}\left(\frac{1}{h_1}\frac{\partial h_1}{\partial y} + \frac{g}{h_1^3}\frac{\partial h_1}{\partial x} - \frac{1}{h_1^2}\frac{\partial g}{\partial x}\right)$$

$$a_2 = \frac{h_1}{q^2}\left(\frac{\partial g}{\partial y} - h_2\frac{\partial h_2}{\partial x} - \frac{g}{h_2}\frac{\partial h_2}{\partial y}\right)$$

$$a_3 = \frac{1}{q^2}\left(h_1 h_2\left\{1 + \frac{g^2}{h_1^2 h_2^2}\right\}\frac{\partial h_1}{\partial y} - 2g\frac{\partial h_2}{\partial x}\right) \qquad \text{(A-1)}$$

$$a_4 = -\frac{h_2^2 h_1}{q^2}$$

$$a_5 = \frac{g h_1}{q^2}$$

$$b_1 = \frac{h_2^2}{q^2}\left(\frac{\partial g}{\partial x} - h_1\frac{\partial h_1}{\partial y} - \frac{g}{h_1}\frac{\partial h_1}{\partial x}\right)$$

$$b_2 = \frac{g h_2}{q^2}\left(\frac{1}{h_2}\frac{\partial h_2}{\partial x} + \frac{g}{h_2^3}\frac{\partial h_2}{\partial y} - \frac{1}{h_2^2}\frac{\partial g}{\partial y}\right)$$

$$b_3 = \frac{1}{q^2}\left(h_1 h_2\left\{1 + \frac{g^2}{h_1^2 h_2^2}\right\}\frac{\partial h_2}{\partial x} - 2g\frac{\partial h_1}{\partial y}\right)$$

$$b_4 = \frac{g h_2}{q^2}$$

$$b_5 = -\frac{h_1^2 h_2}{q^2}$$

Appendix B

The integral functions in the x,y,z coordinate system

$$\Theta_{111} = \int_0^\delta \frac{\rho u}{\rho_e U_e}\left(\frac{u_1^2}{U_e^2} - \frac{u}{U_e^2}\right) dz \qquad \Theta_{112} = \int_0^\delta \frac{\rho v}{\rho_e U_e}\left(\frac{u_1^2}{U_e^2} - \frac{u^2}{U_e^2}\right) dz$$

$$\Theta_{221} = \int_0^\delta \frac{\rho u}{\rho_e U_e}\left(\frac{v_1^2}{U_e^2} - \frac{v^2}{U_e^2}\right) dz \qquad \Theta_{222} = \int_0^\delta \frac{\rho v}{\rho_e U_e}\left(\frac{v_1^2}{U_e^2} - \frac{v}{U_e^2}\right) dz$$

$$\Theta_{11} = \int_0^\delta \frac{\rho u}{\rho_e U_e}\left(\frac{u_1}{U_e} - \frac{u}{U_e}\right) dz \qquad \Theta_{12} = \int_0^\delta \frac{\rho v}{\rho_e U_e}\left(\frac{u_1}{U_e} - \frac{u}{U_e}\right) dz$$

$$\Theta_{21} = \int_0^\delta \frac{\rho u}{\rho_e U_e}\left(\frac{v_1}{U_e} - \frac{v}{U_e}\right) dz \qquad \Theta_{22} = \int_0^\delta \frac{\rho v}{\rho_e U_e}\left(\frac{v_1}{U_e} - \frac{v}{U_e}\right) dz \qquad \text{(B-1)}$$

$$\Theta_{12i} = \int_0^\delta \frac{v}{U_e}\left(\frac{u_1}{U_e} - \frac{\rho u}{\rho_e U_e}\right) dz \qquad \Theta_{21i} = \int_0^\delta \frac{u}{U_e}\left(\frac{v_1}{U_e} - \frac{\rho v}{\rho_e U_e}\right) dz$$

$$\Delta_1^x = \int_0^\delta \left(\frac{u_1}{U_e} - \frac{\rho u}{\rho_e U_e}\right) dz \qquad \Delta_2^x = \int_0^\delta \left(\frac{v_1}{U_e} - \frac{\rho v}{\rho_e U_e}\right) dz$$

$$\Delta_{1i}^x = \int_0^\delta \left(\frac{u_1}{U_e} - \frac{u}{U_e}\right) dz \qquad \Delta_{2i}^x = \int_0^\delta \left(\frac{v_1}{U_e} - \frac{v}{U_e}\right) dz$$

$$c_{f_x} = \frac{2}{\rho_e U_e}\left(\mu \frac{\partial \frac{u}{U_e}}{\partial z}\right)_{z=0} \qquad c_{f_y} = \frac{2}{\rho_e U_e}\left(\mu \frac{\partial \frac{v}{U_e}}{\partial z}\right)_{z=0}$$

For laminar flows the dissipation integrals S_x and S_y can be written as /54

$$S_x = \frac{1}{\rho_e U_e} \int_0^\delta \mu \left(\frac{\partial \frac{u}{U_e}}{\partial z} \right)^2 dz$$

$$S_y = \frac{1}{\rho_e U_e} \int_0^\delta \mu \left(\frac{\partial \frac{v}{U_e}}{\partial z} \right)^2 dz \qquad \text{(B-2)}$$

μ is here the dynamic viscosity of the gas

Appendix C

Relation between the integral functions in the x,y,z and t,n,z coordinate system

$$\Theta_{111} = \frac{1}{\sin^3\lambda}\Big[\theta_{111}\sin^3(\lambda-\alpha) - \{3\theta_{112} + 2\delta_2^x\}\sin^2(\lambda-\alpha)\cos(\lambda-\alpha) + 3\theta_{221}\sin(\lambda-\alpha)\cos^2(\lambda-\alpha) - \theta_{222}\cos^3(\lambda-\alpha)\Big]$$

$$\Theta_{112} = \frac{1}{\sin^3\lambda}\Big[\theta_{111}\sin\alpha\sin^2(\lambda-\alpha) - \{\theta_{112} + \delta_2^x\}2\sin\alpha\sin(\lambda-\alpha)\cos(\lambda-\alpha) + \theta_{221}\sin\alpha\cos^2(\lambda-\alpha) + \theta_{112}\cos\alpha\sin^2(\lambda-\alpha) - 2\theta_{221}\cos\alpha\sin(\lambda-\alpha)\cos(\lambda-\alpha) + \theta_{222}\cos\alpha\cos^2(\lambda-\alpha)\Big] \qquad (C-1)$$

$$\Theta_{221} = \frac{1}{\sin^3\lambda}\Big[\theta_{111}\sin^2\alpha\sin(\lambda-\alpha) + \{\theta_{112} + \delta_2^x\}2\sin\alpha\cos\alpha\sin(\lambda-\alpha) + \theta_{221}\cos^2\alpha\sin(\lambda-\alpha) - \theta_{112}\sin^2\alpha\cos(\lambda-\alpha) - 2\theta_{221}\sin\alpha\cos\alpha\cos(\lambda-\alpha) - \theta_{222}\cos^2\alpha\cos(\lambda-\alpha)\Big]$$

$$\Theta_{222} = \frac{1}{\sin^3\lambda}\Big[\theta_{111}\sin^3\alpha + \{3\theta_{112} + 2\delta_2^x\}\sin^2\alpha\cos\alpha + 3\theta_{221}\sin\alpha\cos^2\alpha + \theta_{222}\cos^3\alpha\Big]$$

Continuation: /56

$$\Theta_{11} = \frac{1}{\sin^2\lambda}\Big[\theta_{11}\sin^2(\lambda-\alpha) - \{\theta_{12}+\theta_{21}\}\sin(\lambda-\alpha)\cos(\lambda-\alpha) + \theta_{22}\cos^2(\lambda-\alpha)\Big]$$

$$\Theta_{12} = \frac{1}{\sin^2\lambda}\Big[\theta_{11}\sin\alpha\sin(\lambda-\alpha) + \theta_{12}\sin(\lambda-\alpha)\cos\alpha - \theta_{21}\cos(\lambda-\alpha)\sin\alpha - \theta_{22}\cos\alpha\cos(\lambda-\alpha)\Big] \qquad (C-1)$$

$$\Theta_{21} = \frac{1}{\sin^2\lambda}\Big[\theta_{11}\sin\alpha\sin(\lambda-\alpha) + \theta_{21}\sin(\lambda-\alpha)\cos\alpha - \theta_{12}\cos(\lambda-\alpha)\sin\alpha - \theta_{22}\cos\alpha\cos(\lambda-\alpha)\Big]$$

$$\Theta_{22} = \frac{1}{\sin^2\lambda}\Big[\theta_{11}\sin^2\alpha + \{\theta_{12}+\theta_{21}\}\cos\alpha\sin\alpha + \theta_{22}\cos^2\alpha\Big]$$

$$\Theta_{12i} = \frac{1}{\sin^2\lambda}\Big[\theta_{11i}\sin\alpha\sin(\lambda-\alpha) - \theta_{21}\sin\alpha\cos(\lambda-\alpha) + \theta_{12i}\cos\alpha\sin(\lambda-\alpha) - \theta_{22}\cos\alpha\cos(\lambda-\alpha)\Big]$$

$$\Theta_{21i} = \frac{1}{\sin^2\lambda}\Big[\theta_{11i}\sin\alpha\sin(\lambda-\alpha) + \theta_{21}\cos\alpha\sin(\lambda-\alpha) - \theta_{12i}\sin\alpha\cos(\lambda-\alpha) - \theta_{22}\cos\alpha\cos(\lambda-\alpha)\Big]$$

$$\Delta_1^x = \frac{1}{\sin\lambda}\Big[\delta_1^x\sin(\lambda-\alpha) - \delta_2^x\cos(\lambda-\alpha)\Big]$$

Continuation: /57

$$\Delta_2^x = \frac{1}{\sin\lambda}\left[\delta_1^x \sin\alpha + \delta_2^x \cos\alpha\right]$$

$$\Delta_{1i}^x = \frac{1}{\sin\lambda}\left[\delta_{1i}^x \sin(\lambda-\alpha) - \delta_{2i}^x \cos(\lambda-\alpha)\right]$$

$$\Delta_{2i}^x = \frac{1}{\sin\lambda}\left[\delta_{1i}^x \sin\alpha + \delta_{2i}^x \cos\alpha\right]$$

$$C_{f_x} = \frac{1}{\sin\lambda}\left[C_{f_t} \sin(\lambda-\alpha) - C_{f_n} \cos(\lambda-\alpha)\right] \qquad \text{(C-1)}$$

$$C_{f_y} = \frac{1}{\sin\lambda}\left[C_{f_t} \sin\alpha + C_{f_n} \cos\alpha\right]$$

$$S_x = \frac{1}{\sin^2\lambda}\left[S_{tt} \sin^2(\lambda-\alpha) - 2 S_{tn} \sin(\lambda-\alpha)\cos(\lambda-\alpha) + S_{nn} \cos^2(\lambda-\alpha)\right]$$

$$S_y = \frac{1}{\sin^2\lambda}\left[S_{tt} \sin^2\alpha + 2 S_{tn} \sin\alpha \cos\alpha + S_{nn} \cos^2\alpha\right]$$

The integral functions appearing in equation (C-1), which are based on velocity profiles in the main flow and crossflow directions, become /58

$$\theta_{111} = \int_0^\delta \frac{\rho U}{\rho_e U_e}\left(1-\frac{U^2}{U_e^2}\right) dz \qquad \theta_{112} = \int_0^\delta \frac{\rho V}{\rho_e U_e}\left(1-\frac{U^2}{U_e^2}\right) dz$$

$$\theta_{221} = -\int_0^\delta \frac{\rho U V^2}{\rho_e U_e^3}\, dz \qquad \theta_{222} = -\int_0^\delta \frac{\rho V^3}{\rho_e U_e^3}\, dz$$

$$\theta_{11} = \int_0^\delta \frac{\rho U}{\rho_e U_e}\left(1-\frac{U}{U_e}\right) dz \qquad \theta_{12} = \int_0^\delta \frac{\rho V}{\rho_e U_e}\left(1-\frac{U}{U_e}\right) dz \qquad \text{(C-2)}$$

$$\theta_{21} = -\int_0^\delta \frac{\rho U V}{\rho_e U_e^2}\, dz \qquad \theta_{22} = -\int_0^\delta \frac{\rho V^2}{\rho_e U_e^2}\, dz$$

$$\theta_{11i} = \int \frac{U}{U_e}\left(1-\frac{\rho U}{\rho_e U_e}\right) dz \qquad \theta_{12i} = \int_0^\delta \frac{V}{U_e}\left(1-\frac{\rho U}{\rho_e U_e}\right) dz$$

$$\delta_1^x = \int_0^\delta \left(1-\frac{\rho U}{\rho_e U_e}\right) dz \qquad \delta_2^x = -\int_0^\delta \frac{\rho V}{\rho_e U_e}\, dz$$

$$\delta_{1i}^x = \int_0^\delta \left(1-\frac{U}{U_e}\right) dz \qquad \delta_{2i}^x = -\int_0^\delta \frac{V}{U_e}\, dz$$

Continuation:

$$c_{f_n} = \frac{2}{\rho_e U_e}\left(\mu \frac{\partial \frac{V}{U_e}}{\partial z}\right)_{z=0} \qquad c_{f_t} = \frac{2}{\rho_e U_e}\left(\mu \frac{\partial \frac{U}{U_e}}{\partial z}\right)_{z=0} \tag{C-2}$$

$$S_{tt} = \frac{1}{\rho_e U_e}\int_0^\delta \mu\left(\frac{\partial \frac{U}{U_e}}{\partial z}\right)^2 dz \qquad S_{tn} = \frac{1}{\rho_e U_e}\int_0^\delta \mu \frac{\partial \frac{U}{U_e}}{\partial z}\frac{\partial \frac{V}{U_e}}{\partial z} dz$$

$$S_{nn} = \frac{1}{\rho_e U_e}\int_0^\delta \mu\left(\frac{\partial \frac{V}{U_e}}{\partial z}\right)^2 dz$$

Appendix D (Turbulent Boundary Layer) /60

Calculation of the integral functions of the boundary layer in the t,n,z coordinate system

The boundary layer integral functions can be expressed as functions of the boundary layer thickness δ, of the pressure gradient parameter π, the wallfriction parameter σ and the parameter A, with the help of the Coles' profiles for the main flow direction and the statements of Mager or Johnston for the crossflow direction. We write $f=f(\pi,\sigma,A)$.

$$\begin{aligned} \Theta_{11} &= \delta f_{11} & \Theta_{12} &= \delta f_{12} & \Theta_{21} &= \delta f_{21} \\ \Theta_{22} &= \delta f_{22} & \delta_1^* &= \delta f_1 & \delta_2^* &= \delta f_2 \end{aligned} \qquad \text{(D-1)}$$

For the integral functions which depend only on the velocity profile in the direction of the main flow we write:

$$f_{11} = \tau (P_1 - \tau P_2) \qquad f_1 = \tau P_1 \qquad \text{(D-2)}$$

For the remaining integral functions:
--Mager Crossflow profiles--

$$\begin{aligned} f_{12} &= A\tau (P_3 - \tau P_5) & f_{21} &= -A\left(\frac{1}{3} - 2\tau P_3 + \tau^2 P_5\right) \\ f_{22} &= -A^2\left(\frac{1}{5} - 2\tau P_4 + \tau^2 P_6\right) & f_2 &= -A\left(\frac{1}{3} - \tau P_3\right) \end{aligned} \qquad \text{(D-3)}$$

Johnston Crossflow profiles-- /61

$$f_{12} = A\tau^2 P_2 \qquad f_{21} = -A\tau(P_1 - \tau P_2)$$

$$f_{22} = -A^2\tau^2 P_2 \qquad f_2 = -A\tau P_1 \qquad \text{(D-4)}$$

For the expression P_i we get:

$$P_1 = \frac{1}{k}(\Pi + 1)$$

$$P_2 = \frac{1}{k^2}\left[\frac{3}{2}\Pi^2 + 2(2 - L_1)\Pi + 2\right]$$

$$P_3 = \frac{1}{k}\left[\Pi\left(\frac{1}{3} + \frac{2}{\pi^2}\right) + \frac{11}{18}\right] \qquad \text{(D-5)}$$

$$P_4 = \frac{1}{k}\left[\Pi\left(\frac{1}{5} + \frac{4}{\pi^2} - \frac{24}{\pi^4}\right) + \frac{137}{300}\right]$$

$$P_5 = \frac{1}{k^2}\left[\Pi^2\left(\frac{1}{2} + \frac{17}{24\pi^2}\right) + \Pi\left(\frac{29}{9} - \frac{10}{\pi^2} - 2L_1 + \frac{4}{\pi^2}\left\{L_1 + L_2\right\} + \frac{85}{54}\right]\right.$$

$$P_6 = \frac{1}{k^2}\left[\Pi^2\left(\frac{3}{10} + \frac{17}{2\pi^2} - \frac{195}{4\pi^4}\right) + \Pi\left(\frac{437}{150} - 2L_1\left\{1 - \frac{12}{\pi^2} + \frac{24}{\pi^4}\right\}\right.\right.$$

$$\left.\left. + \frac{8}{\pi^2}L_2\left\{1 - \frac{6}{\pi^2}\right\} - \frac{34}{\pi^2} + \frac{172}{\pi^4}\right) + \frac{12019}{9000}\right]$$

k=0.41 is here the von Kármon constant and L_1 and L_2 calculate /62. to:

$$L_1 = -\sum_{n=1}^{\infty} (-1)^n \frac{\pi^{2n}}{(2n+1)\,[(2n+1)!]} \qquad \text{(D-6)}$$

$$L_2 = -\sum_{n=1}^{\infty} (-1)^n \frac{\pi^{2n}}{2n\,(2n!)}$$

The derivations needed for the calculation

$$\frac{\partial f}{\partial \Pi} = f_{\Pi}\,, \quad \frac{\partial f}{\partial \tau} = f_{\tau} \text{ und } \frac{\partial f}{\partial A} = f_A$$

can be determined from the above equations.

Appendix E (Turbulent Boundary Layer) /63

The integral functions of the boundary layer in the x,y,z coordinate system.

With the aid of the relations between the integral functions in the t,n,z and x,y,z coordinate systems, as determined from appendix C and the f functions determined from appendix D, the integral functions in the x,y,z coordinate system can be named.

$$\Theta_{11} = \delta \phi_{11} \qquad \Theta_{12} = \delta \phi_{12} \qquad \Theta_{21} = \delta \phi_{21}$$

$$\Theta_{22} = \delta \phi_{22} \qquad \Delta_1^x = \delta \phi_1 \qquad \Delta_2^x = \delta \phi_2 \qquad \text{(E-1)}$$

$$\frac{u_1}{U_e}\delta - \Delta_1^x = \delta \phi_3 \qquad \frac{v_1}{U_e}\delta - \Delta_2^x = \delta \phi_4$$

where $\phi = \phi(\alpha, \lambda, \pi, \sigma, A)$

The functions ϕ are as follows:

$$\phi_{11} = \frac{1}{\sin^2\lambda}\left[f_{11}\sin^2(\lambda-\alpha) - \left\{f_{12}+f_{21}\right\}\sin(\lambda-\alpha)\cos(\lambda-\alpha) + f_{22}\cos^2(\lambda-\alpha)\right] \qquad \text{(E-2)}$$

Continuation: /64

$$\Phi_{12} = \frac{1}{\sin^2\lambda}\left[f_{11}\sin\alpha\sin(\lambda-\alpha) + f_{12}\cos\alpha\sin(\lambda-\alpha) - f_{21}\cos\alpha\sin(\lambda-\alpha) - f_{22}\cos\alpha\cos(\lambda-\alpha)\right]$$

$$\Phi_{21} = \frac{1}{\sin^2\lambda}\left[f_{11}\sin\alpha\sin(\lambda-\alpha) - f_{12}\sin\alpha\cos(\lambda-\alpha) + f_{12}\cos\alpha\sin(\lambda-\alpha) - f_{22}\cos\alpha\cos(\lambda-\alpha)\right]$$

$$\Phi_{22} = \frac{1}{\sin^2\lambda}\left[f_{11}\sin^2\alpha + \{f_{12}+f_{21}\}\cos\alpha\sin\alpha + f_{22}\cos^2\alpha\right]$$

$$\Phi_{1} = \frac{1}{\sin\lambda}\left[f_{1}\sin(\lambda-\alpha) - f_{2}\cos(\lambda-\alpha)\right]$$

$$\Phi_{2} = \frac{1}{\sin\lambda}\left[f_{1}\sin\alpha + f_{2}\cos\alpha\right]$$

$$\Phi_{3} = \frac{1}{\sin\lambda}\left[\{1-f_{1}\}\sin(\lambda-\alpha) + f_{2}\cos(\lambda-\alpha)\right]$$

$$\Phi_{4} = \frac{1}{\sin\lambda}\left[\{1-f_{1}\}\sin\alpha - f_{2}\cos\alpha\right]$$

The f coefficients that appear in the equations (E-2) are given in appendix D. /65

The derivations required for the calculations

$$\frac{\partial \phi}{\partial \alpha} = \phi_\alpha \,,\ \frac{\partial \phi}{\partial \lambda} = \phi_\lambda \,,\ \frac{\partial \phi}{\partial \tau} = \phi_\tau \,,\ \frac{\partial \phi}{\partial \pi} = \phi_\pi \text{ und } \frac{\partial \phi}{\partial A} = \phi_A$$

can be easily determined.

The right-hand sides of equations (31)-(36)

The expressions I on the right-hand sides of the equations (31)-(36) produce

$$
\begin{aligned}
I_1 = {} & \frac{c_{fx}}{2} h_1 - \delta \Big[\phi_{11_\alpha} \frac{\partial \alpha}{\partial x} + \phi_{11_\lambda} \frac{\partial \lambda}{\partial x} + \frac{h_1}{h_2} \Big(\phi_{12_\alpha} \frac{\partial \alpha}{\partial y} + \phi_{12_\lambda} \frac{\partial \lambda}{\partial y} \\
& + \phi_{12_\tau} \frac{\partial \tau}{\partial y} + \phi_{12_\Pi} \frac{\partial \Pi}{\partial y} + \phi_{12_A} \frac{\partial A}{\partial y} + \frac{\phi_{12}}{\delta} \frac{\partial \delta}{\partial y} \Big) \\
& + \phi_{11} \Big(\frac{2}{U_e} \frac{\partial U_e}{\partial x} + \frac{h_1}{q} \frac{\partial}{\partial x} \Big[\frac{q}{h_1} \Big] + a_1 h_1 \Big) + \phi_{12} \Big(\frac{h_1}{h_2} \frac{2}{U_e} \frac{\partial U_e}{\partial y} \\
& + \frac{h_1}{q} \frac{\partial}{\partial y} \Big[\frac{q}{h_2} \Big] + a_3 h_1 \Big) + \phi_1 \Big(\frac{1}{U_e} \frac{\partial U_e}{\partial x} + a_1 h_1 \frac{u_1}{U_e} \Big) \\
& + \phi_2 \Big(\frac{h_1}{h_2} \frac{1}{U_e} \frac{\partial U_e}{\partial y} + a_2 h_1 \frac{v_1}{U_e} + a_3 h_1 \frac{u_1}{U_e} \Big) + \phi_{22} h_1 a_2 \Big\}
\end{aligned}
$$

$$
\begin{aligned}
I_2 = {} & \frac{c_{fy}}{2} h_1 - \delta \Big\{ \phi_{21_\alpha} \frac{\partial \alpha}{\partial x} + \phi_{21_\lambda} \frac{\partial \lambda}{\partial x} + \frac{h_1}{h_2} \Big(\phi_{22_\alpha} \frac{\partial \alpha}{\partial y} \\
& + \phi_{22_\lambda} \frac{\partial \lambda}{\partial y} + \phi_{22_\tau} \frac{\partial \tau}{\partial y} + \phi_{22_\Pi} \frac{\partial \Pi}{\partial y} + \phi_{22_A} \frac{\partial A}{\partial y} + \frac{\phi_{22}}{\delta} \frac{\partial \delta}{\partial y} \\
& + \phi_{21} \Big(\frac{2}{U_e} \frac{\partial U_e}{\partial x} + \frac{h_1}{q} \frac{\partial}{\partial x} \Big[\frac{q}{h_1} \Big] + b_3 h_1 \Big) + \phi_{22} \Big(\frac{h_1}{h_2} \frac{2}{U_e} \frac{\partial U_e}{\partial y} \\
& + \frac{h_1}{q} \frac{\partial}{\partial y} \Big[\frac{q}{h_2} \Big] + b_2 h_1 \Big) + \phi_1 \Big(\frac{1}{U_e} \frac{\partial U_e}{\partial x} + b_1 h_1 \frac{u_1}{U_e} \\
& + b_3 h_1 \frac{v_1}{U_e} \Big) + \phi_2 \Big(\frac{h_1}{h_2} \frac{1}{U_e} \frac{\partial U_e}{\partial y} + b_2 h_1 \frac{v_1}{U_e} \Big) + \phi_{11} b_1 h_1 \Big\}
\end{aligned}
\qquad (F-1)
$$

Continuation:

$$J_3 = F h_1 - \delta \left\{ \phi_{3_\alpha} \frac{\partial \alpha}{\partial x} + \phi_{3_\lambda} \frac{\partial \lambda}{\partial x} + \frac{h_1}{h_2} \left(\phi_{4_\alpha} \frac{\partial \alpha}{\partial y} + \phi_{4_\lambda} \frac{\partial \lambda}{\partial y} \right.\right.$$

$$\left. + \phi_{4_\tau} \frac{\partial \tau}{\partial y} + \phi_{4_\pi} \frac{\partial \pi}{\partial y} + \phi_{4_A} \frac{\partial A}{\partial y} + \frac{\phi_4}{\delta} \frac{\partial \delta}{\partial y} \right)$$

$$\left. + \phi_3 \left(\frac{1}{U_e} \frac{\partial U_e}{\partial x} + \frac{h_1}{q} \frac{\partial}{\partial x} \left[\frac{q}{h_1} \right] \right) + \frac{h_1}{h_2} \phi_4 \left(\frac{1}{U_e} \frac{\partial U_e}{\partial y} + \frac{h_2}{q} \frac{\partial}{\partial y} \left[\frac{q}{h_2} \right] \right) \right\}$$

$$J_4 = - \frac{\delta}{U_e} \frac{\partial U_e}{\partial x}$$

$$J_5 = h_1 \frac{U_e}{u_1} \left[\frac{0.1}{\delta} \left(F_G - F \right) - \frac{V_1}{U_e} \frac{1}{h_2} \frac{\partial F}{\partial y} \right]$$

(F-1)

Continuation:

$$
\begin{aligned}
J_6 = {} & \frac{U_e}{u_1}\left\{\phi_1 \frac{\partial \delta}{\partial x} + \delta \phi_{1\tau} \frac{\partial \tau}{\partial x} + \delta \phi_{1\pi} \frac{\partial \Pi}{\partial x} + \delta \phi_{1A} \frac{\partial A}{\partial x}\right\} \\
& - \delta^x \left\{\frac{h_1}{q} \frac{\partial}{\partial x}\left(\frac{q}{h_1}\right) + \frac{1}{u_1} \frac{\partial u_1}{\partial x} + \frac{v_1}{u_1} \frac{h_1}{q} \frac{\partial}{\partial y}\left(\frac{q}{h_2}\right) + \frac{h_1}{h_2} \frac{1}{u_1} \frac{\partial v_1}{\partial y}\right\} \\
& - \frac{h_1}{h_2} \frac{v_1}{u_1} \frac{\partial \delta^x}{\partial y} + \frac{U_e}{u_1} \delta \left\{\phi_{1\alpha} \frac{\partial \alpha}{\partial x} + \phi_{1\lambda} \frac{\partial \lambda}{\partial x} + \frac{h_1}{h_2}\left[\phi_{2\alpha} \frac{\partial \alpha}{\partial y}\right.\right. \\
& \left.\left. + \phi_{2\lambda} \frac{\partial \lambda}{\partial y} + \phi_{2\tau} \frac{\partial \tau}{\partial y} + \phi_{2\pi} \frac{\partial \Pi}{\partial y} + \phi_{2A} \frac{\partial A}{\partial y} + \frac{\phi_2}{\delta} \frac{\partial \delta}{\partial y}\right]\right\} \\
& + \delta \phi_1 \left\{\frac{U_e}{u_1} \frac{h_1}{q} \frac{\partial}{\partial x}\left(\frac{q}{h_1}\right) + \frac{1}{u_1} \frac{\partial U_e}{\partial x}\right\} + \delta \phi_2 \left\{\frac{U_e}{u_1} \frac{h_1}{q} \frac{\partial}{\partial y}\left(\frac{q}{h_2}\right)\right. \\
& \left. + \frac{h_1}{h_2} \frac{1}{u_1} \frac{\partial U_e}{\partial y}\right\}
\end{aligned}
$$

(F-1)

Appendix G (Turbulent Boundary Layer) /69

Calculation of the initial condition

When recalculating the experiments the initial values of the dependent variables δ, π, σ and A, must be determined at the first test station from the measured values of θ_{11}, H and β.

For the form parameter H we get

$$H = \frac{\delta_1^*}{\theta_{11}} = \frac{f_1}{f_{11}} \tag{G-1}$$

and with equation (D-2)

$$1.5\,\Pi^2 - \Pi\left\{2(L_1-2) + \frac{k}{\sigma}\,\frac{H-1}{H}\right\} + \left(2 - \frac{k}{\sigma}\,\frac{H-1}{H}\right) = 0 \tag{G-2}$$

In addition the following is true

$$\sigma = \frac{k}{\sigma}\,\frac{H\,\theta_{11}}{\Pi+1}$$

$$\frac{1}{\sigma} - \frac{\ln\sigma}{k} = \frac{1}{k}\ln\frac{\delta U_e}{\nu} + \frac{2\Pi}{k} + B \tag{G-3}$$

Equations (G-2) and (G-3) are iterated with an estimated value of π. A can be calculated for Mager profiles from

$$A = \tan\beta \tag{G-4}$$

and for Johnston profiles with equation (22). /70

The initial value for the entrainment coefficient F was the correlation by Head [4].

with

$$F = F(H_1)$$

$$H_1 := \frac{\delta - \delta_1^*}{\Theta_{11}} \qquad \text{(G-5)}$$

Appendix H (Laminar Boundary Layer) /71

The Transformed and Physical Integral Functions

1. The Transformed Integral Functions

Integral functions which depend on profiles in the direction of the main flow ($\eta\delta$ is the transformed boundary layer thickness for which $U/U_e=0.99$)

$$K_1 = \int_0^{\eta_\delta} \left(1 - \frac{U}{U_e}\right) d\eta \tag{H-1}$$

$$K_{11} = \int_0^{\eta_\delta} \frac{U}{U_e}\left(1 - \frac{U}{U_e}\right) d\eta \tag{H-2}$$

$$K_{111} = \int_0^{\eta_\delta} \frac{U}{U_e}\left(1 - \frac{U^2}{U_e^2}\right) d\eta \tag{H-3}$$

$$f_w'' = \left(\frac{\partial \frac{U}{U_e}}{\partial \eta}\right)_w \tag{H-4}$$

$$L_{11} = \int_0^{\eta\delta} \left(\frac{\partial \frac{U}{U_e}}{\partial \eta} \right)^2 d\eta \qquad \text{(H-5)}$$

Integral functions, which depend on profiles in the direction of the crossflow (all functions standardized for $\eta\delta=1$)

$$K_2 = -\int_0^1 \left(\frac{V}{U_e} \right)^x d\eta \qquad \text{(H-6)}$$

$$K_{22} = -\int_0^1 \left(\frac{V}{U_e} \right)^{x^2} d\eta \qquad \text{(H-7)}$$

$$K_{222} = -\int_0^1 \left(\frac{V}{U_e} \right)^{x^3} d\eta \qquad \text{(H-8)}$$

$$g_w'' = \left[\frac{\partial \left(\frac{V}{U_e} \right)^x}{\partial \eta} \right]_w \qquad \text{(H-9)}$$

$$L_{22} = \int_0^1 \left[\frac{\partial \left(\frac{V}{U_e}\right)^x}{\partial \eta} \right]^2 d\eta \qquad \text{(H-10)}$$

Integral functions which depend on profiles in the main flow and crossflow directions ($\eta\delta$ in the crossflow direction is set equal to the $\eta\delta$ of the main flow direction)

$$K_{12} = -\int_0^{\eta\delta} \frac{U}{U_e} \left(\frac{V}{U_e}\right)^x d\eta \qquad \text{(H-11)}$$

$$K_{112} = -\int_0^1 \frac{U^2}{U_e^2} \left(\frac{V}{U_e}\right)^x d\eta \qquad \text{(H-12)}$$

$$K_{221} = -\int_0^1 \frac{U}{U_e} \left(\frac{V}{U_e}\right)^{x^2} d\eta \qquad \text{(H-13)}$$

$$L_{12} = \int_0^{\eta\delta} \frac{\partial \frac{U}{U_e}}{\partial \eta} \frac{\partial \left(\frac{V}{U_e}\right)^x}{\partial \eta} d\eta \qquad \text{(H-14)}$$

. The Physical Integral Functions in the t,n, Coordinate System /74

The definition of these integral functions is given in appendix C. Integral functions which depend on profiles in the main flow direction

$$\delta_1^x = \theta_{11} \left[\frac{K_1}{K_{11}} + m_e^2 \left(\frac{K_1}{K_{11}} + 1 \right) \right] \tag{H-15}$$

$$\delta_{1i}^x = \theta_{11} \left[\frac{K_1}{K_{11}} \left(1 + m_e^2 \right) + m_e^2 \left(1 - \frac{K_{111}}{K_{11}} \right) \right] \tag{H-16}$$

θ_{11} variable

$$\theta_{11_i} = \theta_{11} \left(1 + m_e^2 \frac{K_{111}}{K_{11}} \right) \tag{H-17}$$

$$c_{f_t} = 2 \frac{a c^x}{Re_{\theta_{11}}} \tag{H-18}$$

$$S_{tt} = \frac{L_{11}}{Re_{\theta_{11}}} c^{x} \tag{H-19}$$

Integral functions which depend on profiles in the crossflow direction

$$\delta_2^{x} = \theta_{11} \frac{\eta_\delta}{K_{11}} bc \tag{H-20}$$

$$\delta_{2i}^{x} = \theta_{11} c \left[\frac{\eta_\delta}{K_{11}} b + m_e^2 \left(\frac{\eta_\delta}{K_{11}} b - \frac{K_{112}}{K_{11}} \right) \right] \tag{H-21}$$

$$\theta_{22} = \theta_{11} c^2 \eta_\delta \frac{K_{22}}{K_{11}} \tag{H-22}$$

$$\theta_{122} = \theta_{11} c^3 \eta_\delta \frac{K_{222}}{K_{11}} \tag{H-23}$$

$$c_{f_n} = 2 \frac{q_w''}{Re_{\theta_{11}}} \frac{K_{11}}{\eta_\delta} c c^x \qquad \text{(H-24)}$$

$$S_{nn} = \frac{L_{22}}{Re_{\theta_{11}}} \frac{K_{11}}{\eta_\delta} c^2 c^x \qquad \text{(H-25)}$$

Integral functions which depend on profiles in the main flow and crossflow directions

$$\theta_{12} = \theta_{11} c \left(\frac{K_{12}}{K_{11}} - \frac{\eta_\delta}{K_{11}} b \right) \qquad \text{(H-26)}$$

$$\theta_{12_i} = \theta_{11} c \frac{K_{12}}{K_{11}} - \delta_{2_i}^x \qquad \text{(H-27)}$$

$$\theta_{112} = \theta_{11} c \left(\frac{K_{112}}{K_{11}} - \frac{\eta_\delta}{K_{11}} b \right) \qquad \text{(H-28)}$$

$$\theta_{221} = \theta_{11}\, C^2\, \frac{K_{221}}{K_{11}} \qquad \text{(H-29)}$$

$$S_{tn} = \frac{L_{12}}{Re_{\theta_{11}}}\, K_{11}\, C C^x \qquad \text{(H-30)}$$

θ_{11}, a, b and c are the dependent variables and

$$Re_{\theta_{11}} = \frac{\theta_{11}\, U_e\, \rho_e}{\mu_e} \qquad \text{(H-31)}$$

$$m_e^2 = \frac{\gamma - 1}{2}\, M_e^2 \qquad \text{(H-32)}$$

where γ is the ratio of the specific heat of air.
The Chapman constant c^x is defined as

$$C^x = \left(\frac{T_w}{T_e}\right)^{1/2} \frac{T_e + 102.5}{T_w + 102.5} \qquad \text{(H-33)}$$

T_w and T_e are the static temperatures of the gas at the wall, resp. the outer edge of the boundary layer.

The right-hand sides of the equations (62)-(66)

$$D_1 = h_1 \frac{c_{fx}}{2} - \Theta_{11}\left\{\frac{(2-M_e^2)}{U_e}\frac{\partial U_e}{\partial x} + \frac{h_1}{q}\frac{\partial}{\partial x}\left(\frac{q}{h_1}\right) + a_1 h_1\right\}$$

$$- \frac{h_1}{h_2}\left\{\Theta_{12\theta_{11}}\frac{\partial \theta_{11}}{\partial y} + \Theta_{12a}\frac{\partial a}{\partial y} + \Theta_{12b}\frac{\partial b}{\partial y} + \Theta_{12c}\frac{\partial c}{\partial y} + \Theta_{12\alpha}\frac{\partial \alpha}{\partial y}\right.$$

$$\left. + \Theta_{12\lambda}\frac{\partial \lambda}{\partial y}\right\} - \Theta_{12}\left\{\frac{(2-M_e^2)}{U_e}\frac{h_1}{h_2}\frac{\partial U_e}{\partial y} + \frac{h_1}{q}\frac{\partial}{\partial y}\left(\frac{q}{h_2}\right) + a_3 h_1\right\}$$

$$-\Delta_1^x\left\{\frac{1}{U_e}\frac{\partial u_1}{\partial x} + a_1 h_1 \frac{u_1}{U_e}\right\} - \Delta_2^x\left\{\frac{h_1}{h_2}\frac{1}{U_e}\frac{\partial u_1}{\partial y} + a_2 h_1 \frac{v_1}{U_e} + a_3 h_1 \frac{u_1}{U_e}\right\}$$

$$- h_1 \Theta_{22} a_2 - \Theta_{11\alpha}\frac{\partial \alpha}{\partial x} - \Theta_{11\lambda}\frac{\partial \lambda}{\partial x} \qquad (I-1)$$

$$D_2 = h_1 \frac{c_{fy}}{2} - \Theta_{21}\left\{\frac{(2-M_e^2)}{U_e}\frac{\partial U_e}{\partial x} + \frac{h_1}{q}\frac{\partial}{\partial x}\left(\frac{q}{h_1}\right) + h_1 b_3\right\} - \frac{h_1}{h_2}\left\{\Theta_{22\theta_{11}}\frac{\partial \theta_{11}}{\partial y}\right.$$

$$\left. + \Theta_{22a}\frac{\partial a}{\partial y} + \Theta_{22b}\frac{\partial b}{\partial y} + \Theta_{22c}\frac{\partial c}{\partial y} + \Theta_{22\alpha}\frac{\partial \alpha}{\partial y} + \Theta_{22\lambda}\frac{\partial \lambda}{\partial y}\right\}$$

$$- \Theta_{22}\left\{\frac{(2-M_e^2)}{U_e}\frac{h_1}{h_2}\frac{\partial U_e}{\partial y} + \frac{h_1}{q}\frac{\partial}{\partial y}\left(\frac{q}{h_2}\right) + b_2 h_1\right\} - \Delta_1^x\left\{\frac{1}{U_e}\frac{\partial v_1}{\partial x} + h_1 b_1 \frac{u_1}{U_e}\right.$$

$$\left. + b_3 h_1 \frac{v_1}{U_e}\right\} - \Delta_2^x\left\{\frac{h_1}{h_2}\frac{1}{U_e}\frac{\partial v_1}{\partial y} + h_1 b_2 \frac{v_1}{U_e}\right\} - h_1 b_1 \Theta_{11}$$

$$- \Theta_{21\alpha}\frac{\partial \alpha}{\partial x} - \Theta_{21\lambda}\frac{\partial \lambda}{\partial x} \qquad (I-2)$$

$$D_3 = 2h_1 S_x - \Theta_{111}\left\{\frac{(3-M_e^2)}{U_e}\frac{\partial U_e}{\partial x} + \frac{h_1}{q}\frac{\partial}{\partial x}\left(\frac{q}{h_1}\right) + 2h_1 a_1\right\} - \frac{h_1}{h_2}\left\{\Theta_{221\theta_{11}}\frac{\partial \theta_{11}}{\partial y}\right.$$

$$\left. + \Theta_{221a}\frac{\partial a}{\partial y} + \Theta_{221b}\frac{\partial b}{\partial y} + \Theta_{221c}\frac{\partial c}{\partial y} + \Theta_{221\alpha}\frac{\partial \alpha}{\partial y} + \Theta_{221\lambda}\frac{\partial \lambda}{\partial y}\right\}$$

$$- \Theta_{2212}\left\{\frac{(3-M_e^2)}{U_e}\frac{h_1}{h_2}\frac{\partial U_e}{\partial y} + \frac{h_1}{q}\frac{\partial}{\partial y}\left(\frac{q}{h_2}\right) + 2h_1 a_3\right\} - 2(\Delta_1^x - \Delta_{1i}^x)\left\{\frac{u_1}{U_e^2}\frac{\partial u_1}{\partial x}\right.$$

$$\left. + a_1 h_1 \frac{u_1^2}{U_e^2} + a_2 h_1 \frac{v_1^2}{U_e^2}\right\} - 2(\Theta_{21i} - \Theta_{12})\left\{\frac{h_1}{h_2}\frac{1}{U_e}\frac{\partial u_1}{\partial y} + h_1 a_3 \frac{u_1}{U_e}\right\}$$

$$- 2h_1 a_2 \Theta_{221} - \Theta_{111\alpha}\frac{\partial \alpha}{\partial x} - \Theta_{111\lambda}\frac{\partial \lambda}{\partial x} \qquad \text{(I-3)}$$

$$D_4 = 2h_1 S_y - \Theta_{221}\left\{\frac{(3-M_e^2)}{U_e}\frac{\partial U_e}{\partial x} + \frac{h_1}{q}\frac{\partial}{\partial x}\left(\frac{q}{h_1}\right) + 2h_1 b_3\right\}$$

$$- \frac{h_1}{h_2}\left\{\Theta_{222\theta_{11}}\frac{\partial \theta_{11}}{\partial y} + \Theta_{222a}\frac{\partial a}{\partial y} + \Theta_{222b}\frac{\partial b}{\partial y} + \Theta_{222c}\frac{\partial c}{\partial y} + \Theta_{222\alpha}\frac{\partial \alpha}{\partial y}\right.$$

$$\left. + \Theta_{222\lambda}\frac{\partial \lambda}{\partial y}\right\} - \Theta_{222}\left\{\frac{(3-M_e^2)}{U_e}\frac{h_1}{h_2}\frac{\partial U_e}{\partial y} + \frac{h_1}{q}\frac{\partial}{\partial y}\left(\frac{q}{h_2}\right) + 2h_1 b_2\right\}$$

$$- 2(\Delta_2^x - \Delta_{2i}^x)\left\{\frac{h_1}{h_2}\frac{v_1}{U_e^2}\frac{\partial v_1}{\partial y} + b_1 h_1 \frac{u_1^2}{U_e^2} + b_2 h_1 \frac{v_1^2}{U_e^2}\right\}$$

$$- 2(\Theta_{12i} - \Theta_{21})\left\{\frac{1}{U_e}\frac{\partial v_1}{\partial x} + b_3 h_1 \frac{v_1}{U_e}\right\} - 2b_1 h_1 \Theta_{112} - \Theta_{221\alpha}\frac{\partial \alpha}{\partial x} \qquad \text{(I-4)}$$

$$- \Theta_{221\lambda}\frac{\partial \lambda}{\partial x}$$

$$D_S = \frac{U_e}{u_1}\frac{\partial \Delta_1^x}{\partial x} + \Delta_1^x\left\{\frac{1}{u_1}\frac{\partial U_e}{\partial x} + \frac{U_e}{u_1}\frac{h_1}{q}\frac{\partial}{\partial x}\left(\frac{q}{h_1}\right) - \frac{M_e^2}{u_1}\frac{\partial U_e}{\partial x}\right\}$$

$$+ \Delta_2^x\left\{\frac{U_e}{u_1}\frac{h_1}{q}\frac{\partial}{\partial y}\left(\frac{q}{h_2}\right) + \frac{h_1}{h_2}\frac{1}{u_1}\frac{\partial U_e}{\partial y}(1-M_e^2)\right\} + \frac{h_1}{h_2}\frac{U_e}{u_1}\frac{\partial \Delta_2^x}{\partial y}$$

$$- \delta^x\left\{\frac{1}{u_1}\frac{\partial u_1}{\partial x} + \frac{h_1}{q}\frac{\partial}{\partial x}\left(\frac{q}{h_1}\right) - \frac{M_e^2}{U_e}\frac{\partial U_e}{\partial x} + \frac{h_1}{h_2}\frac{1}{u_1}\frac{\partial v_1}{\partial y}\right.$$

$$\left. + \frac{v_1}{u_1}\frac{h_1}{q}\frac{\partial}{\partial y}\left(\frac{q}{h_2}\right) - \frac{h_1}{h_2}\frac{v_1}{u_1}\frac{M_e^2}{U_e}\frac{\partial U_e}{\partial y}\right\} - \frac{h_1}{h_2}\frac{v_1}{u_1}\frac{\partial \delta^x}{\partial y}$$

(I-5)

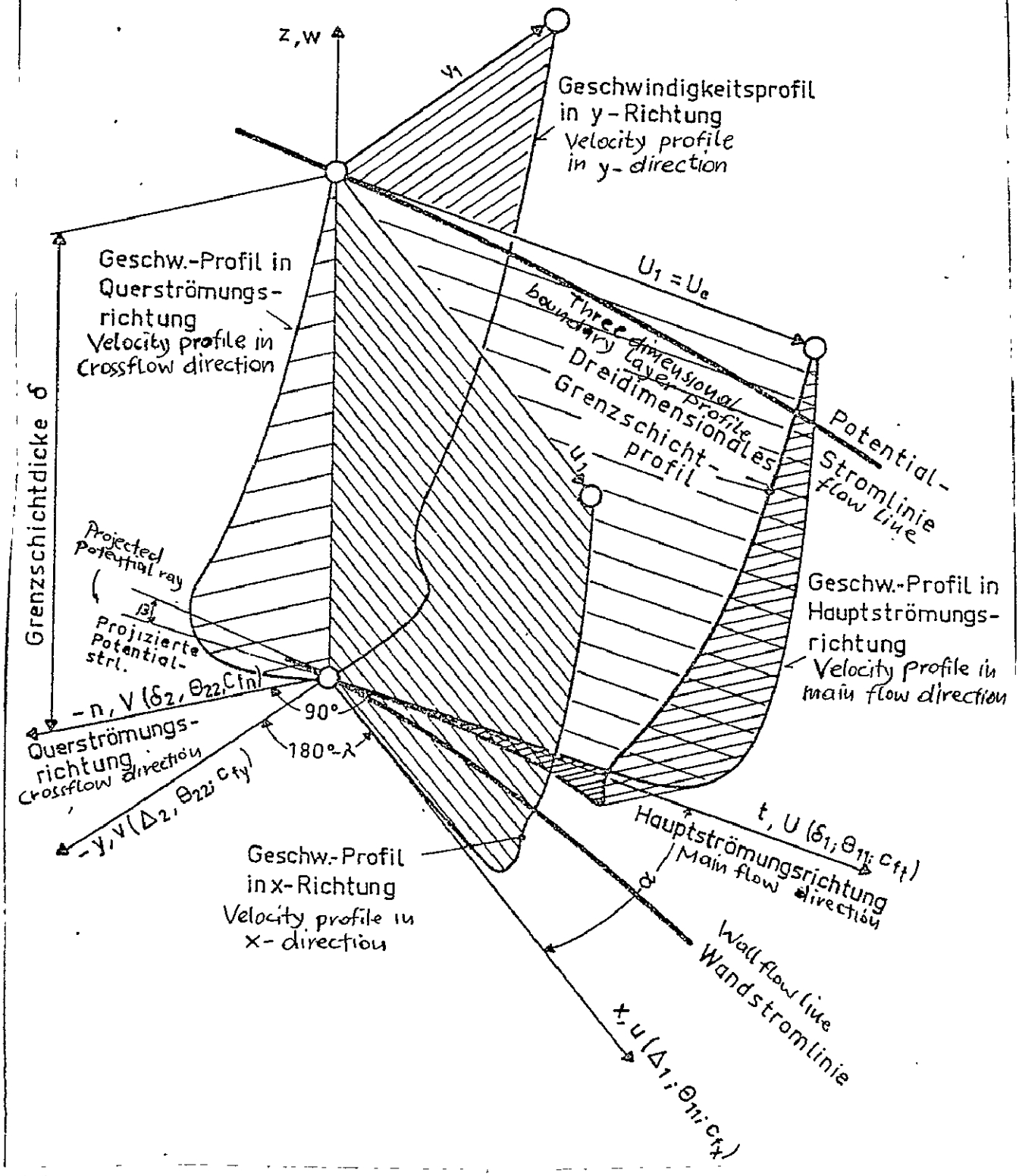

Fig. 1. Three-dimensional Boundary Layer Flow

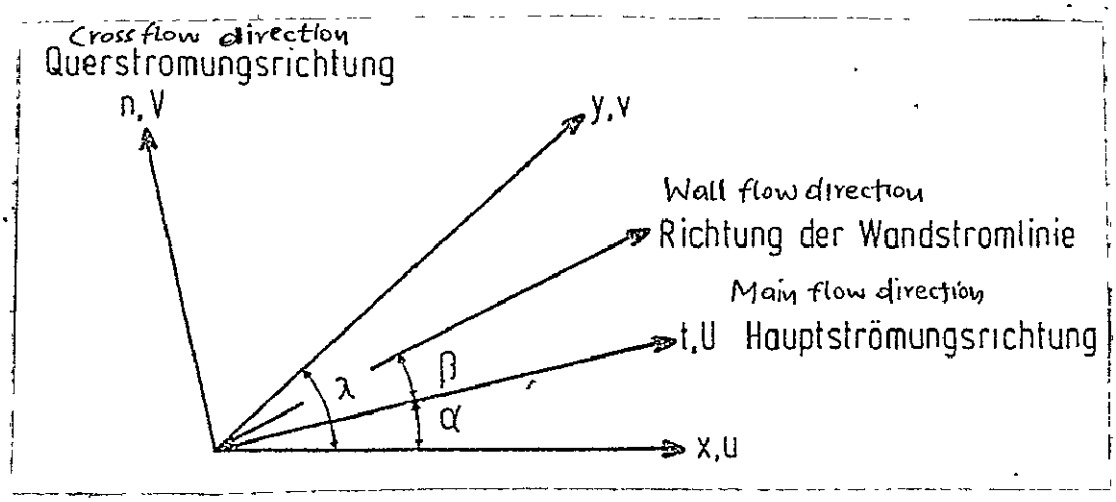

Fig. 2. View of the Plane Tangential to the Body Surface

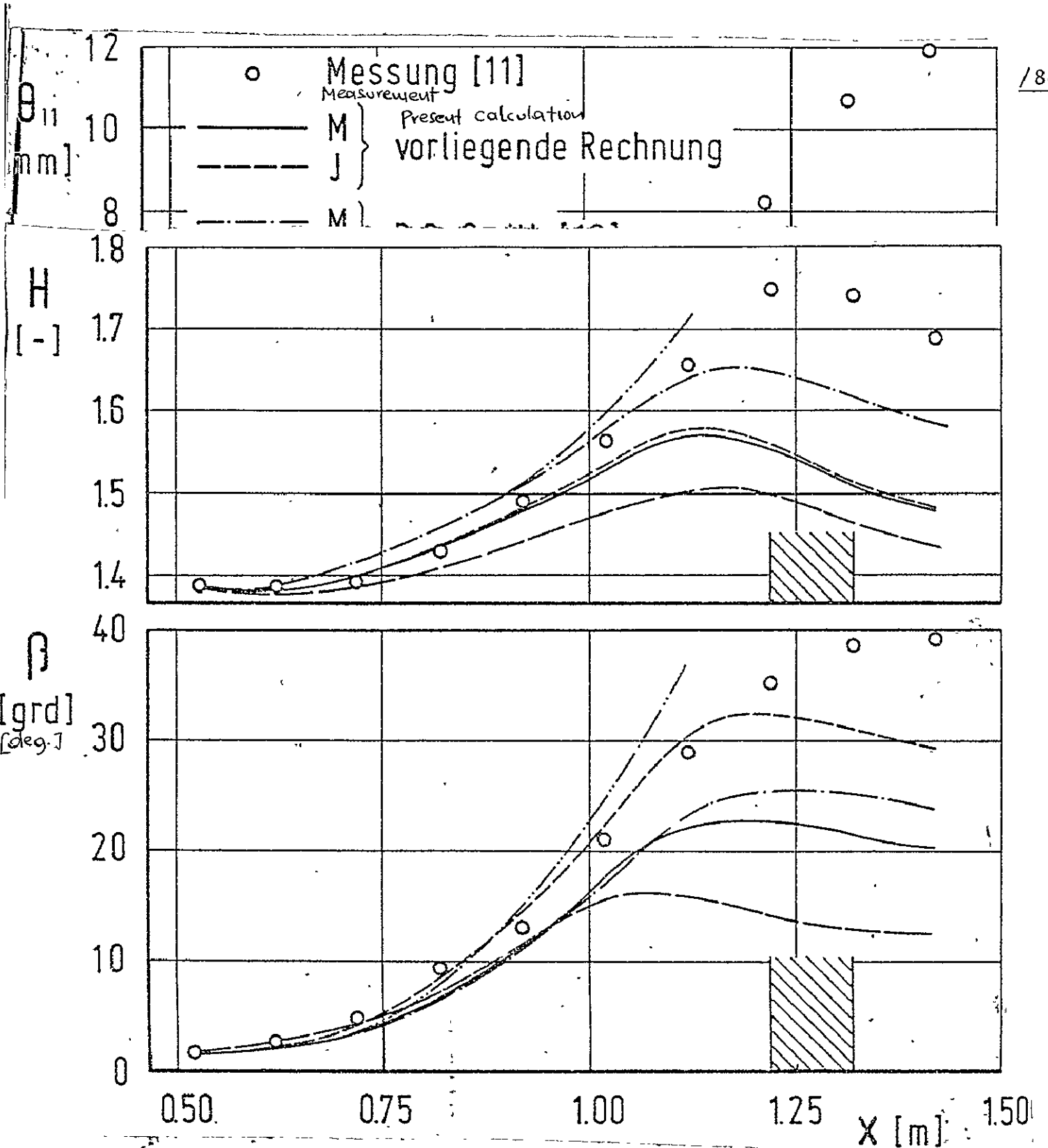

Fig. 3. Course of the moment loss thickness θ_{11} of the form parameter H and of the wallflow line angle β

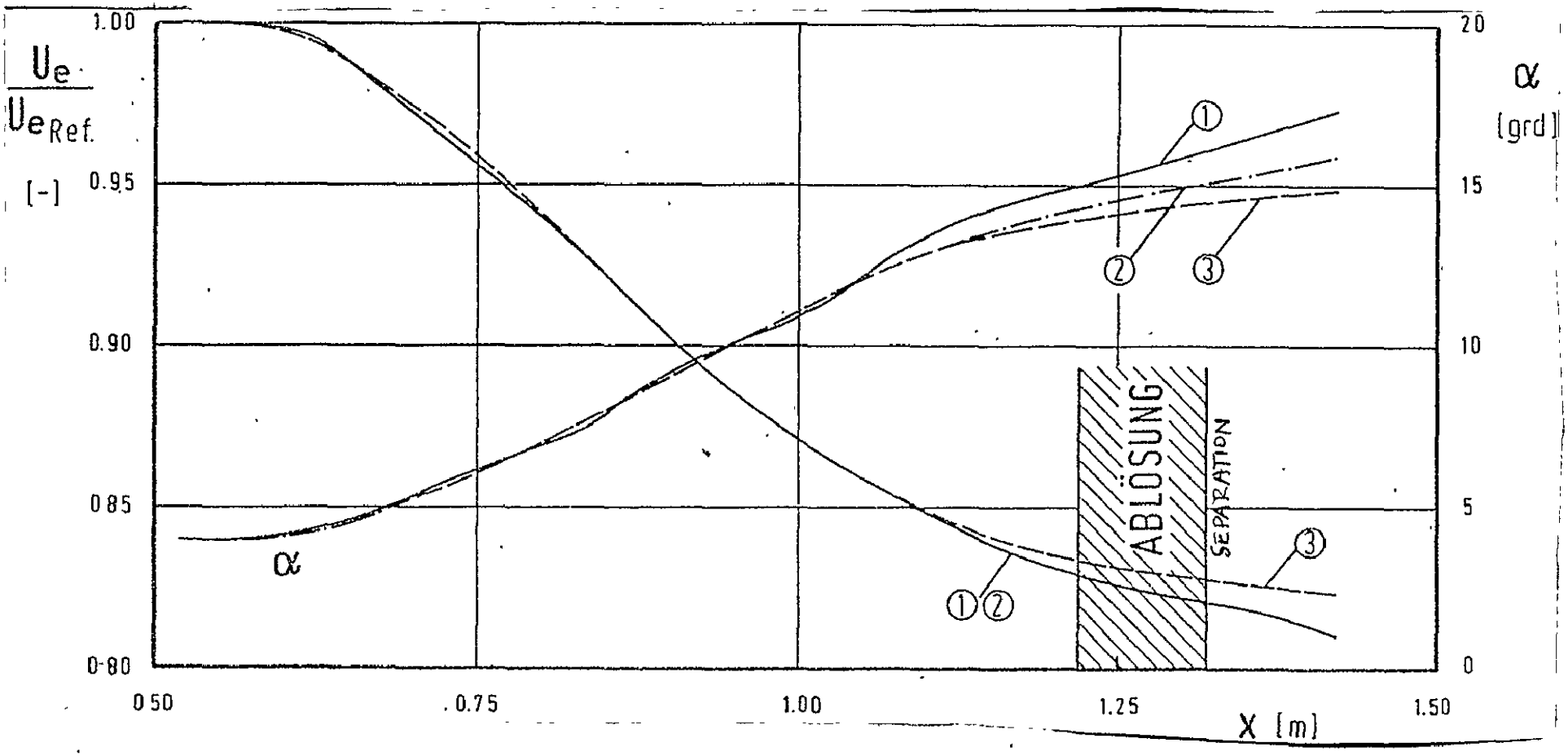

Fig. 4. Data of the potential flow from Berg and Elsenaar's tests

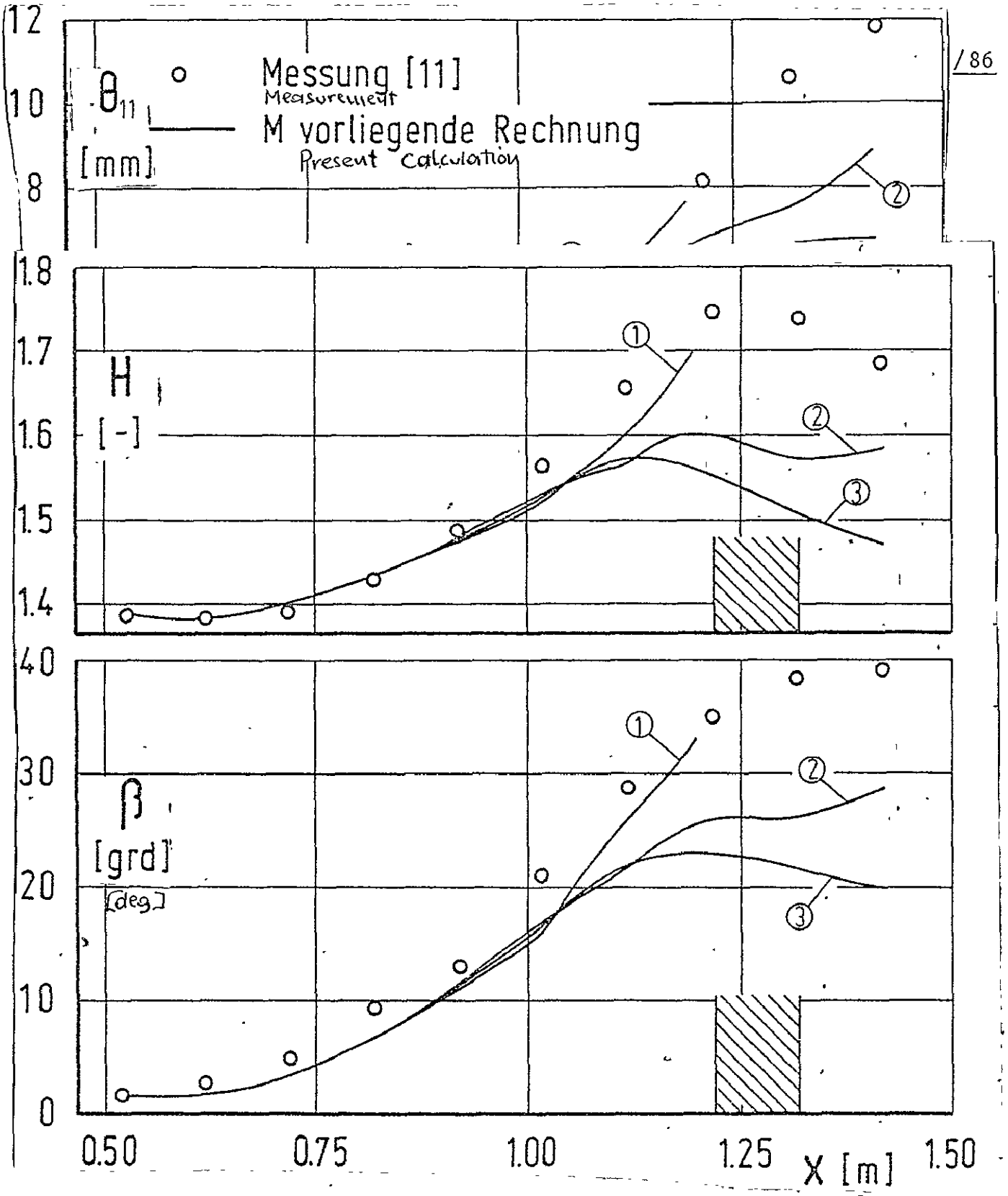

Fig. 5. Results for Mager crossflow profiles for input of various data of the potential flow

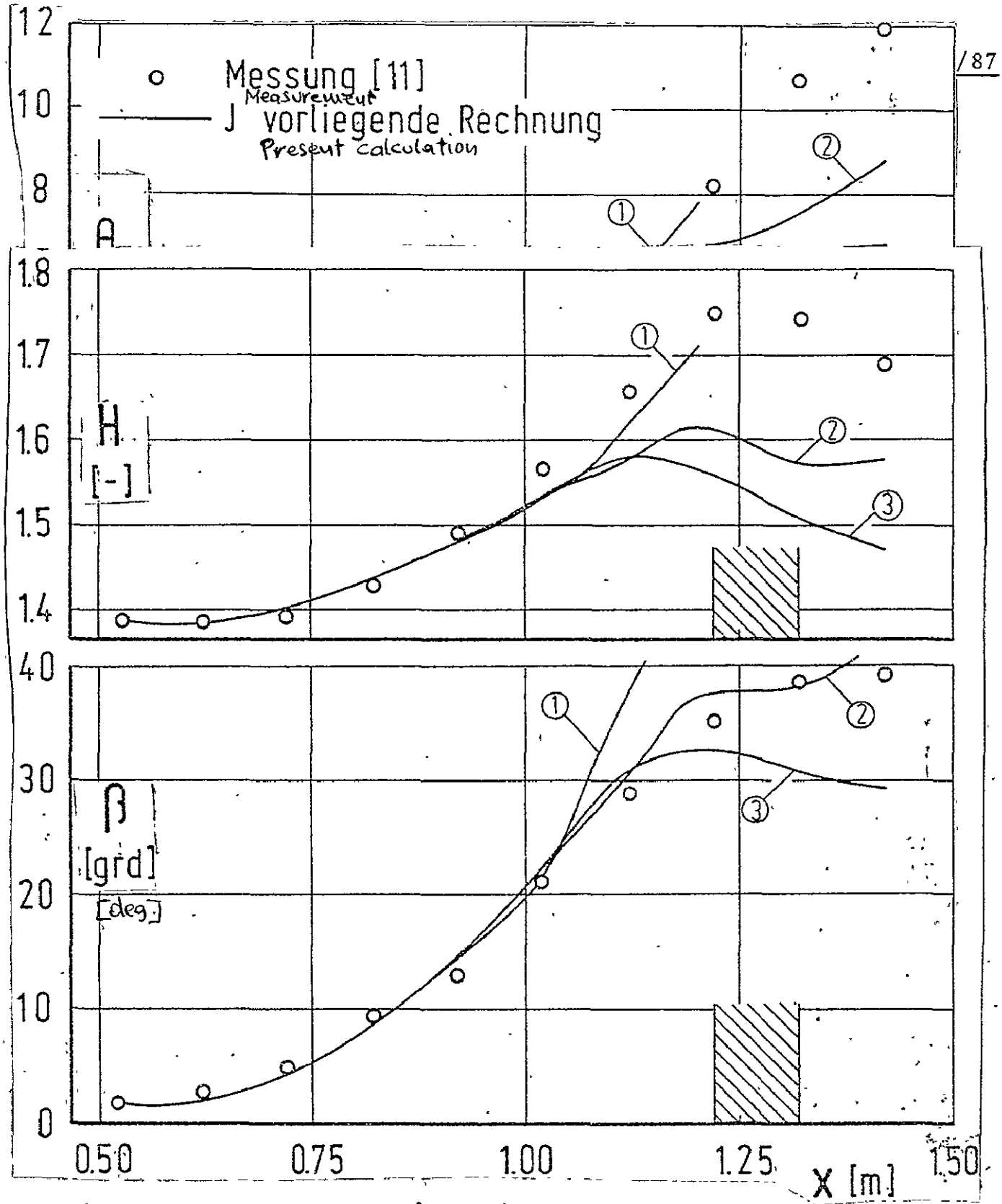

Fig. 6. Results for Johnston crossflow profiles for input of various data of the potential flow

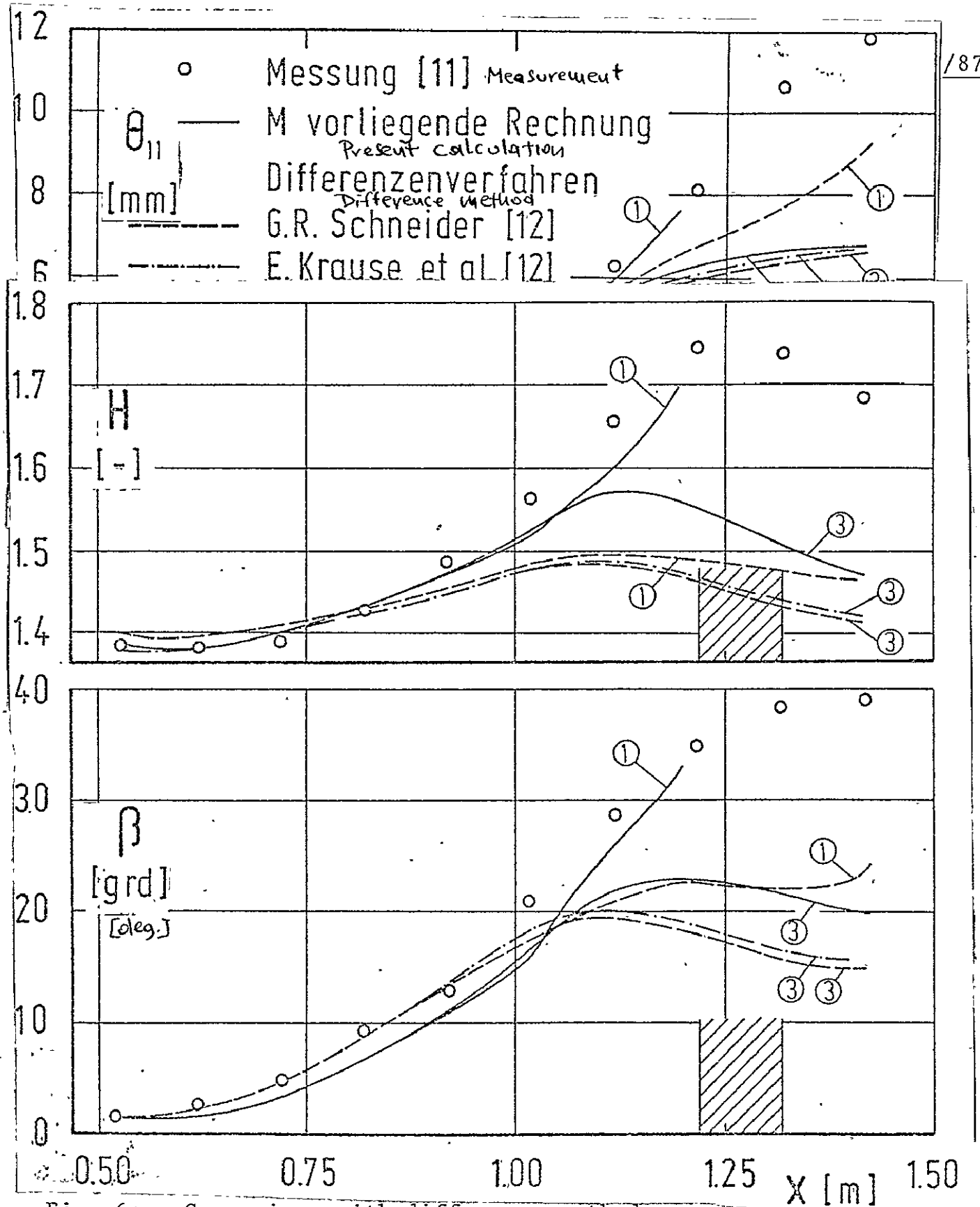

Fig. 6a. Comparison with difference methods

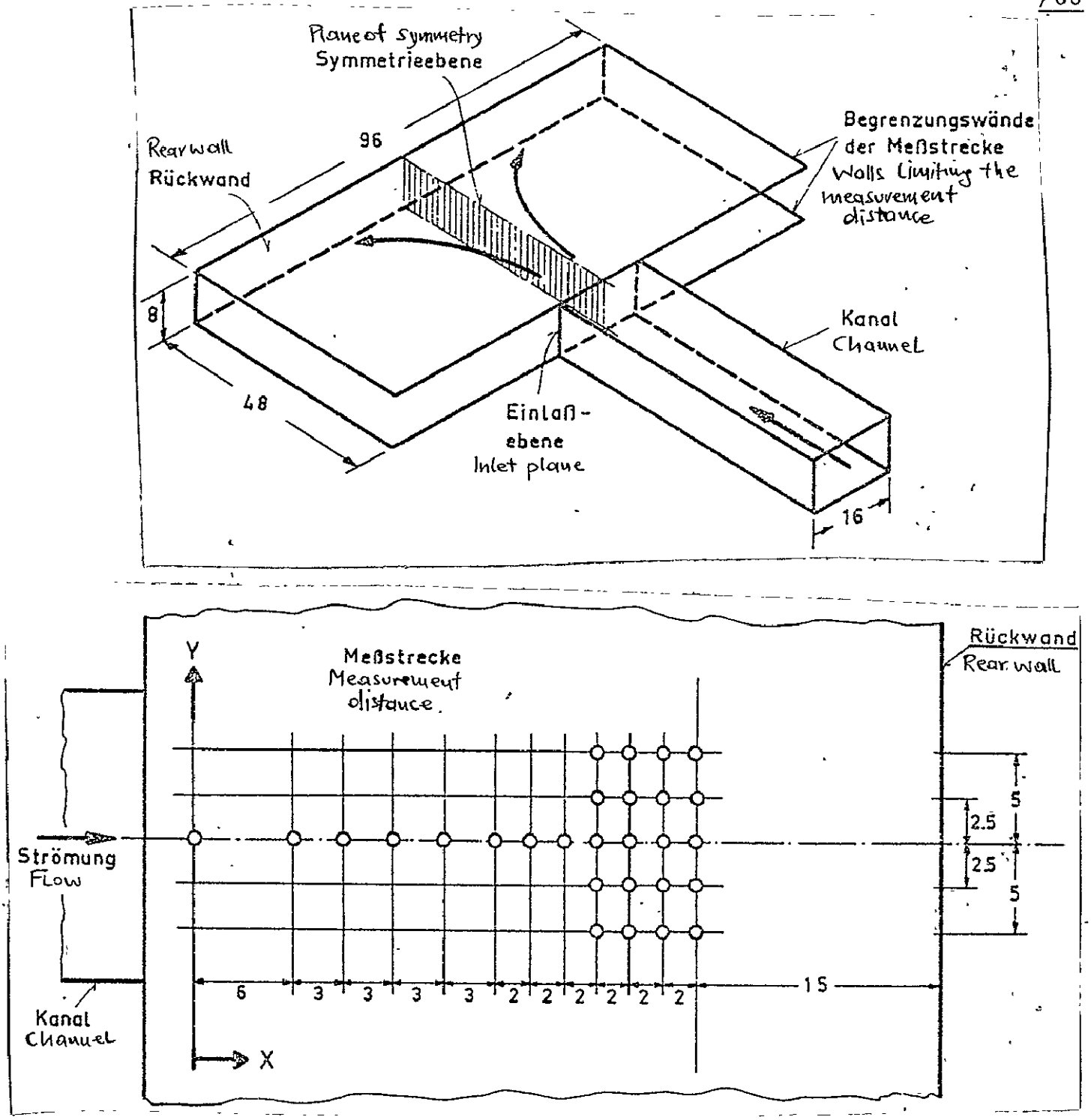

Fig. 7. Description of test arrangement

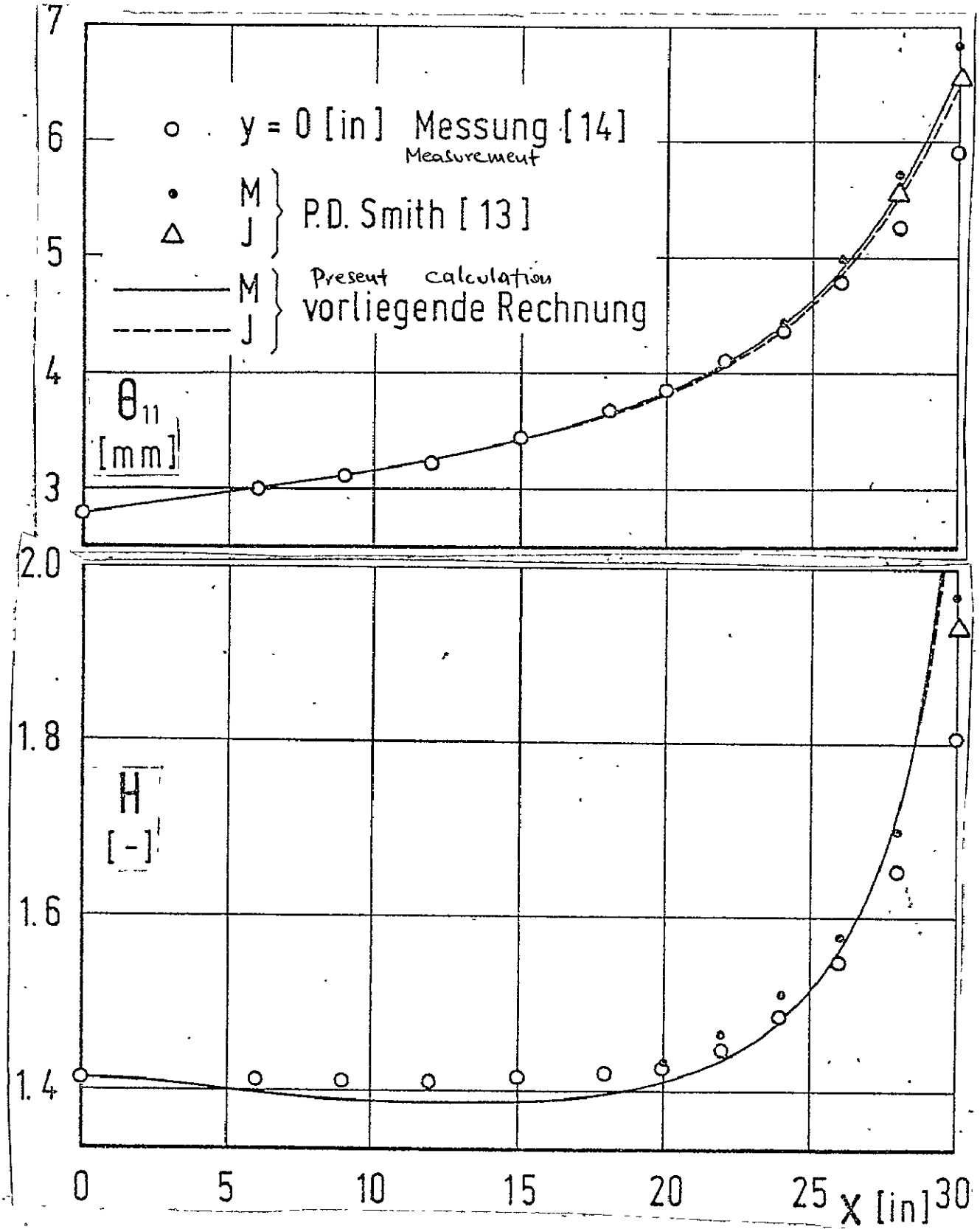

Fig. 8. Course of the moment loss thickness θ_{11}, of the form parameter H and of the wallflow line angle β

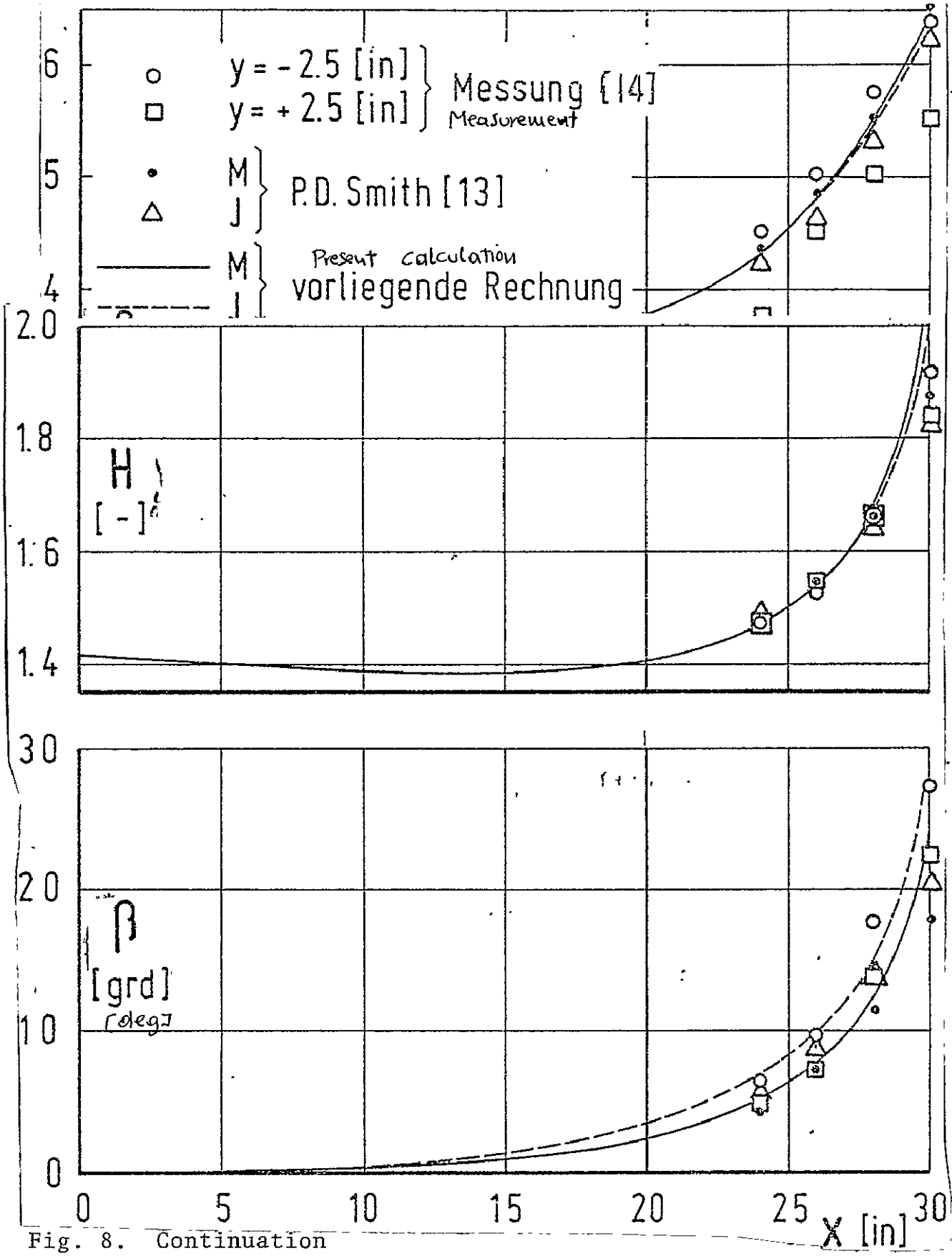

Fig. 8. Continuation

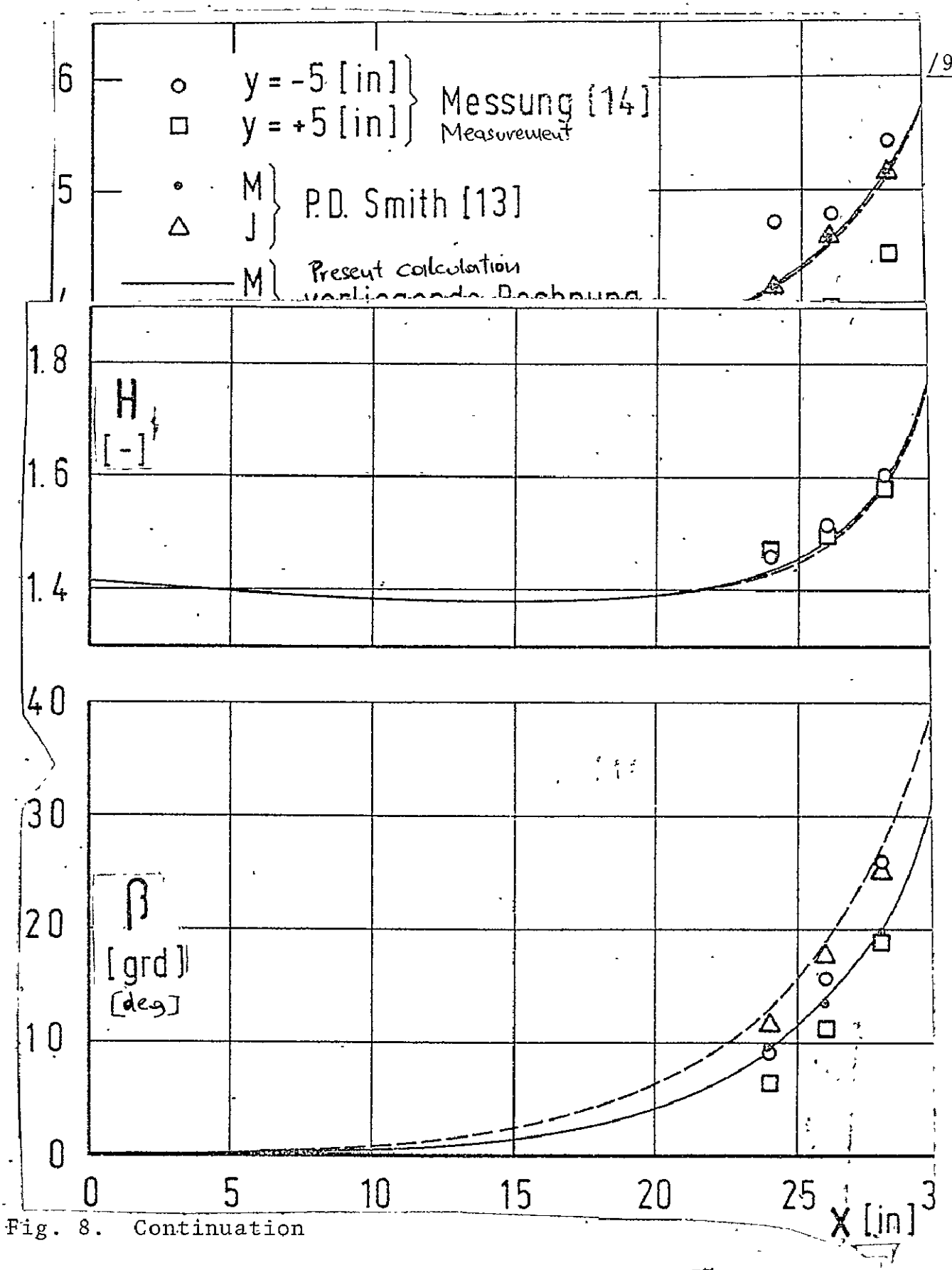

Fig. 8. Continuation

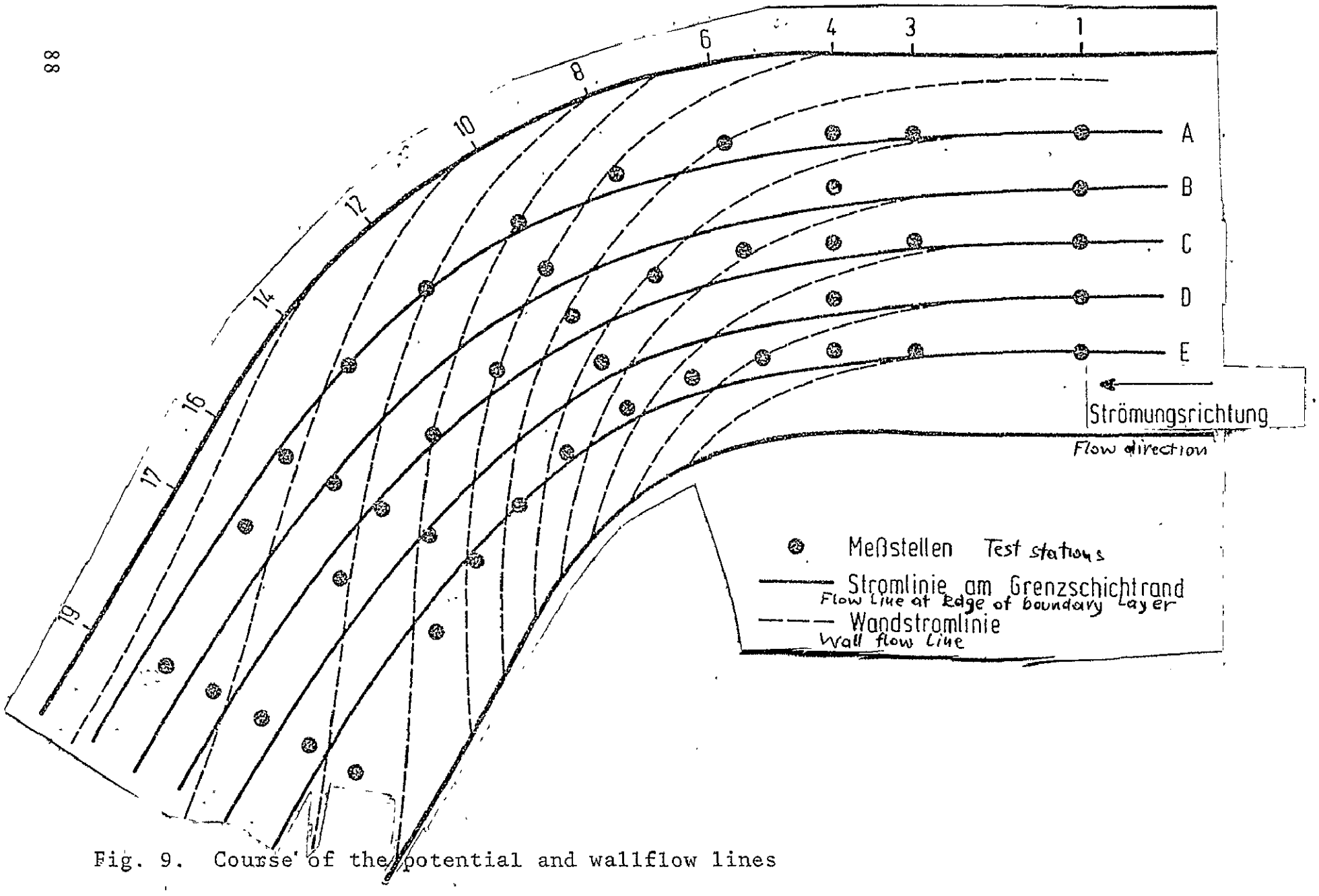

Fig. 9. Course of the potential and wallflow lines

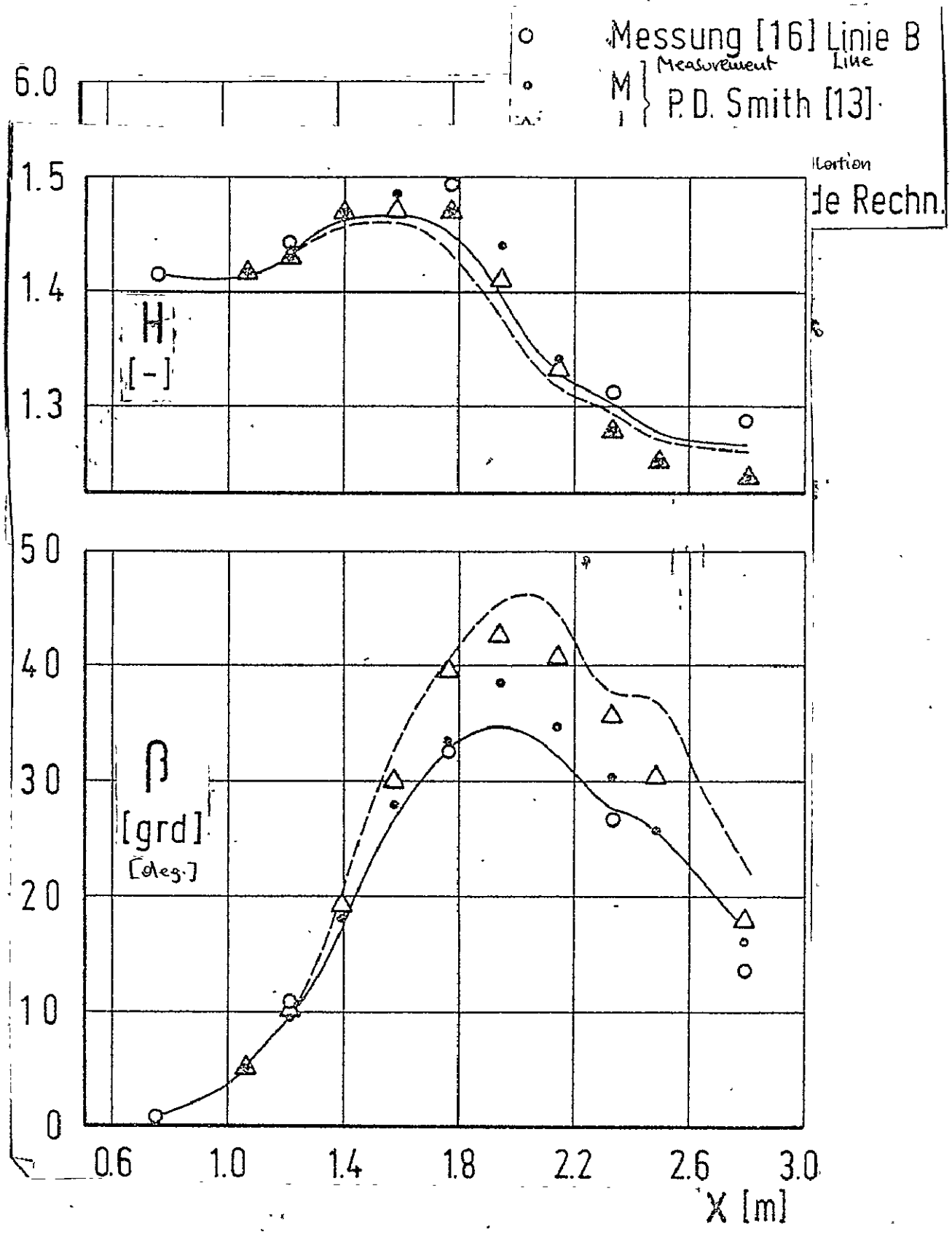

Fig. 10. Course of the moment loss thickness θ_{11} of the form parameter H and of the wallflow line angle β.

C-2

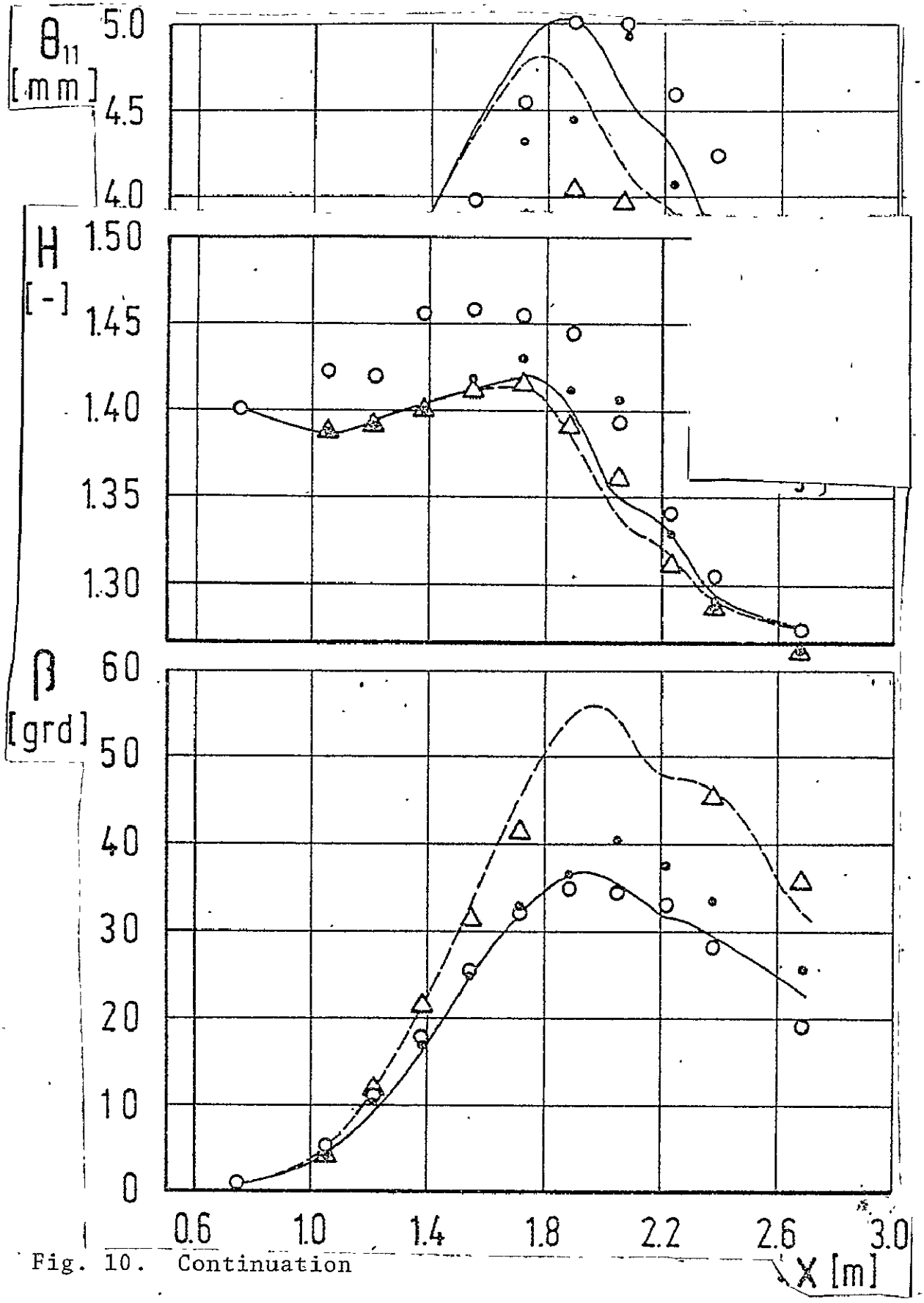

Fig. 10. Continuation

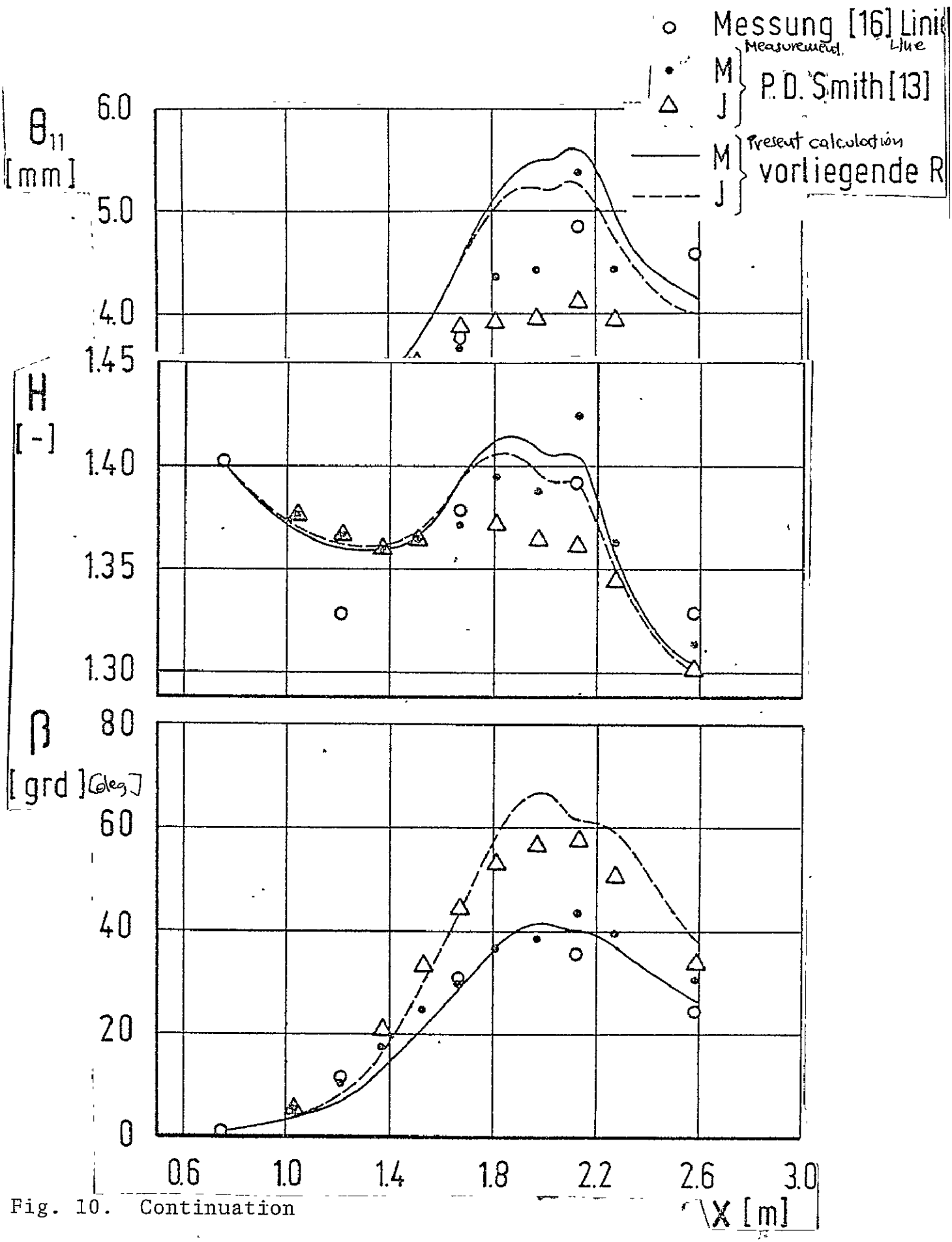

Fig. 10. Continuation

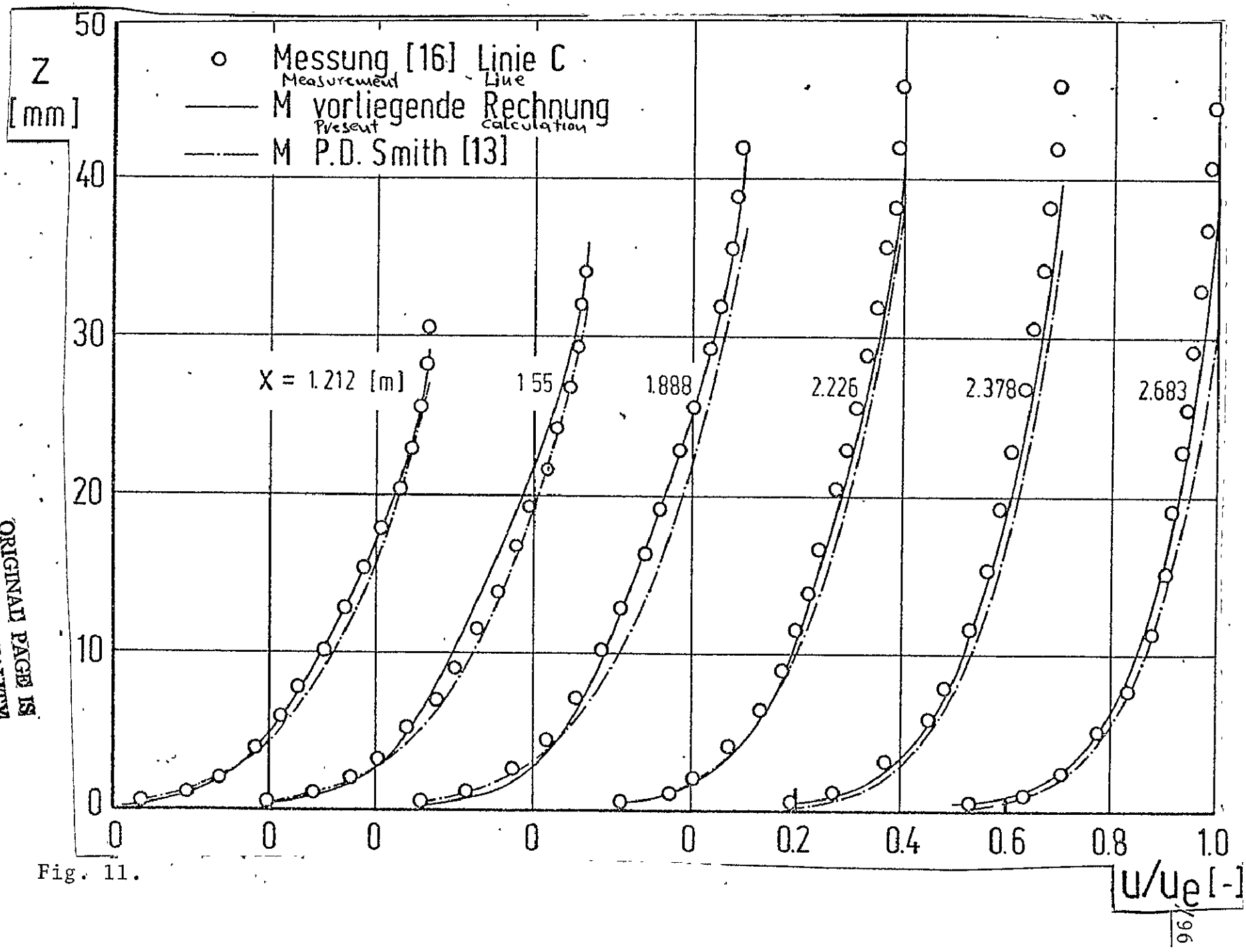

Fig. 11.

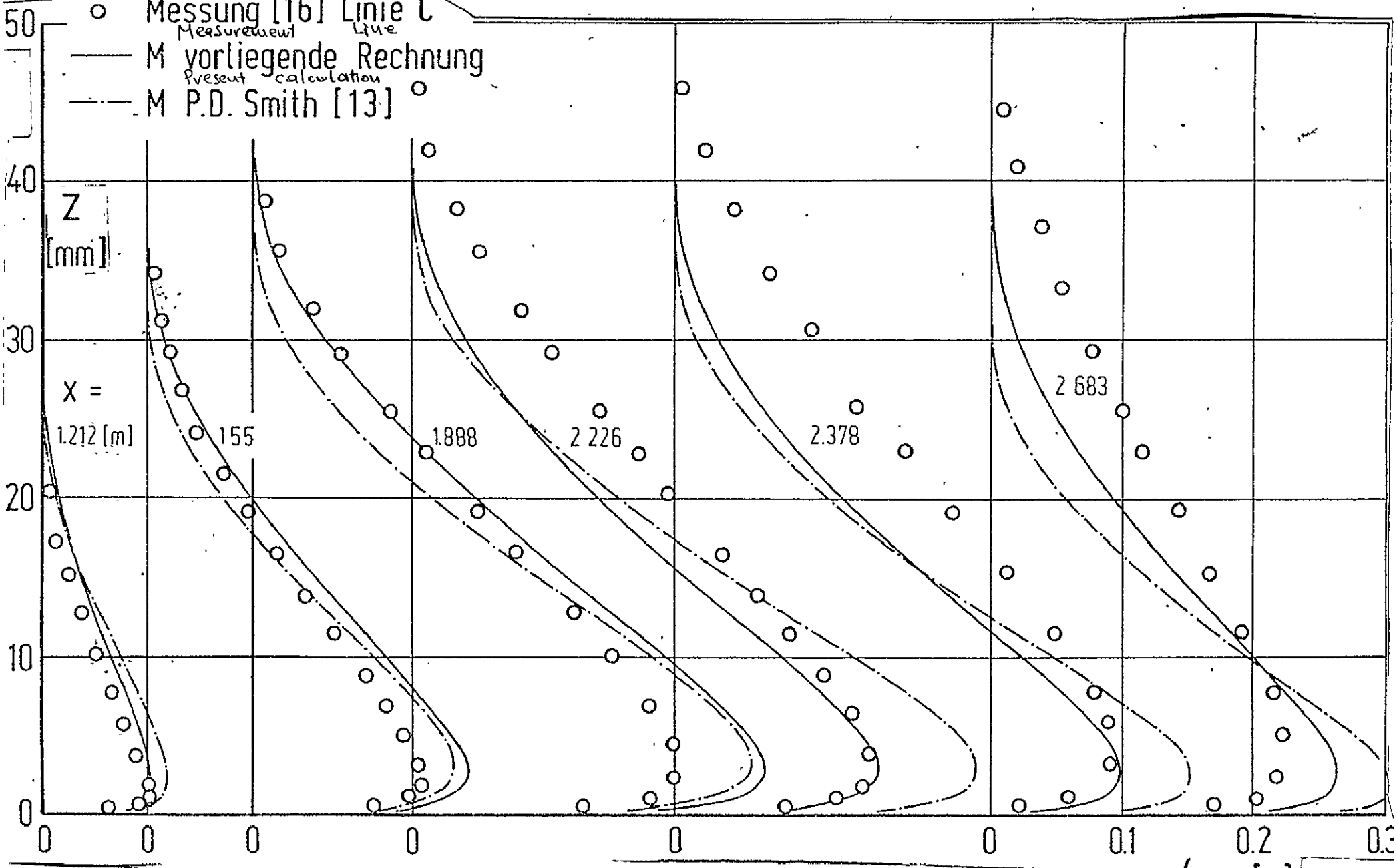

Fig. 12. Comparison of the measured and calculated velocity profiles in the crossflow direction

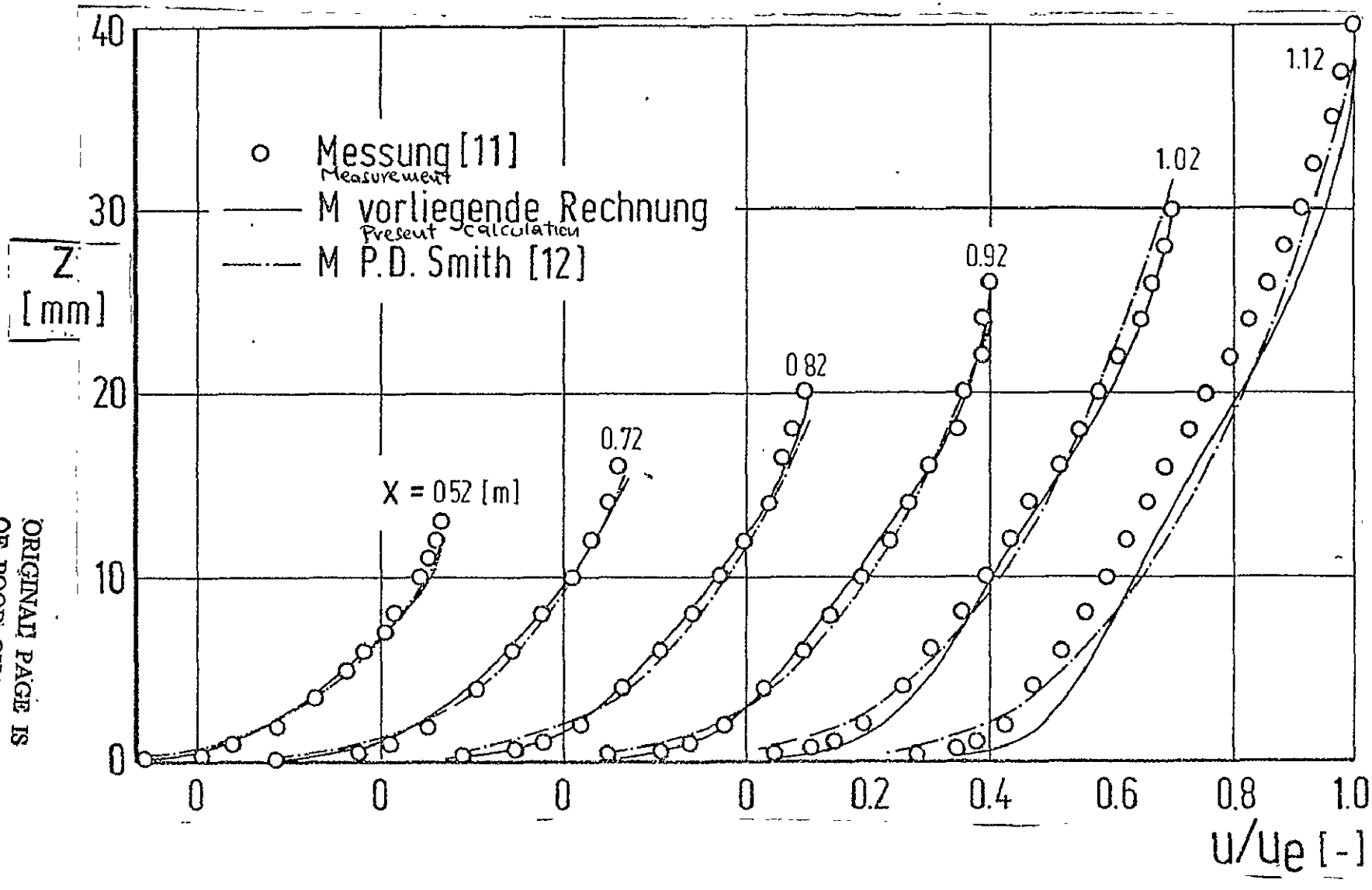

Fig. 13. Comparison of the measured and calculated velocity profiles in the main flow direction

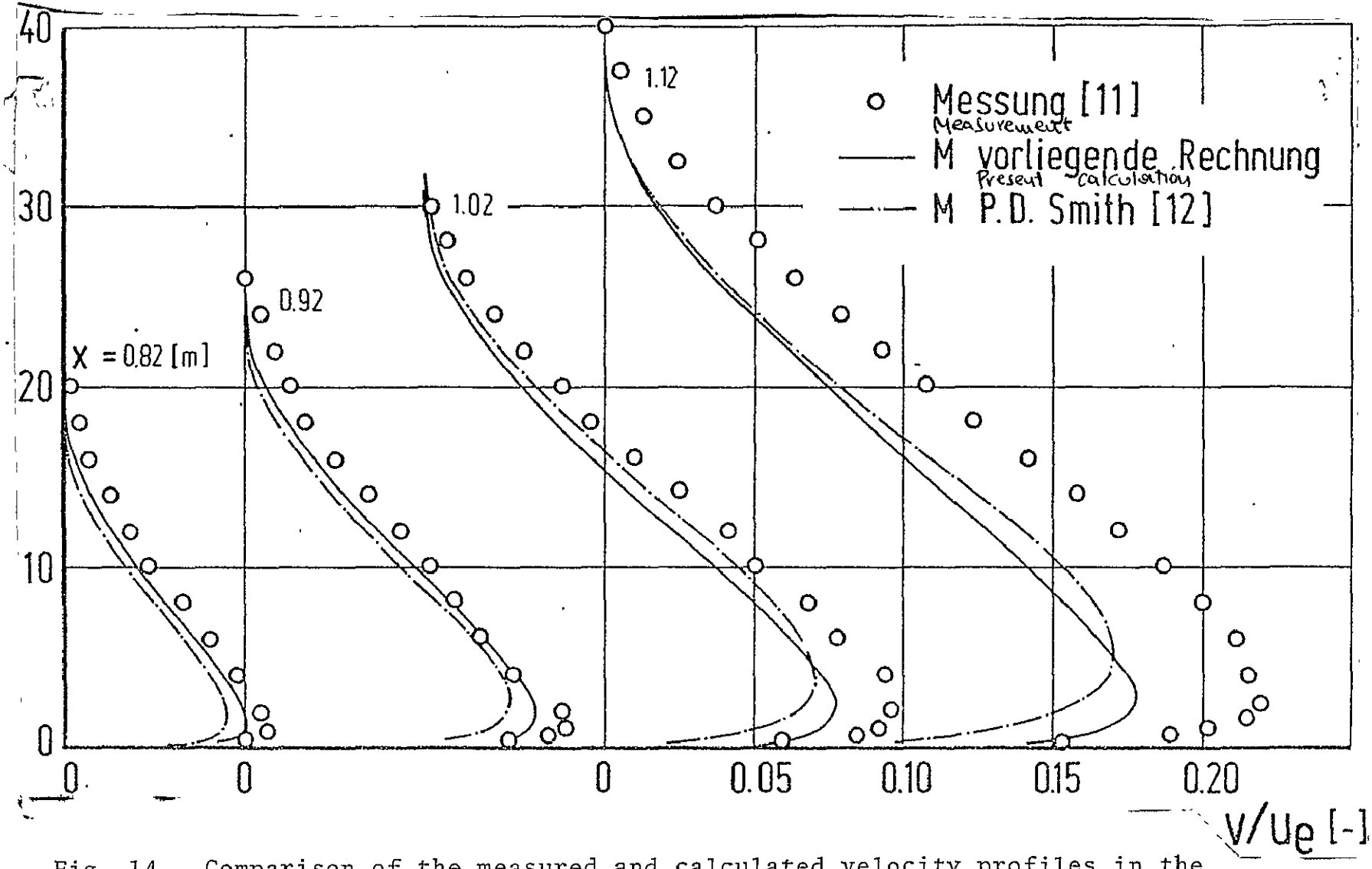

Fig. 14. Comparison of the measured and calculated velocity profiles in the crossflow direction

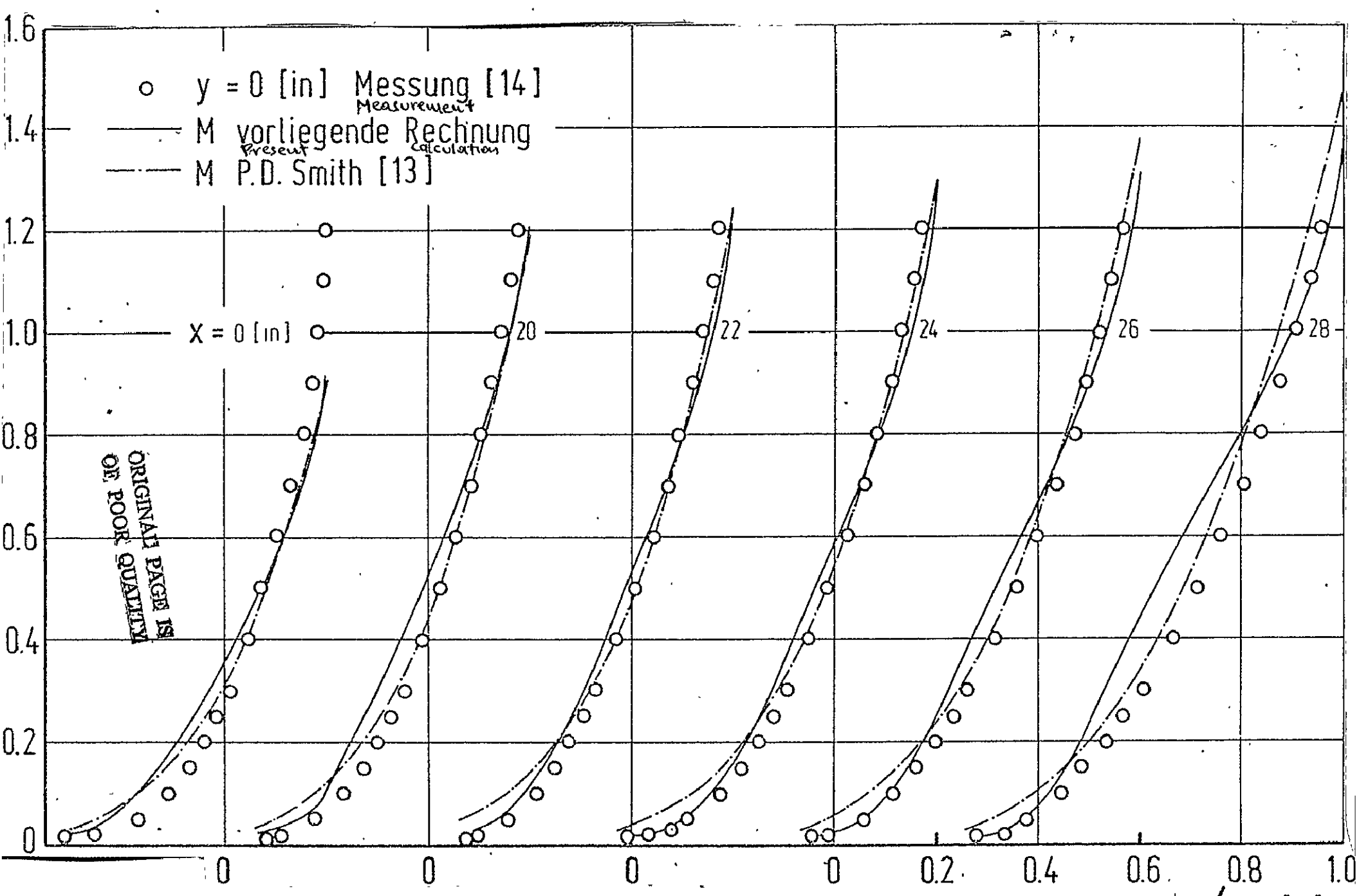

Fig. 15. Comparison of the measured and calculated velocity profiles in the main flow direction

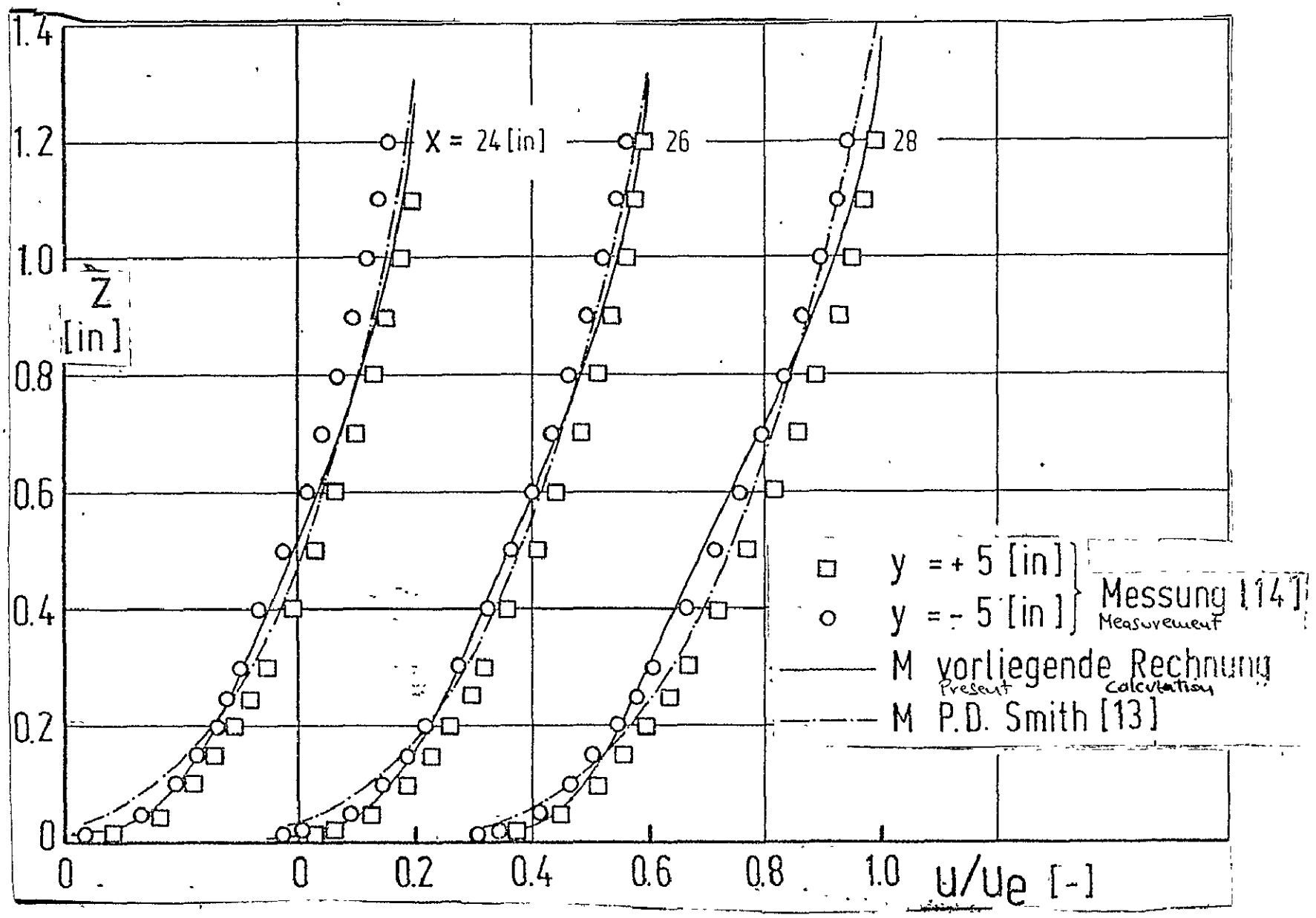

Fig. 16. Comparison of the measured and calculated velocity profiles in the main flow direction

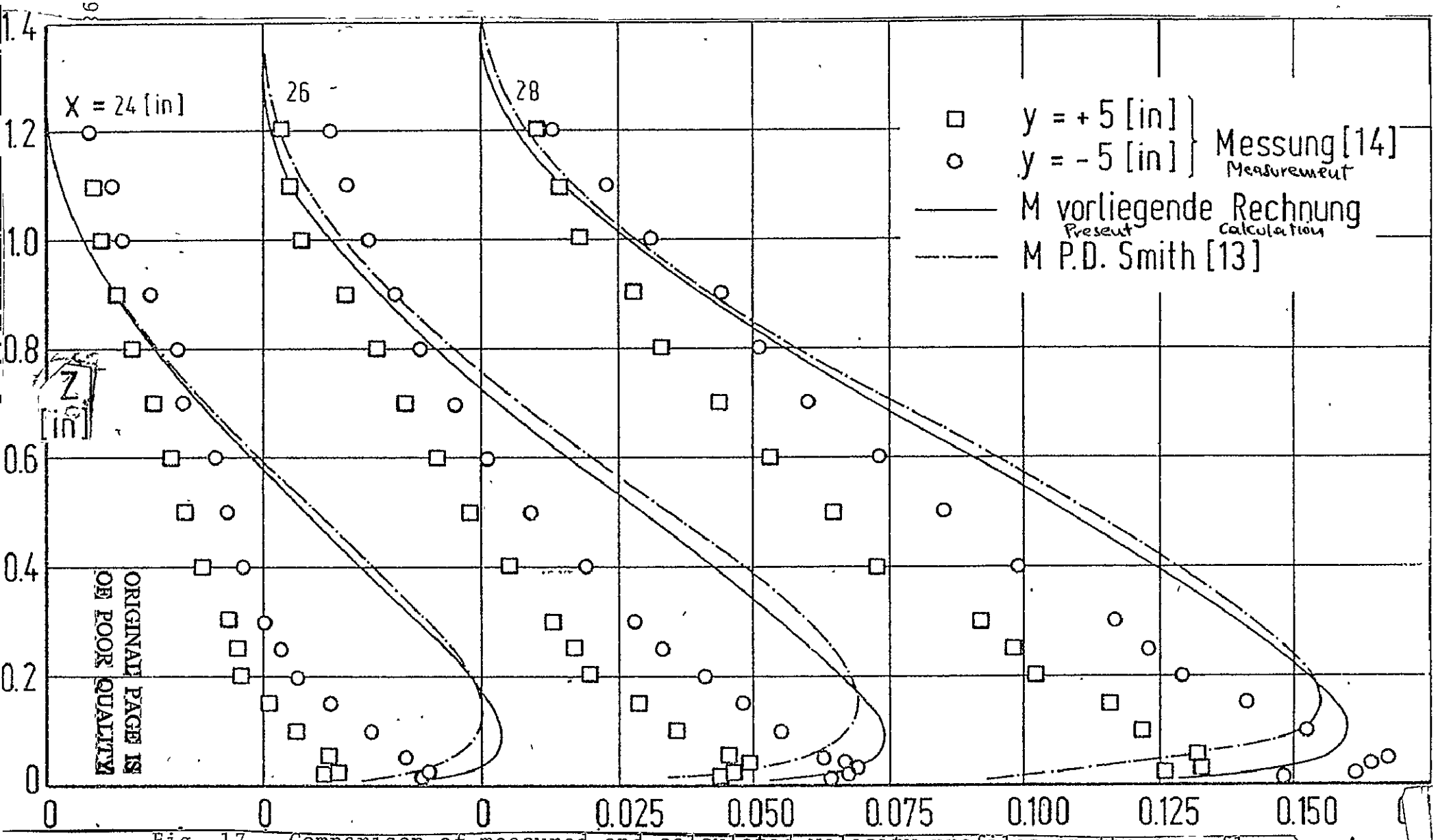

Fig. 17. Comparison of measured and calculated velocity profiles in the crossflow direction

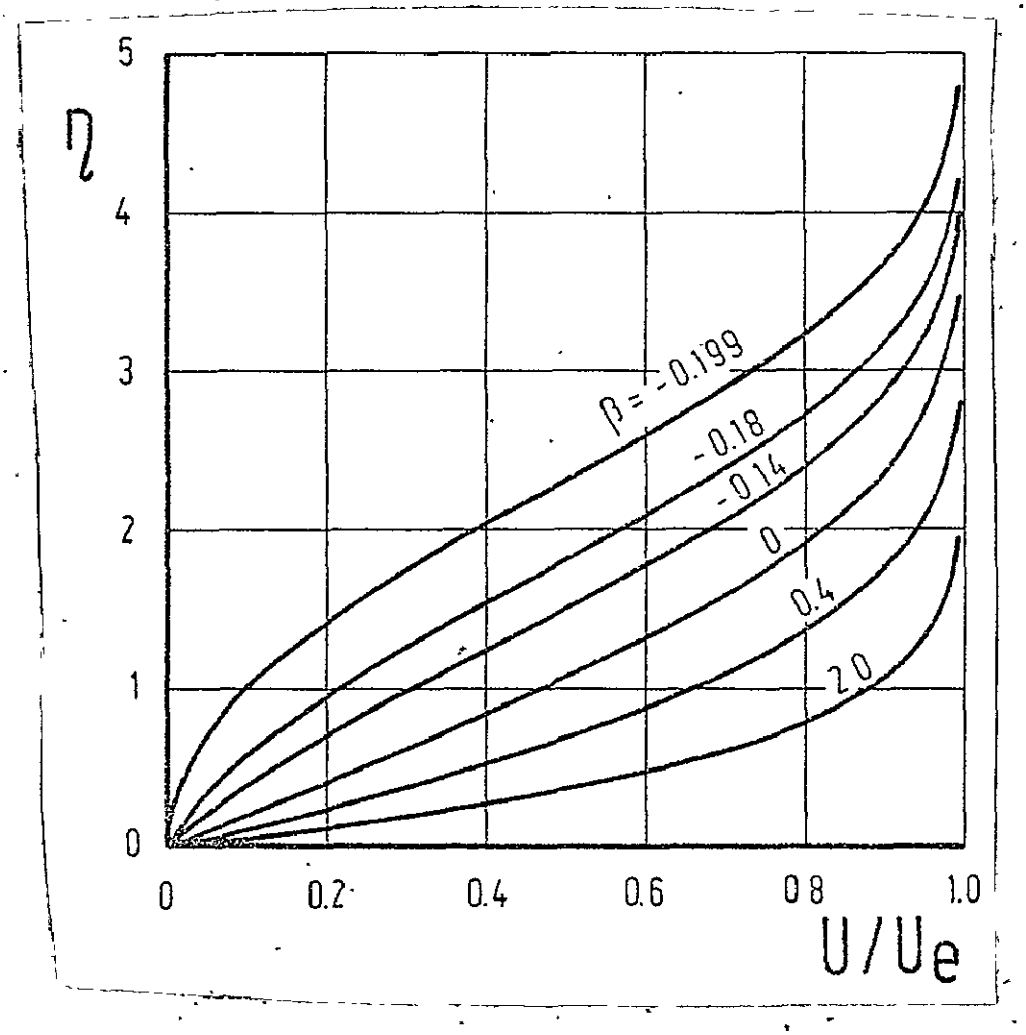

Fig. 18. Velocity profiles (laminar) in the main flow direction

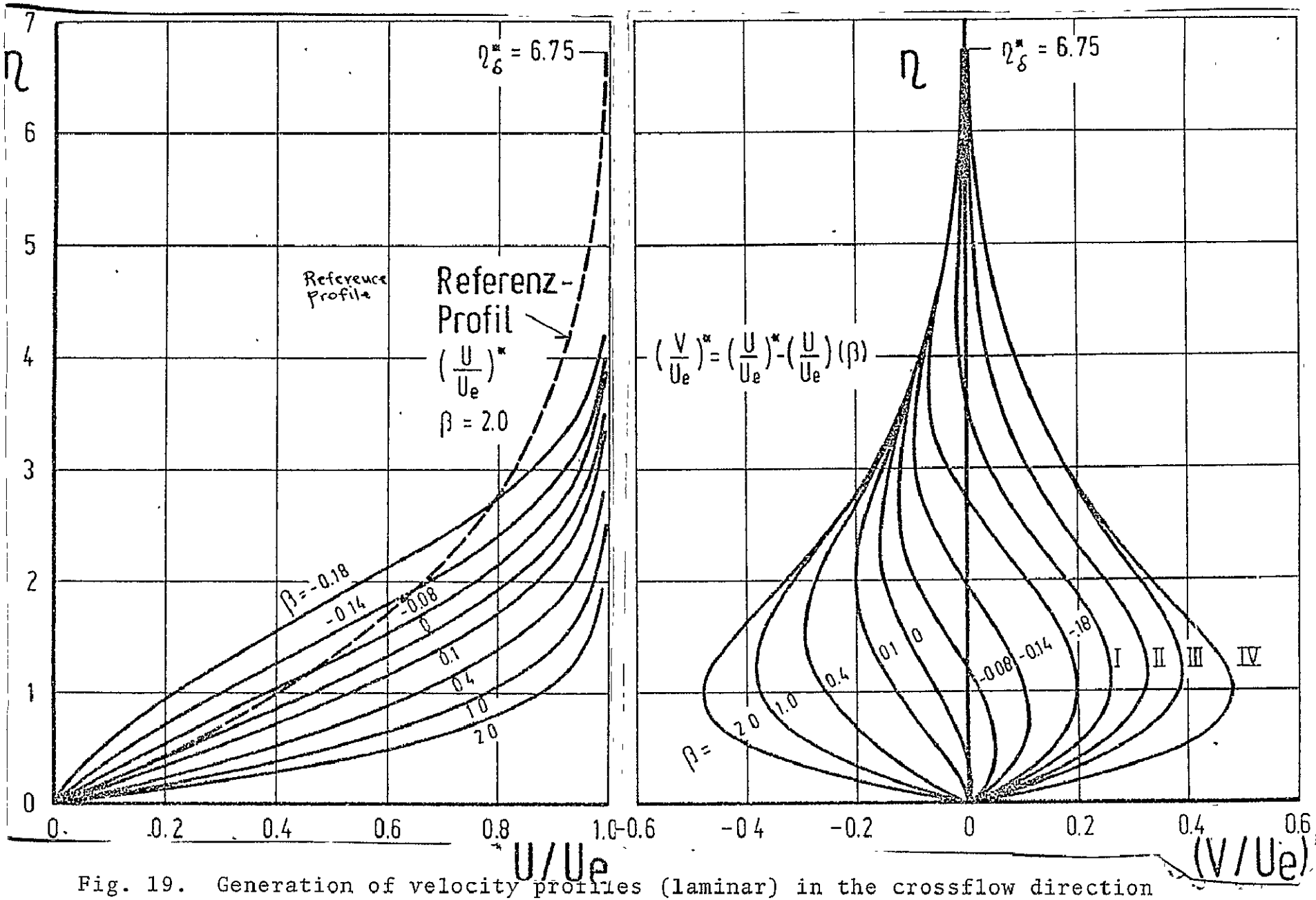

Fig. 19. Generation of velocity profiles (laminar) in the crossflow direction

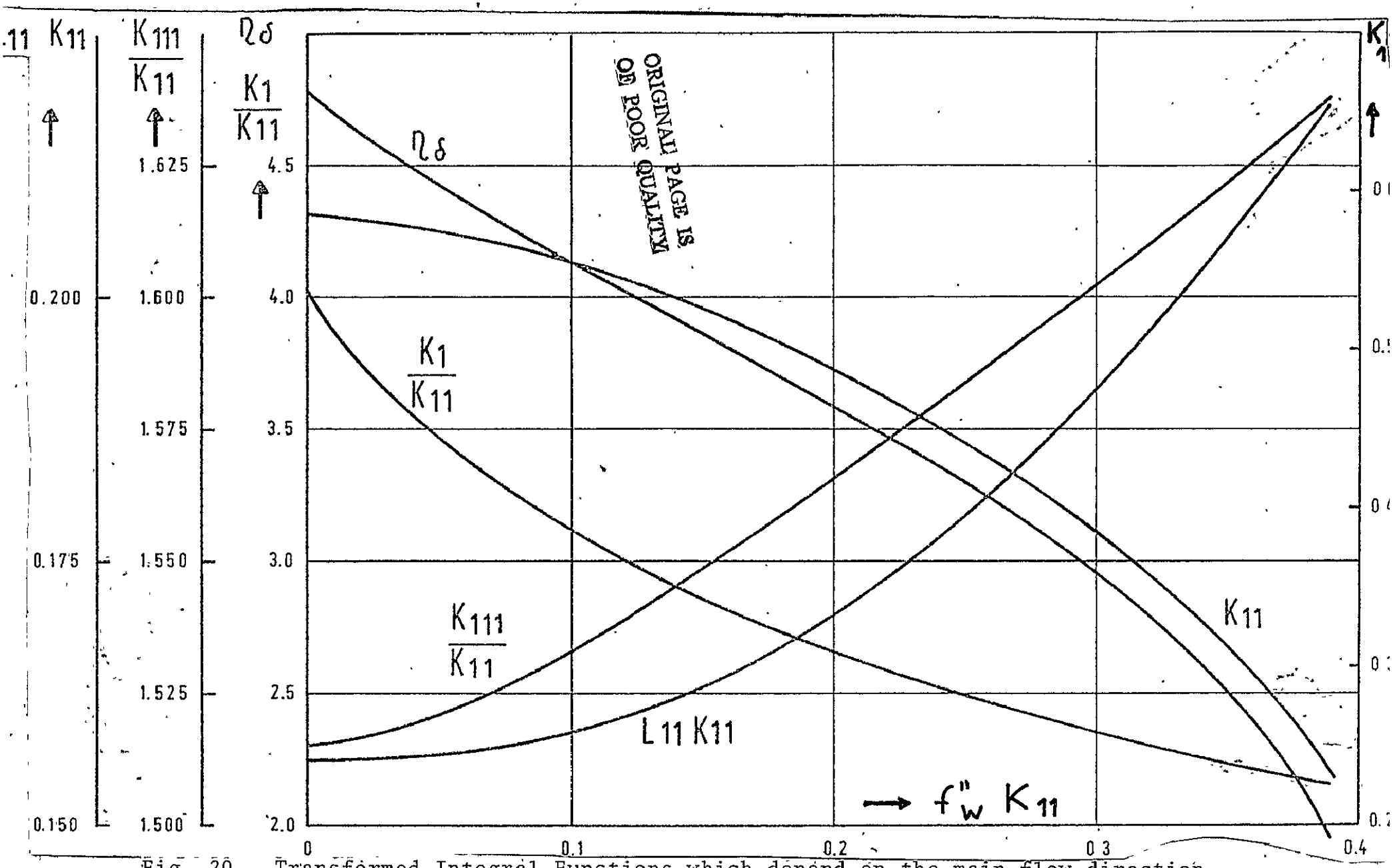

Fig. 20. Transformed Integral Functions which depend on the main flow direction

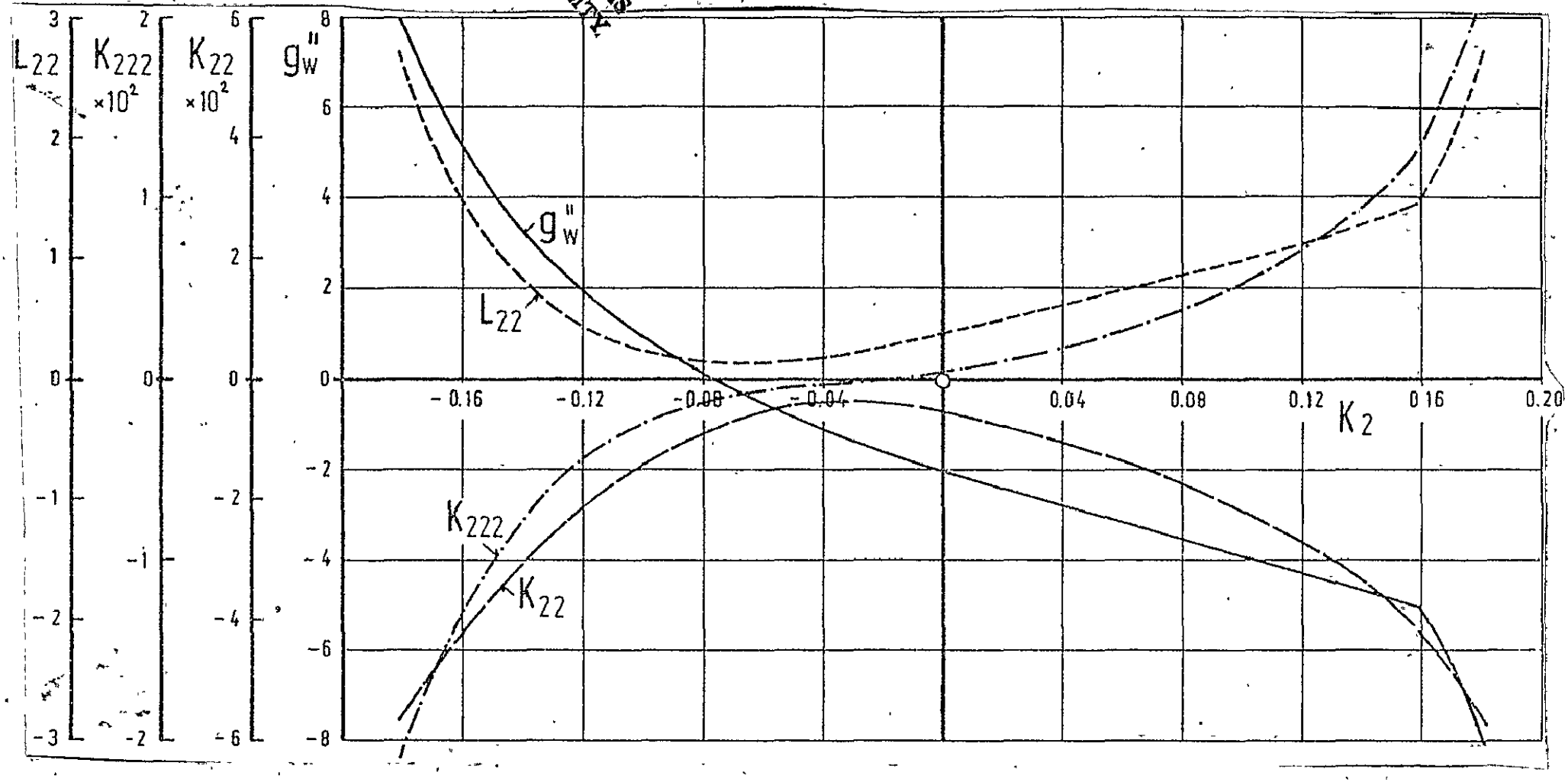

Fig. 21. Transformed integral functions, which depend on profiles in the cross-flow direction

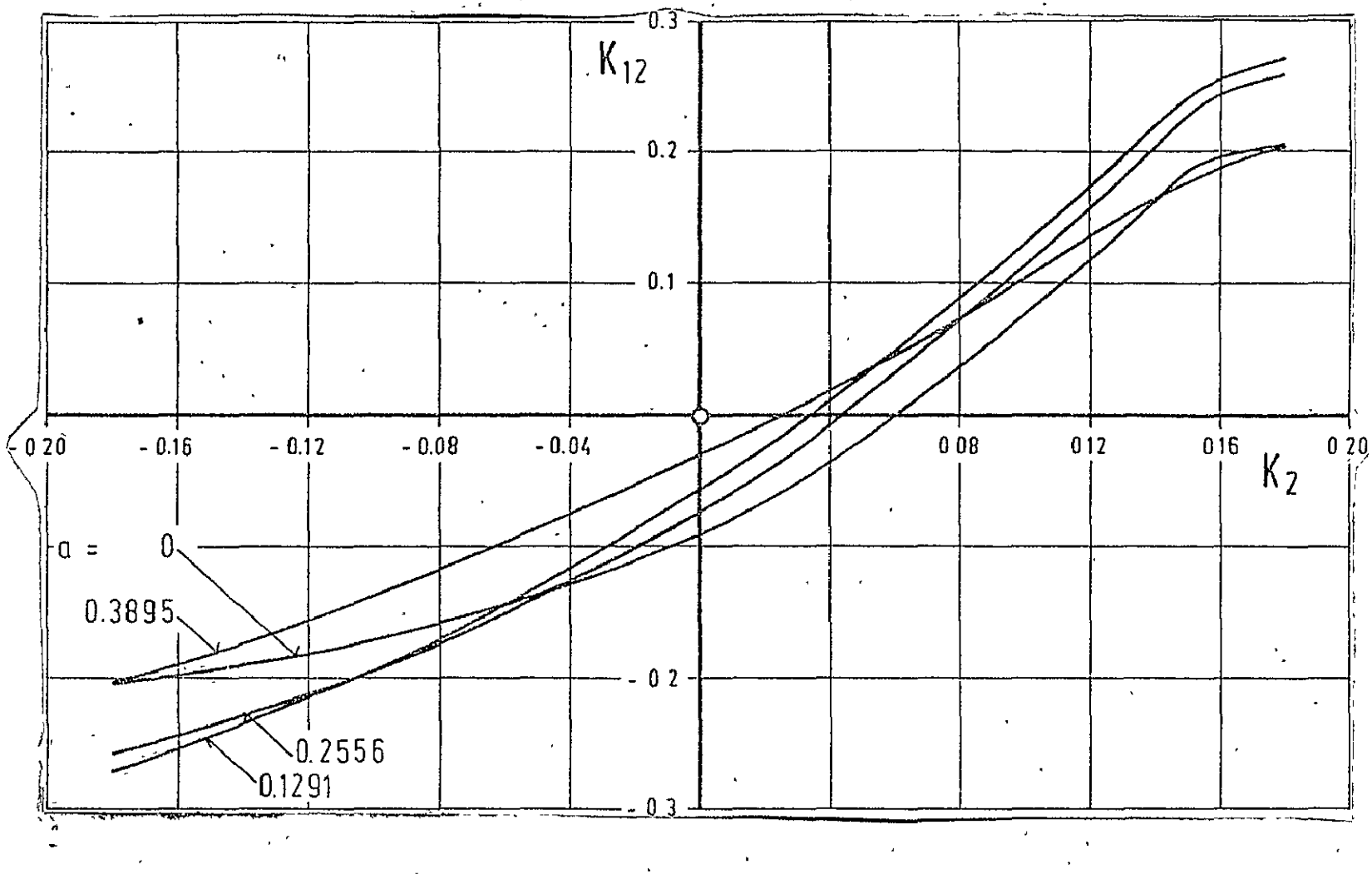

Fig. 22. Moment loss thickness K_{12} over displacement thickness K_2 of the cross-flow profile (transformed functions)

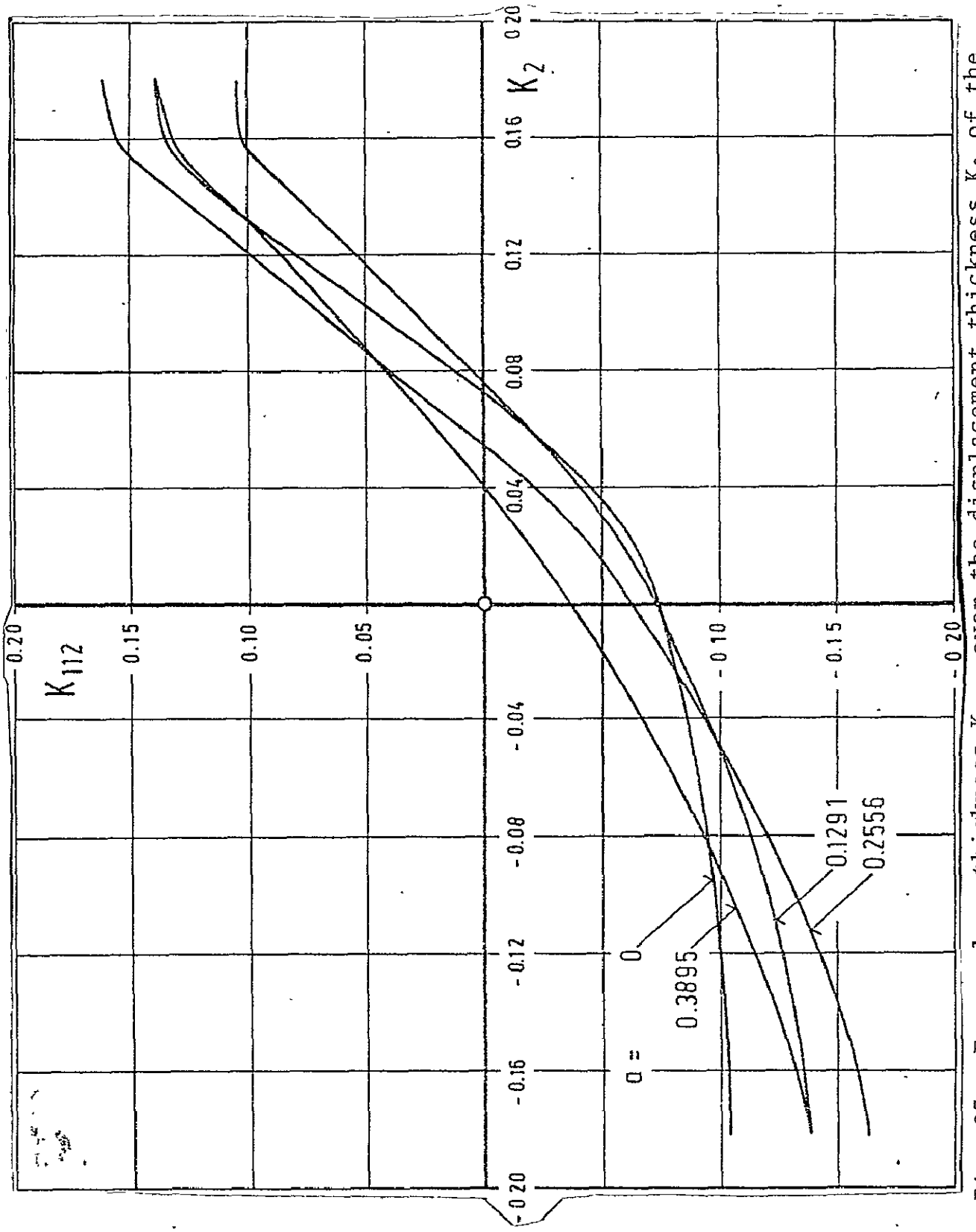

Fig. 23.. Energy loss thickness K_{112} over the displacement thickness K_2 of the crossflow profiles (transformed functions)

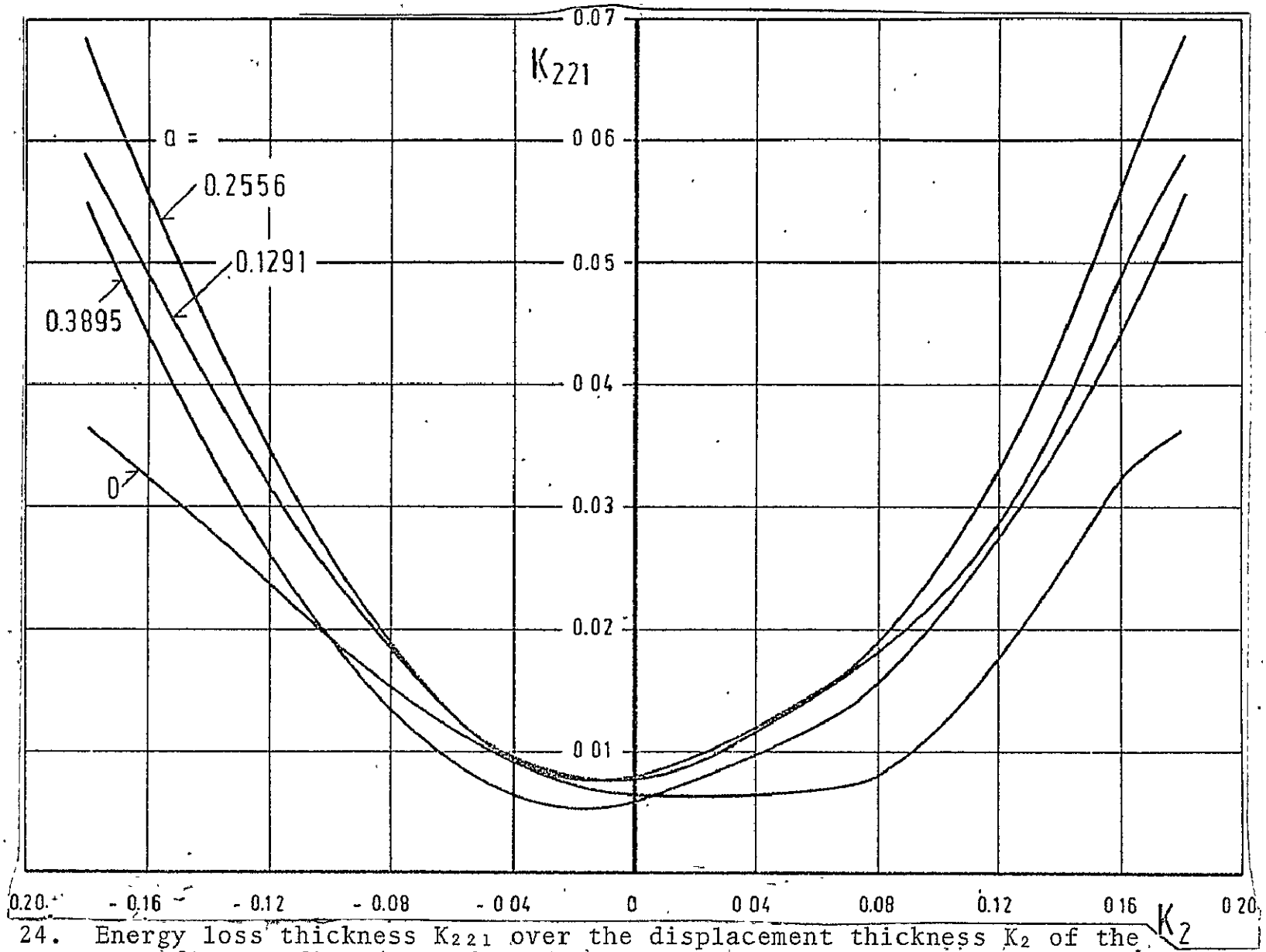

Fig. 24. Energy loss thickness K_{221} over the displacement thickness K_2 of the crossflow profile (transformed functions)

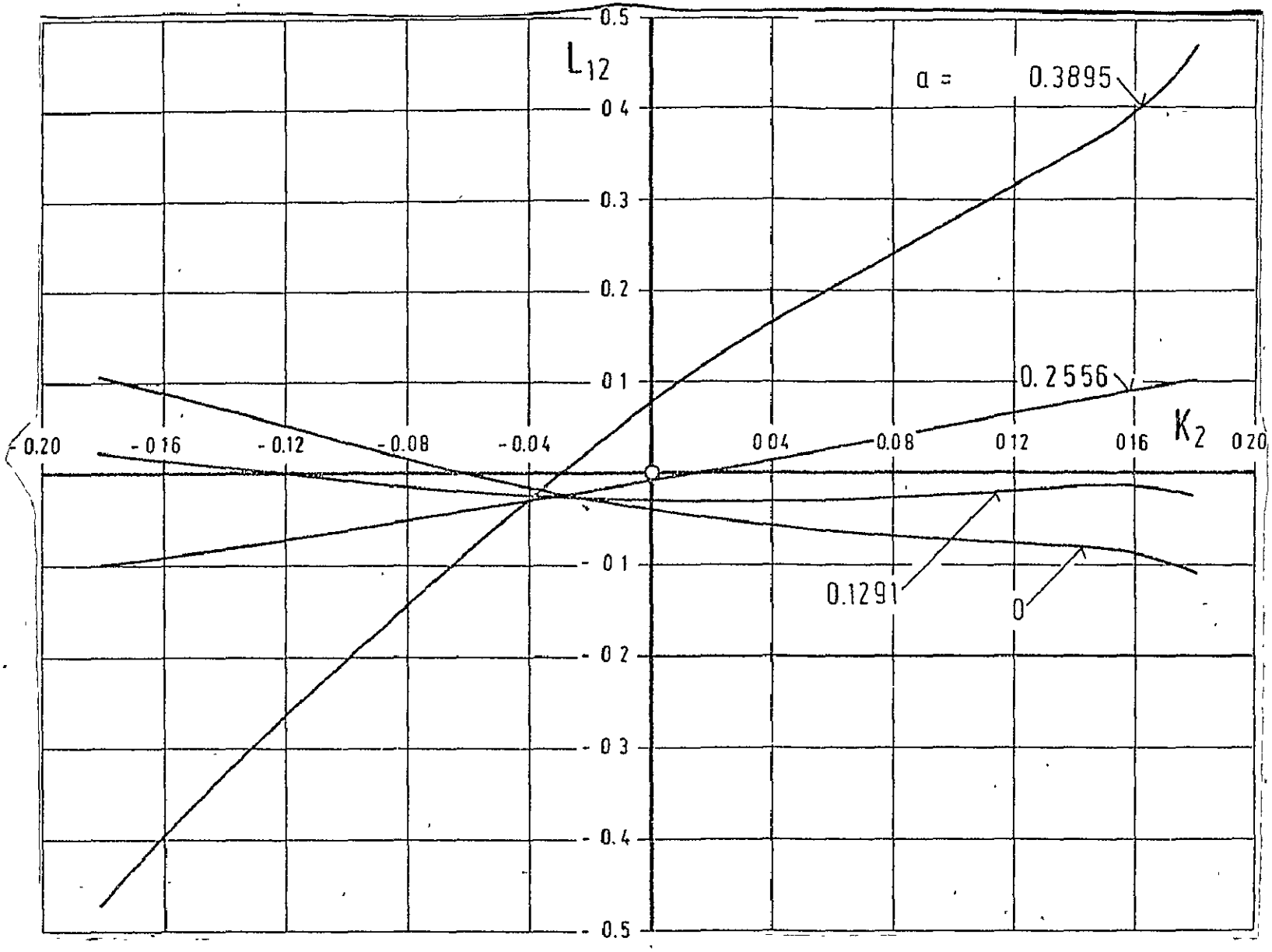

Fig. 25. Dissipation integral L_{12} over the displacement thickness K_2 of the crossflow profile (transformed functions)

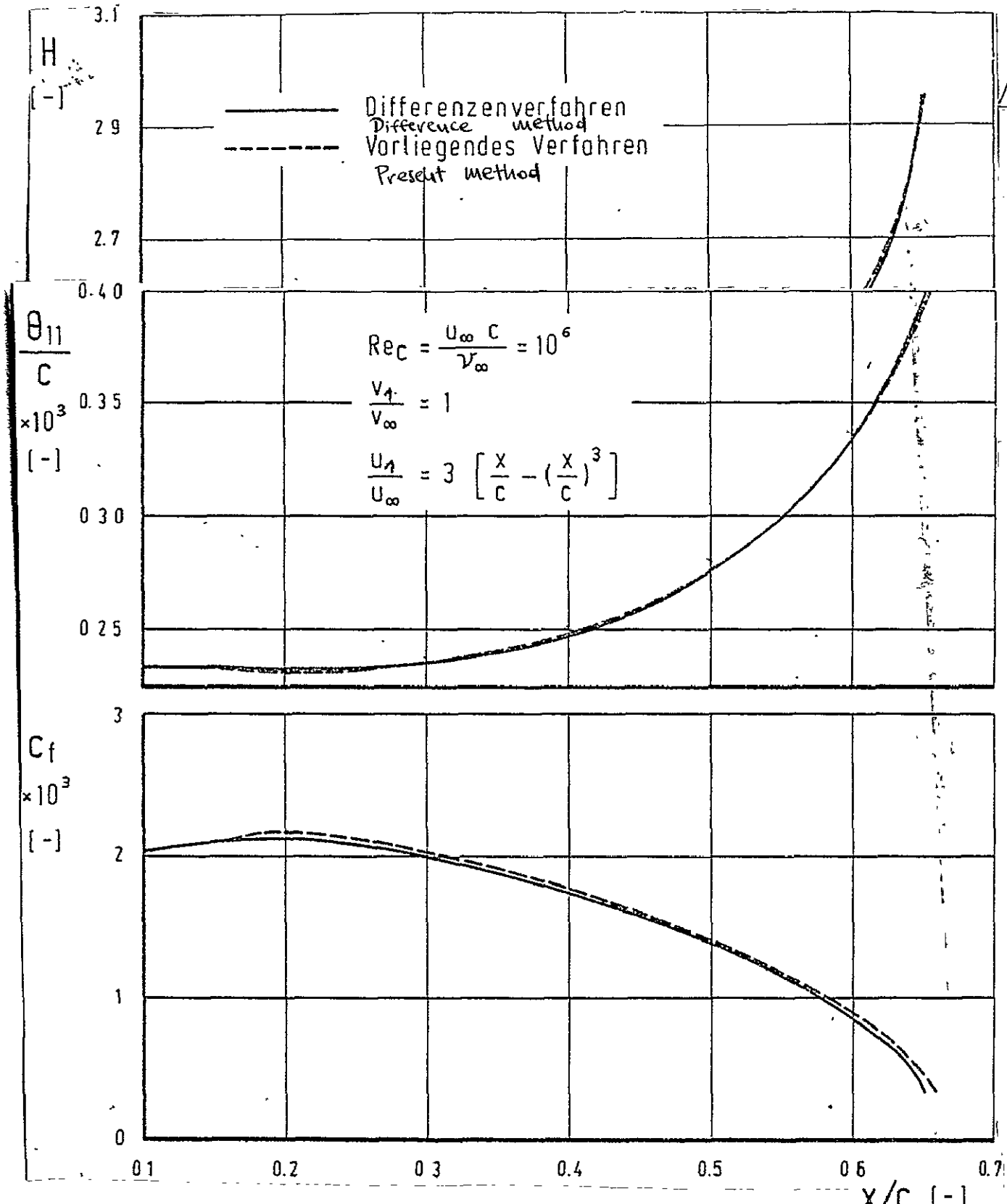

Fig. 26. Comparison of the results of calculation according to a difference method with the present method (Laminar boundary layer, test case 1)

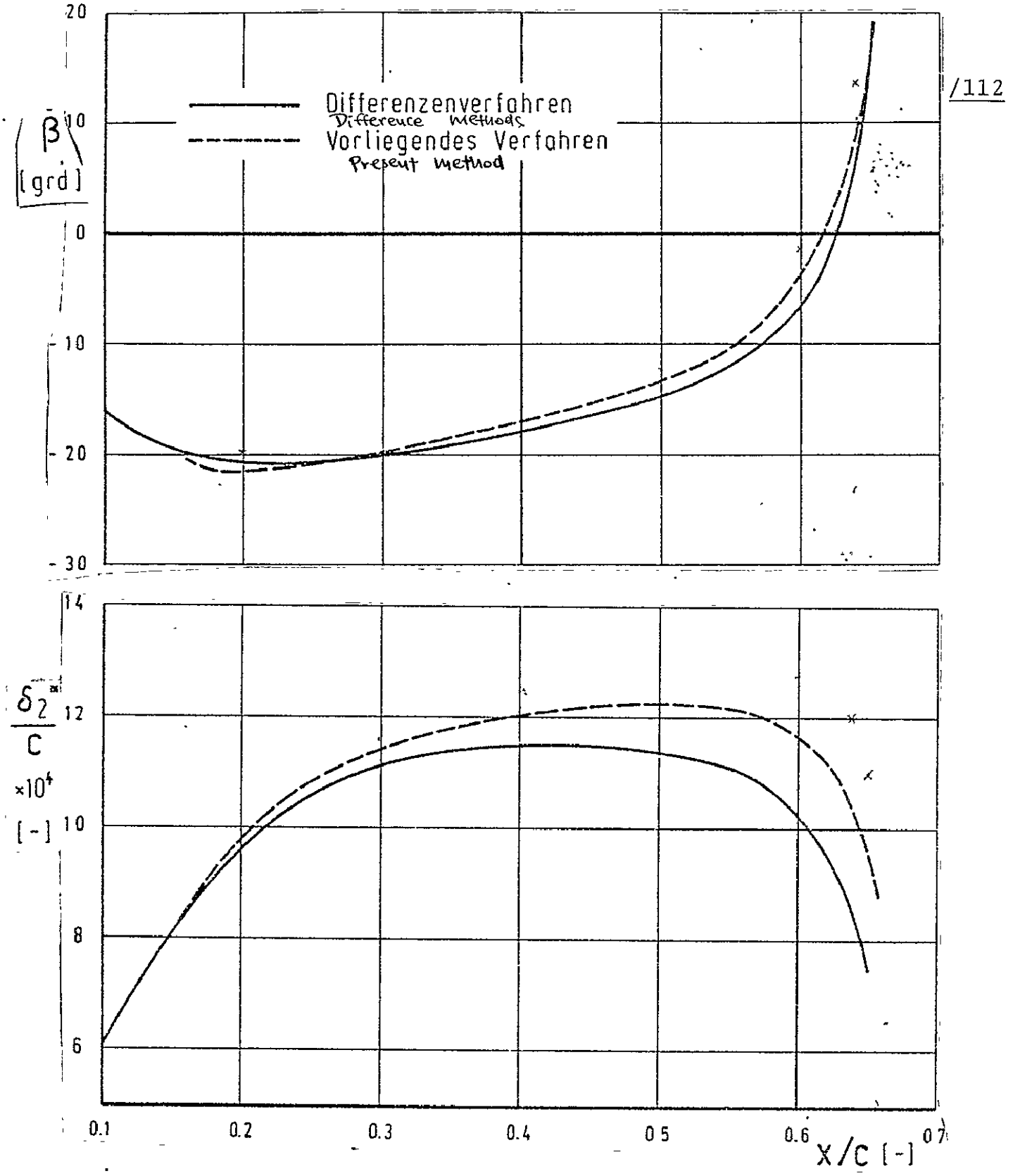

/112

Fig. 26. Continuation

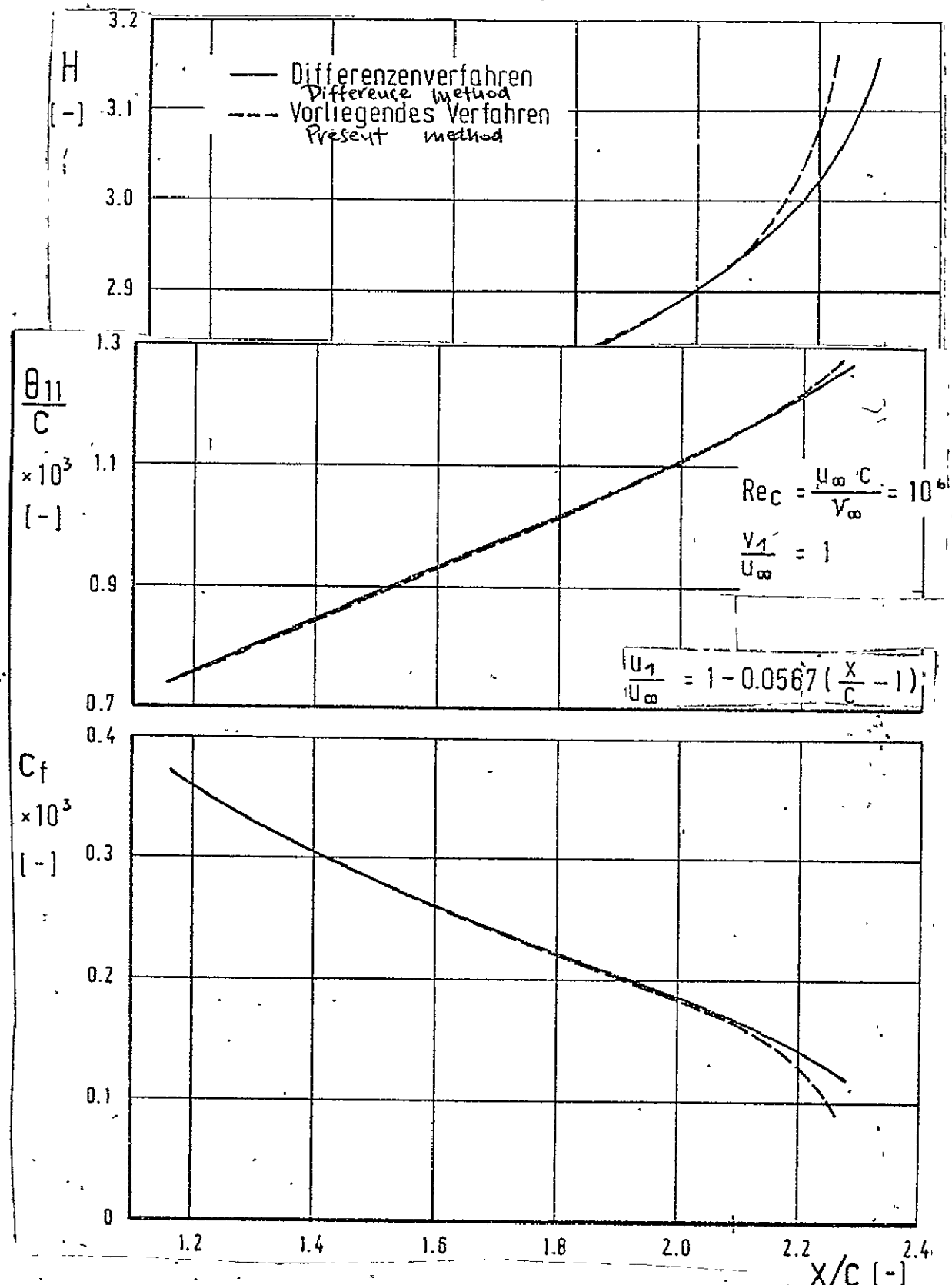

Fig. 27. Comparison of the calculation results of a difference method with the present method
(Laminar boundary layer, test case 2)

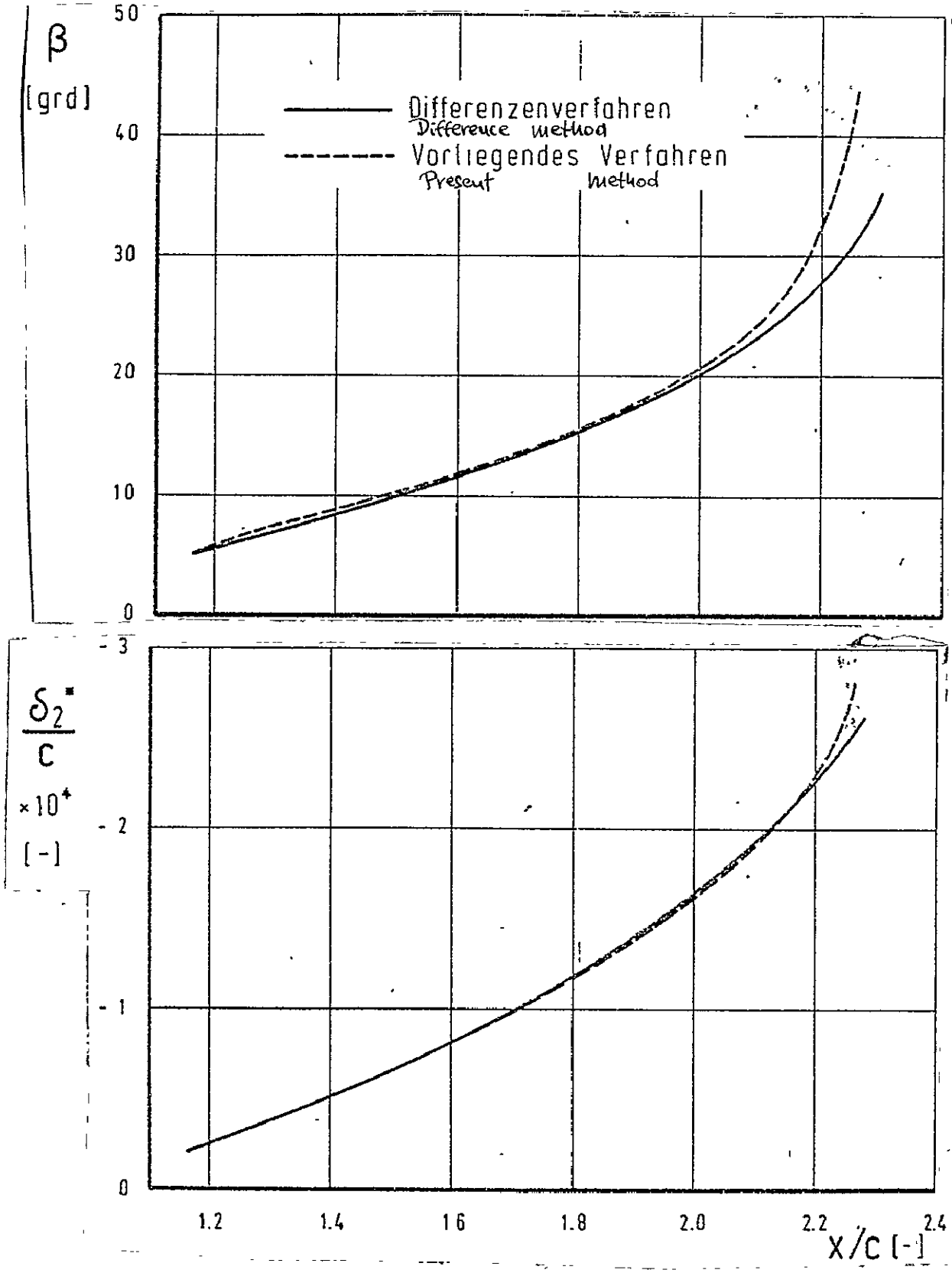

Fig. 27. Continuation

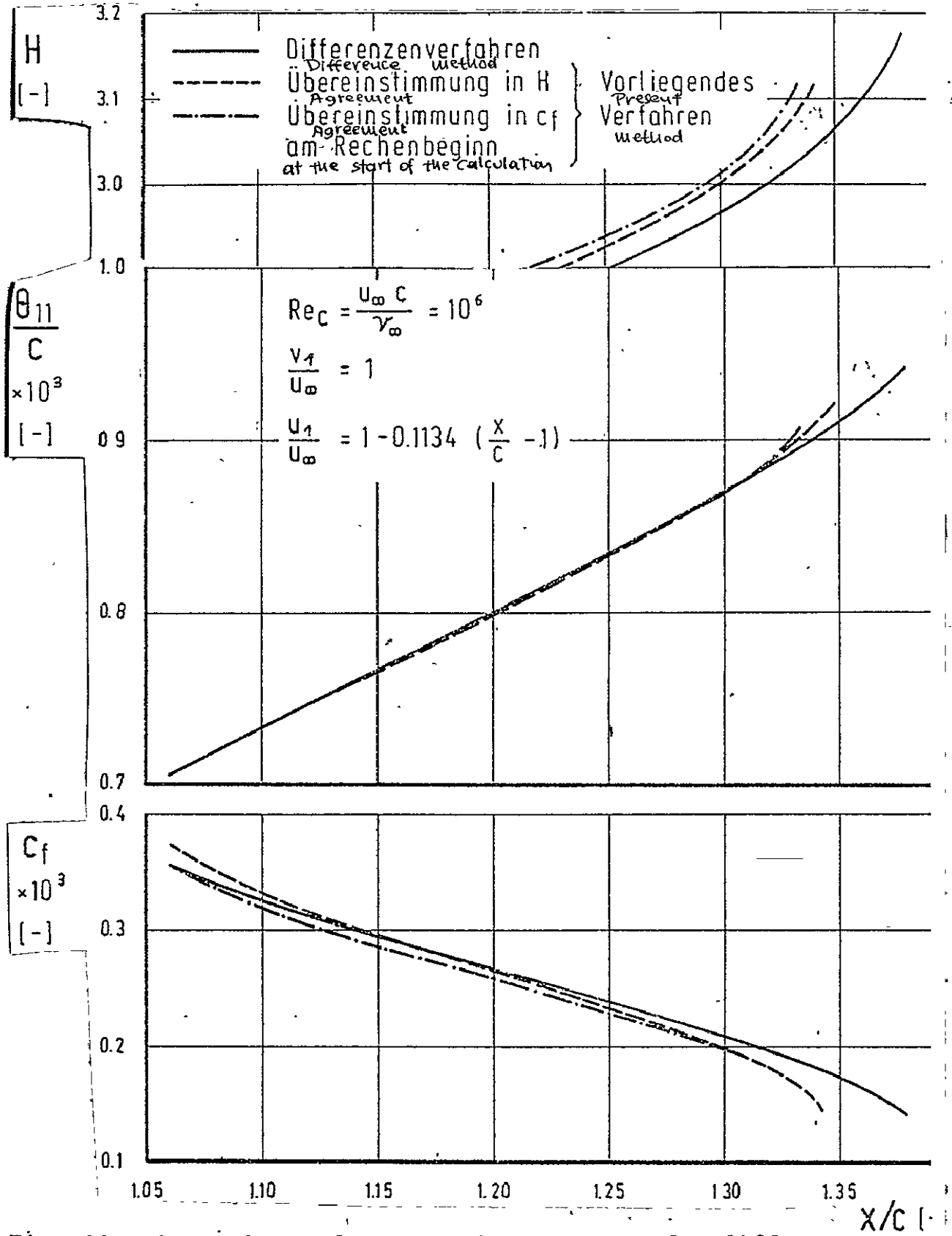

Fig. 28. Comparison of calculation results of a difference method with the present integral method (Laminar boundary layer, test case 3)

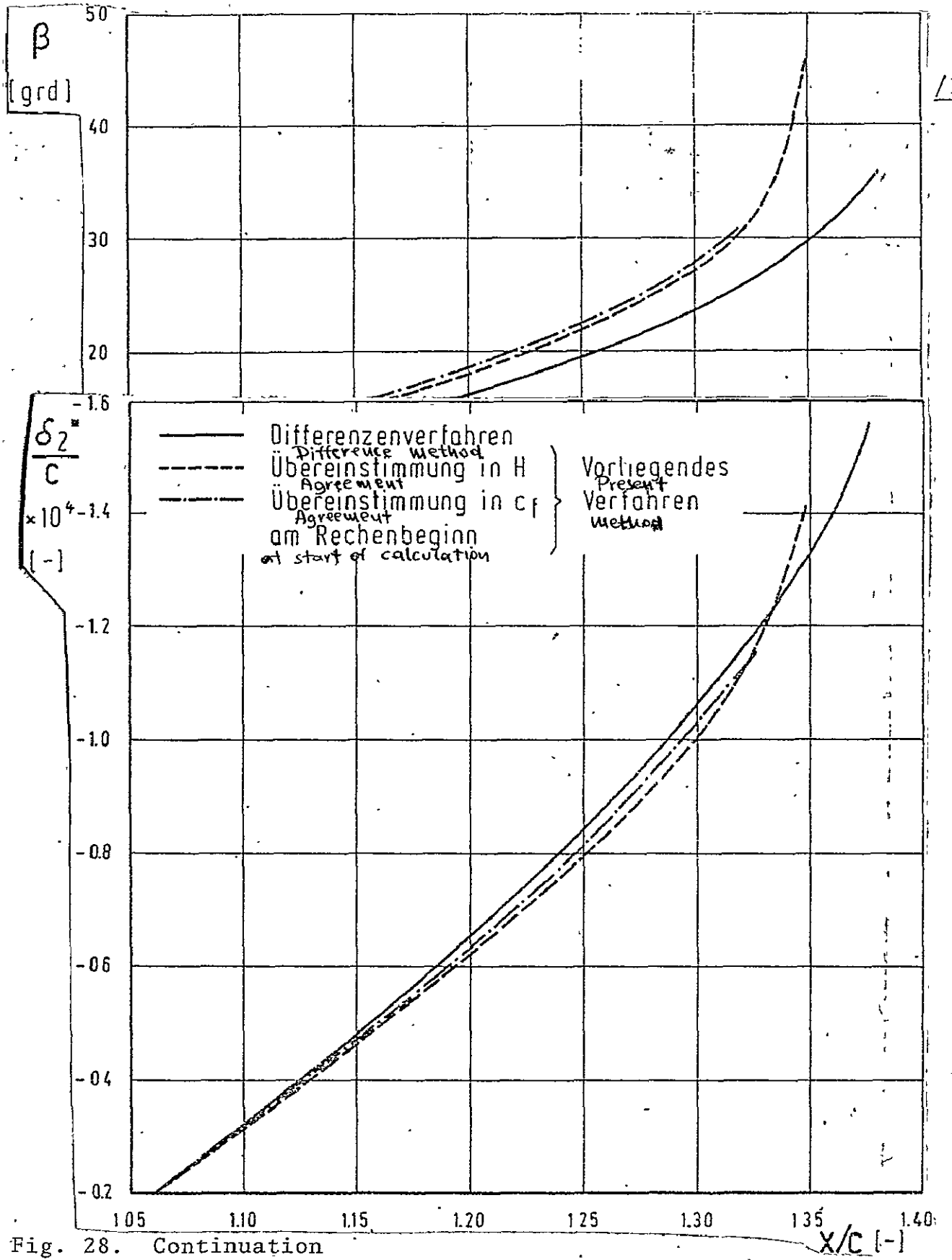

Fig. 28. Continuation

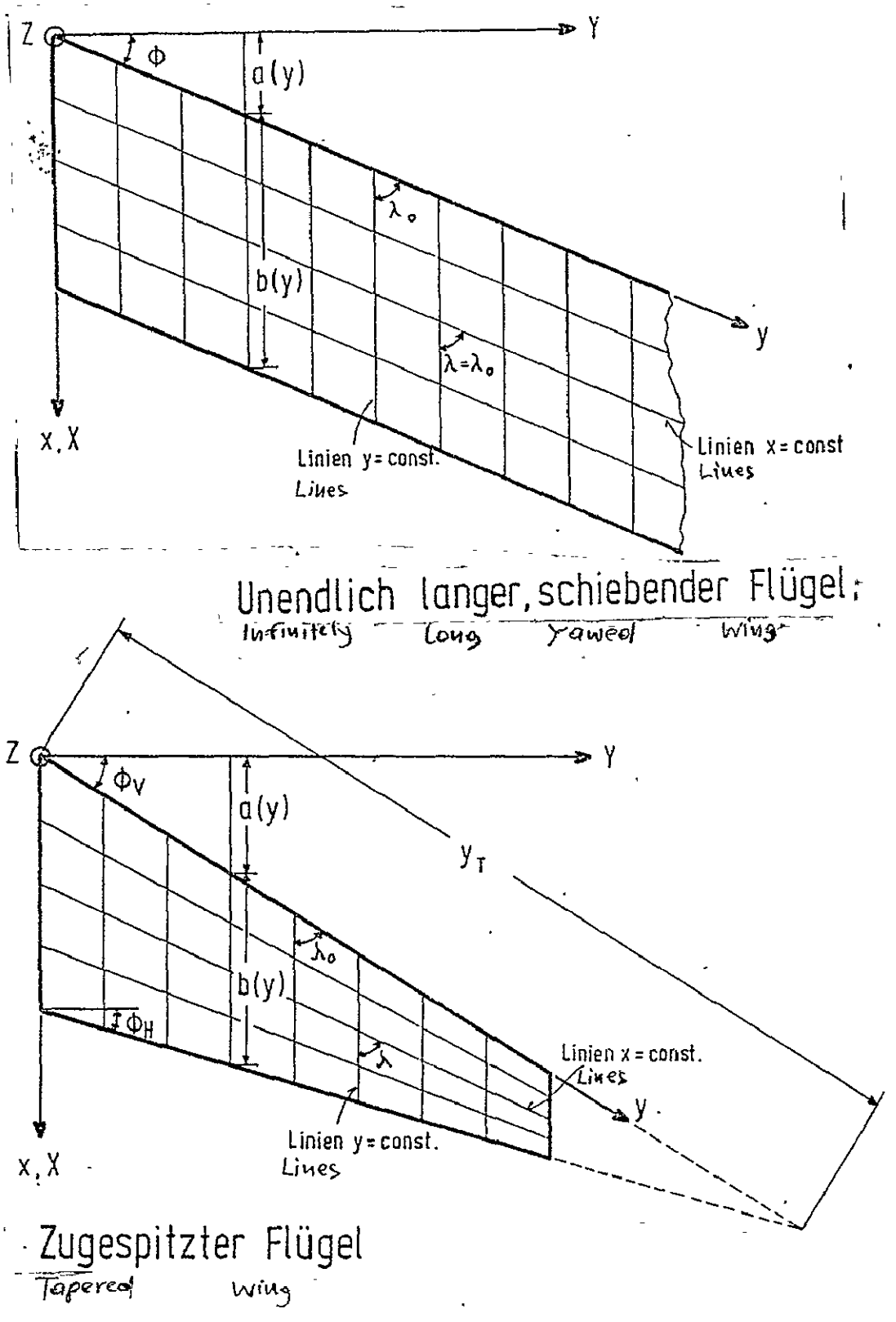

Fig. 29. Coordinate systems at tapered and untapered wings

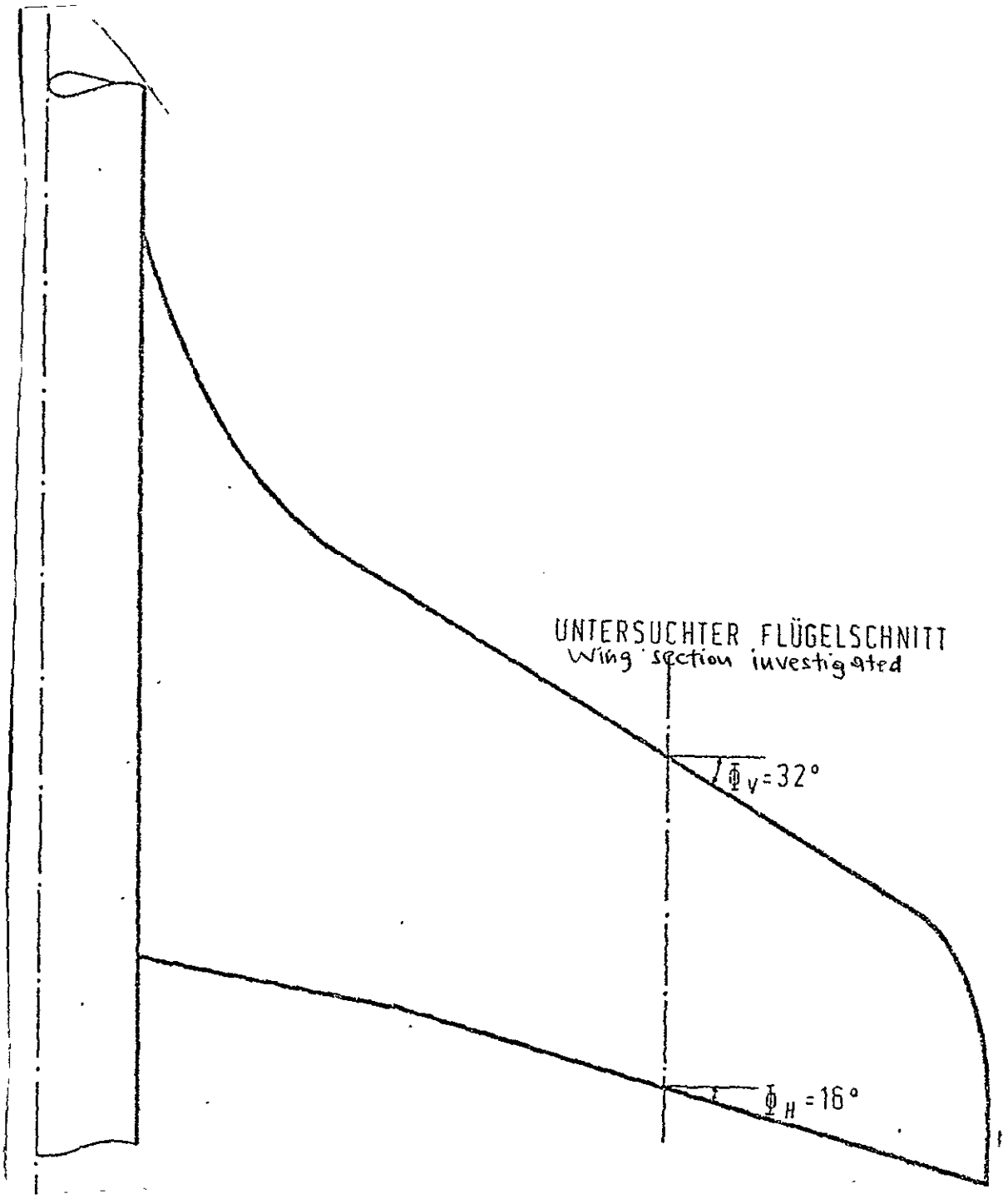

Fig. 30. Top view of the wing

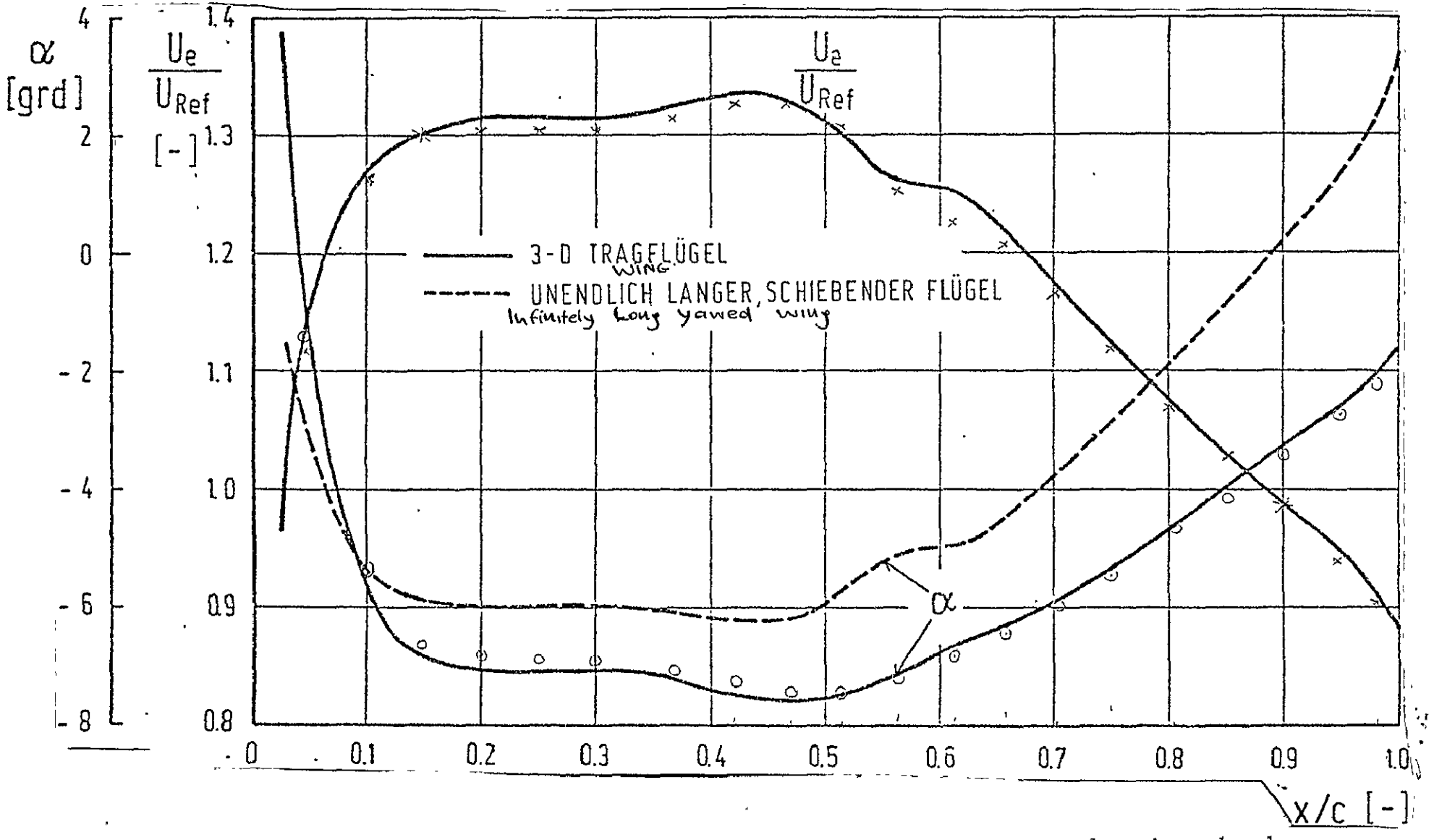

Fig. 31. Distribution of velocity U_e/U_{Ref} and of the angle α over the wing chord

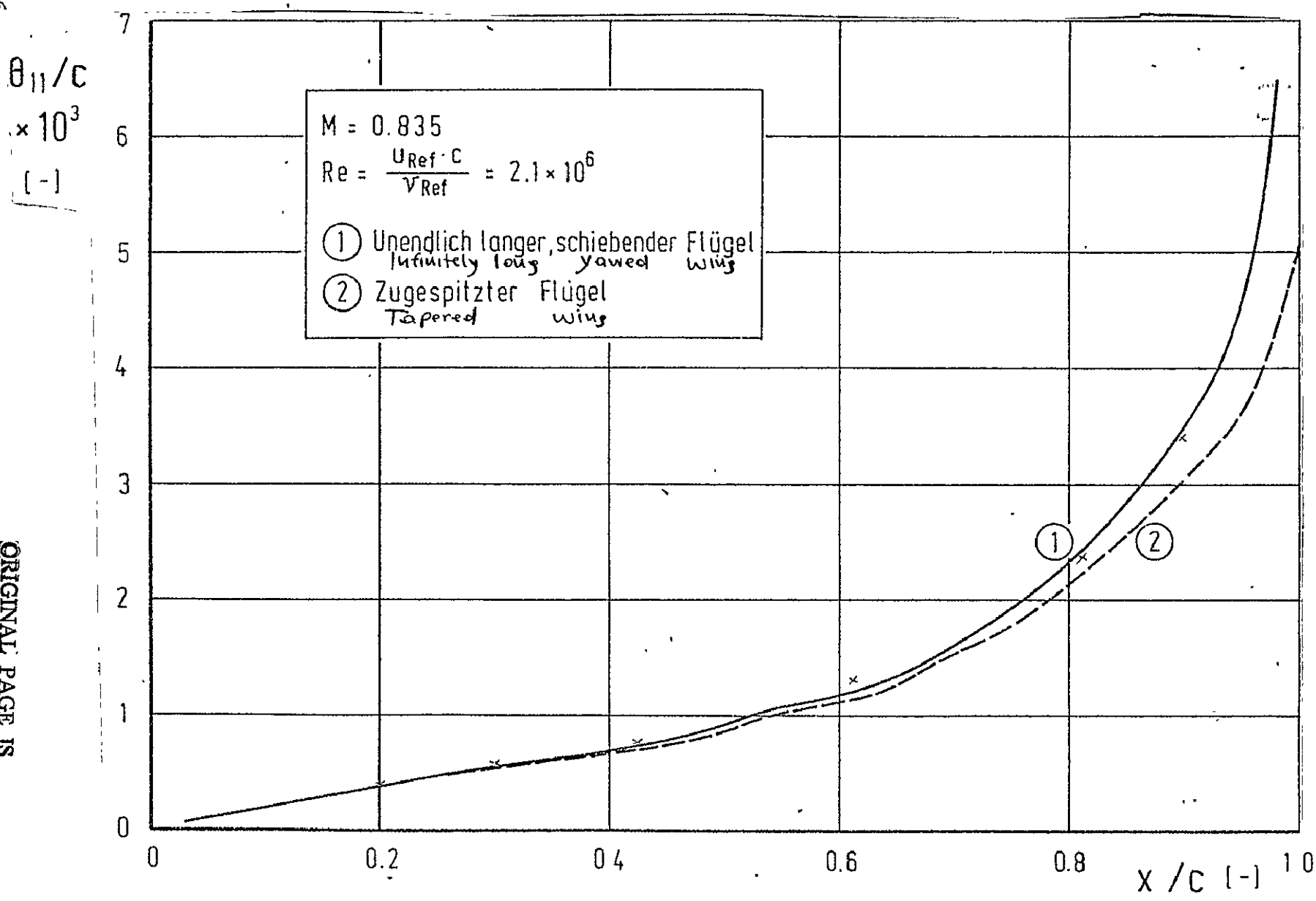

Fig. 32. Trace of the moment loss thickness over the wing chord

/120

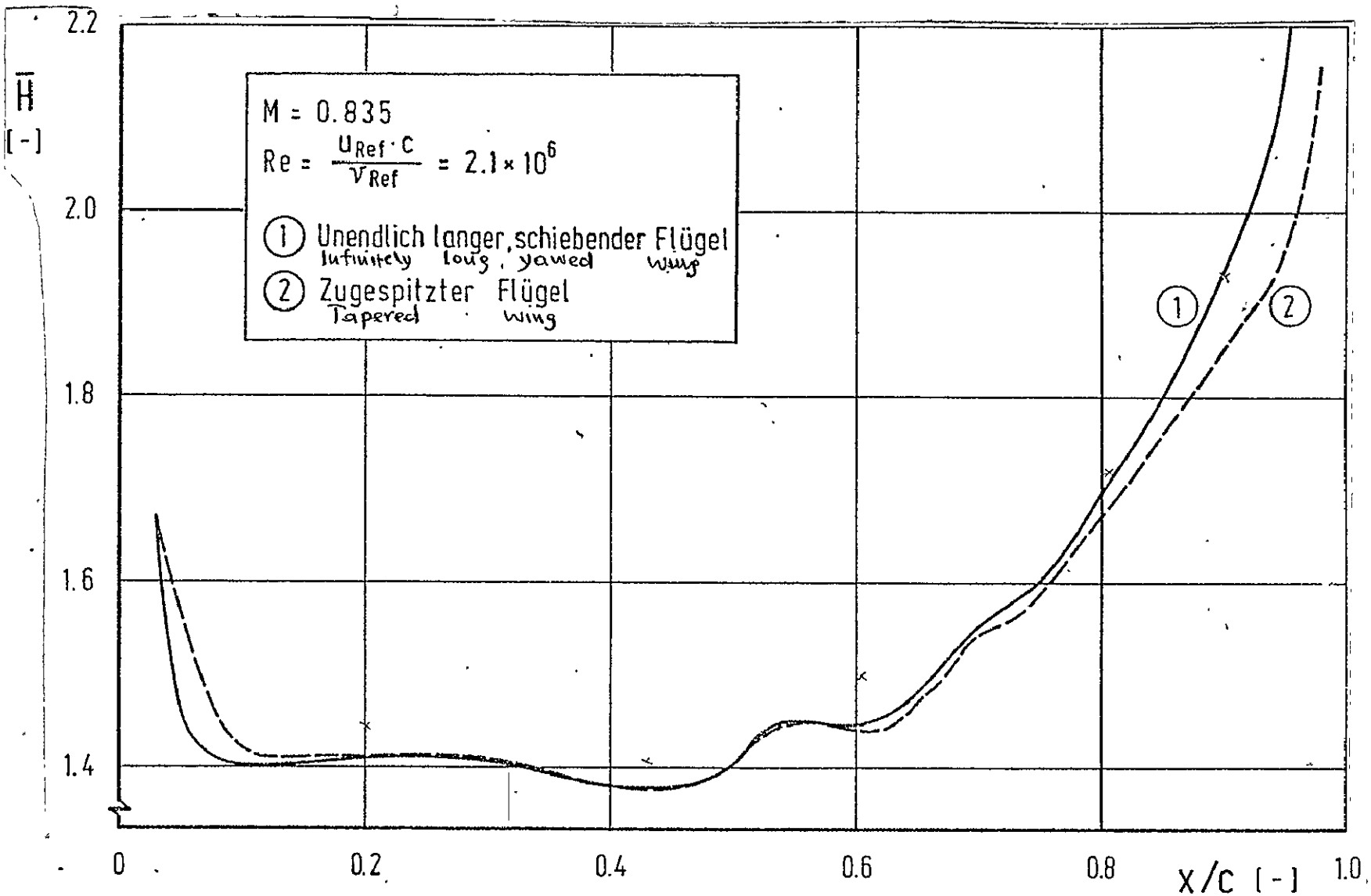

Fig. 33. Trace of the form parameter over the wing chord

/121

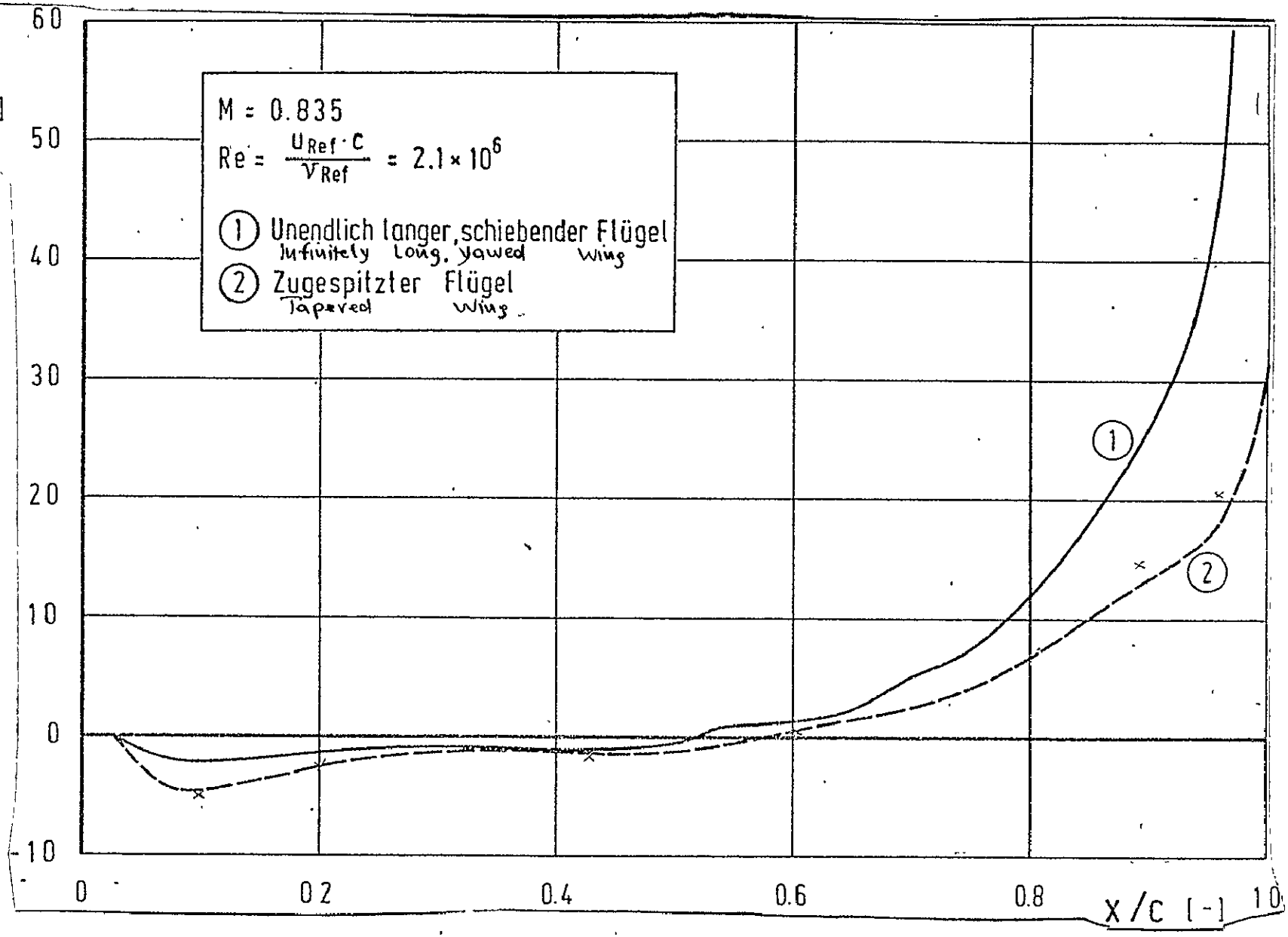

Fig. 34. Trace of the wallflow line angle over the wing chord

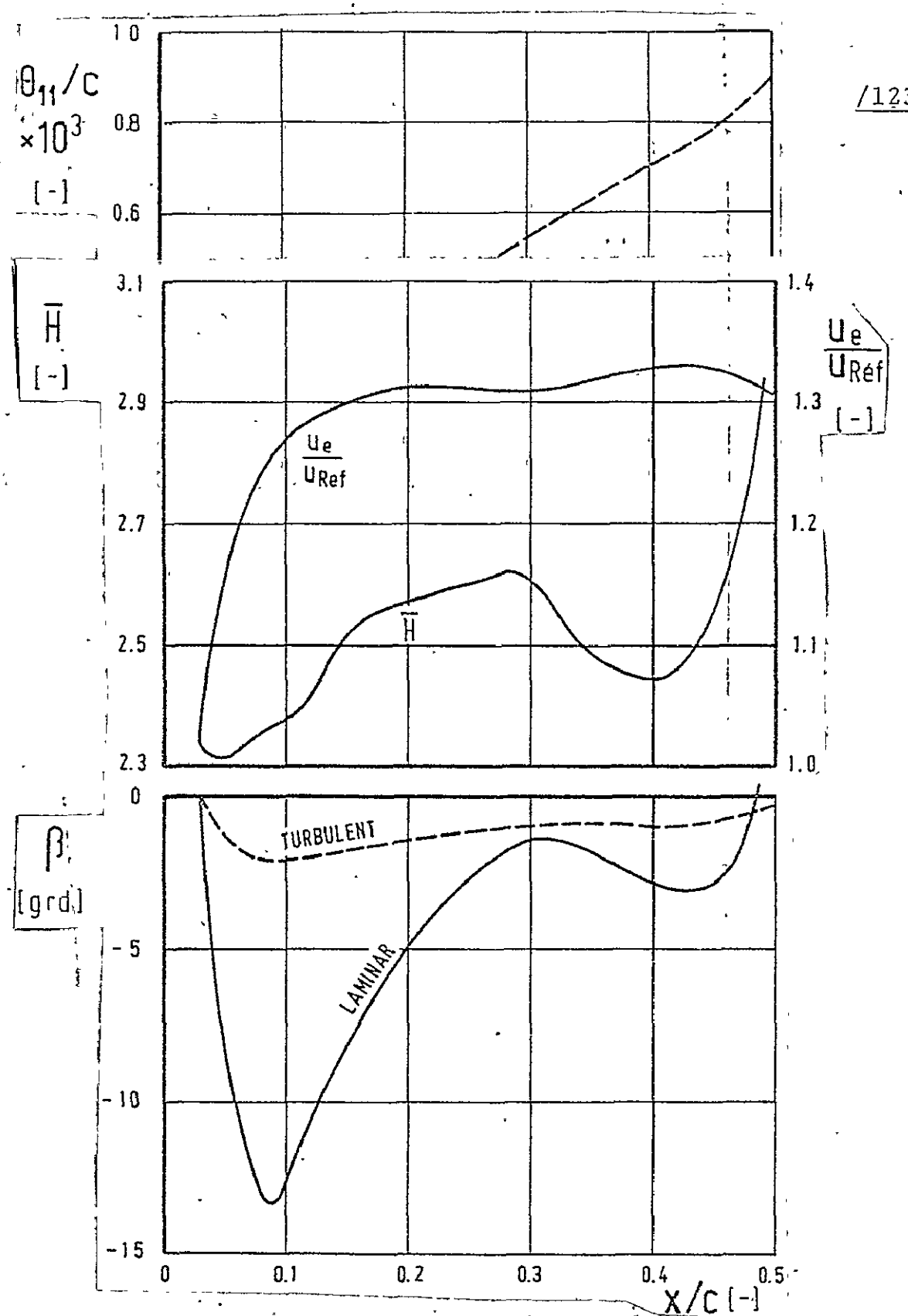

Fig. 35. Comparison of the laminar and turbulent boundary layer development at an infinitely long, yawed wing

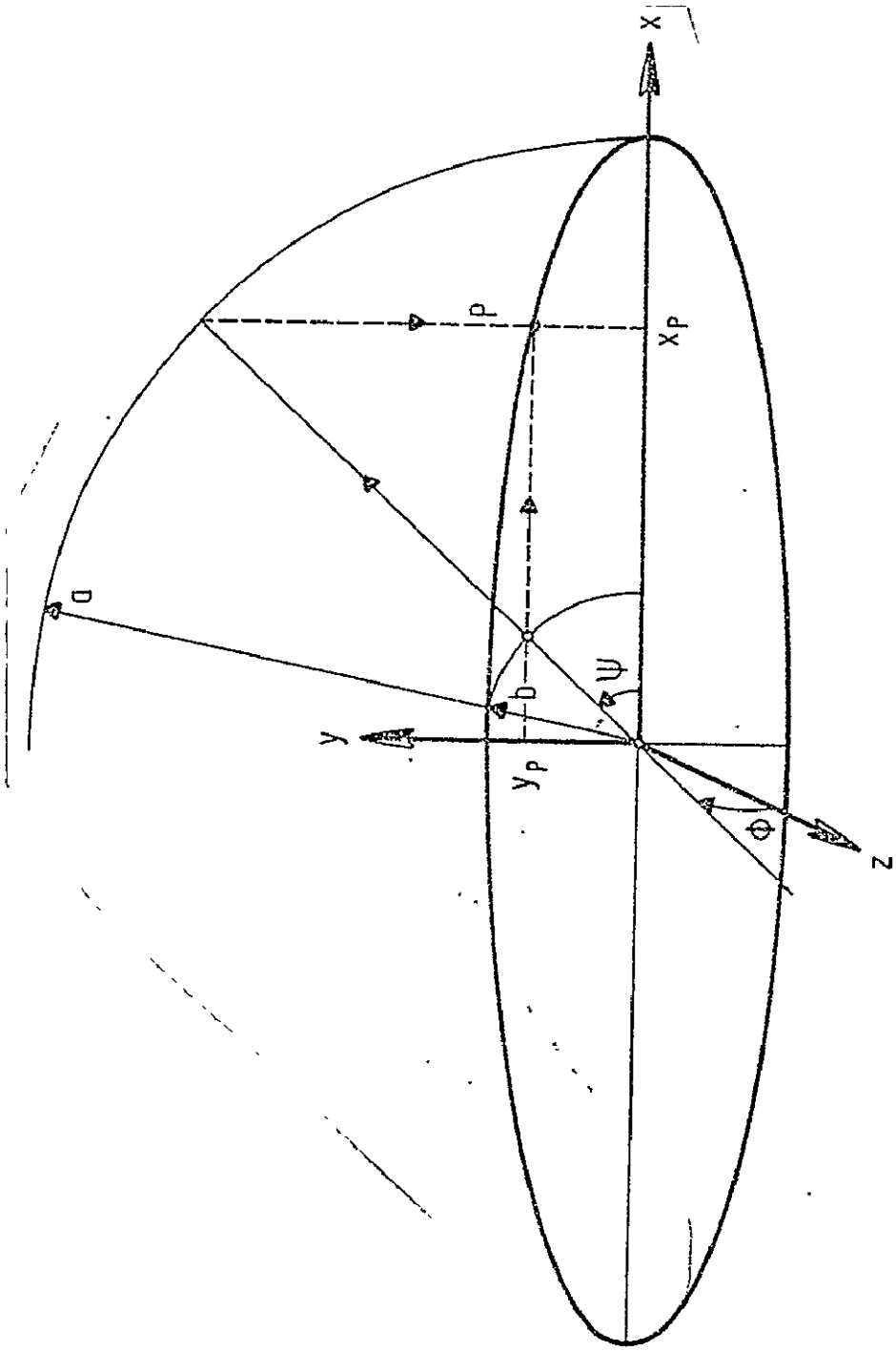

Fig. 36. Definition of the coordinates ϕ and ψ for the revolution ellipsoid

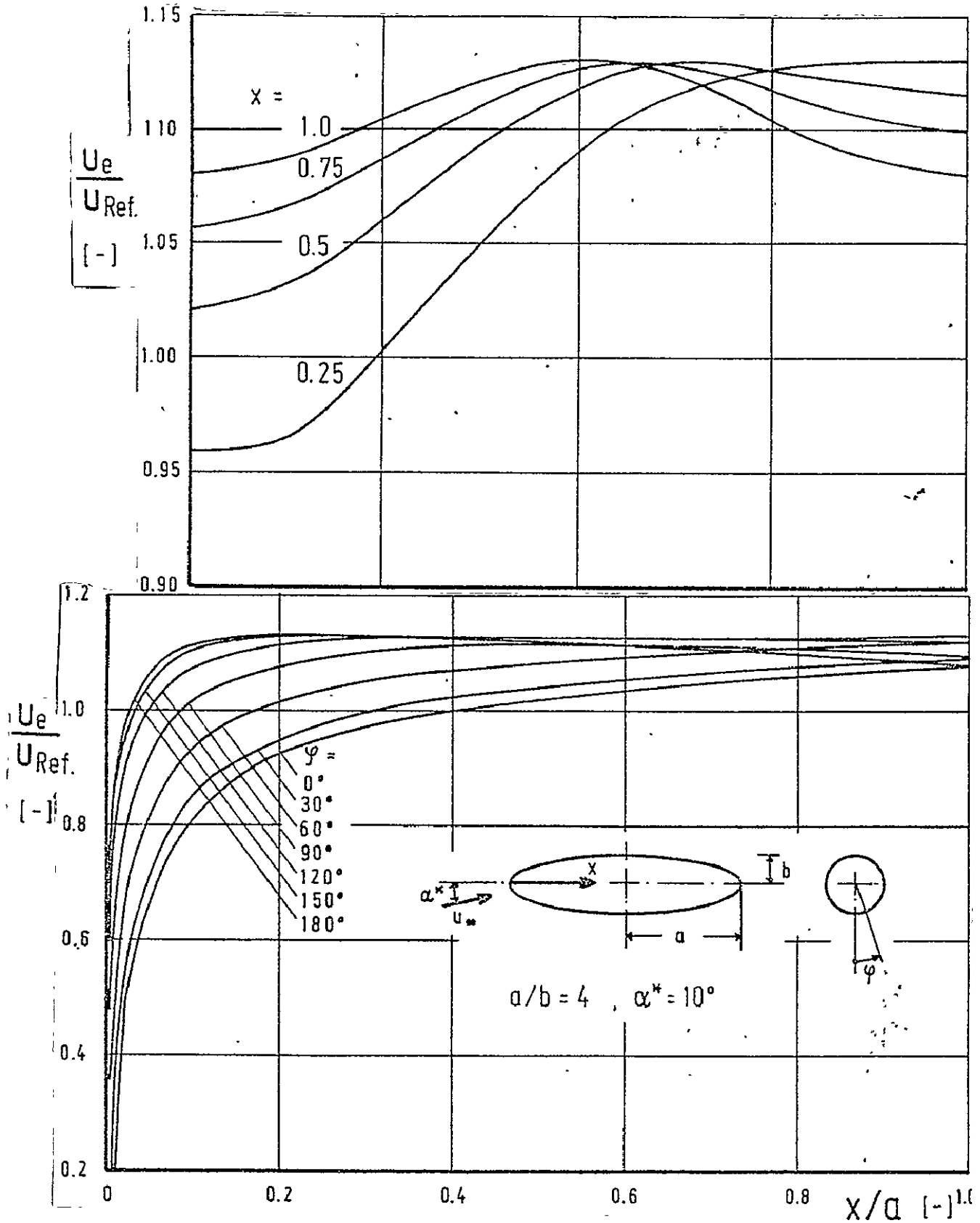

Fig. 37. Velocity distribution of the potential flow for the incident revolution ellipsoid

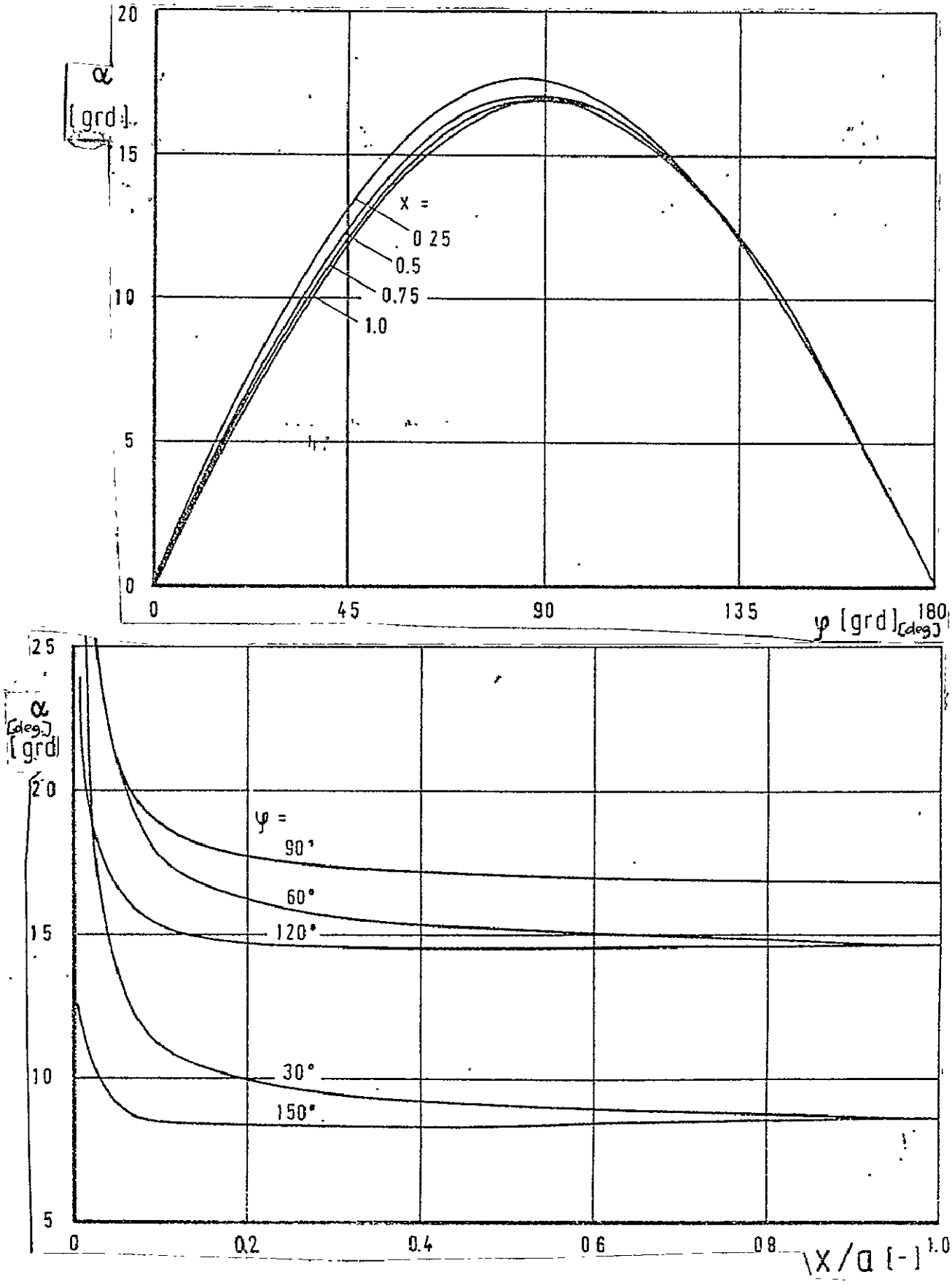

Fig. 38. Distribution of the angle α at the incident revolution ellipsoid

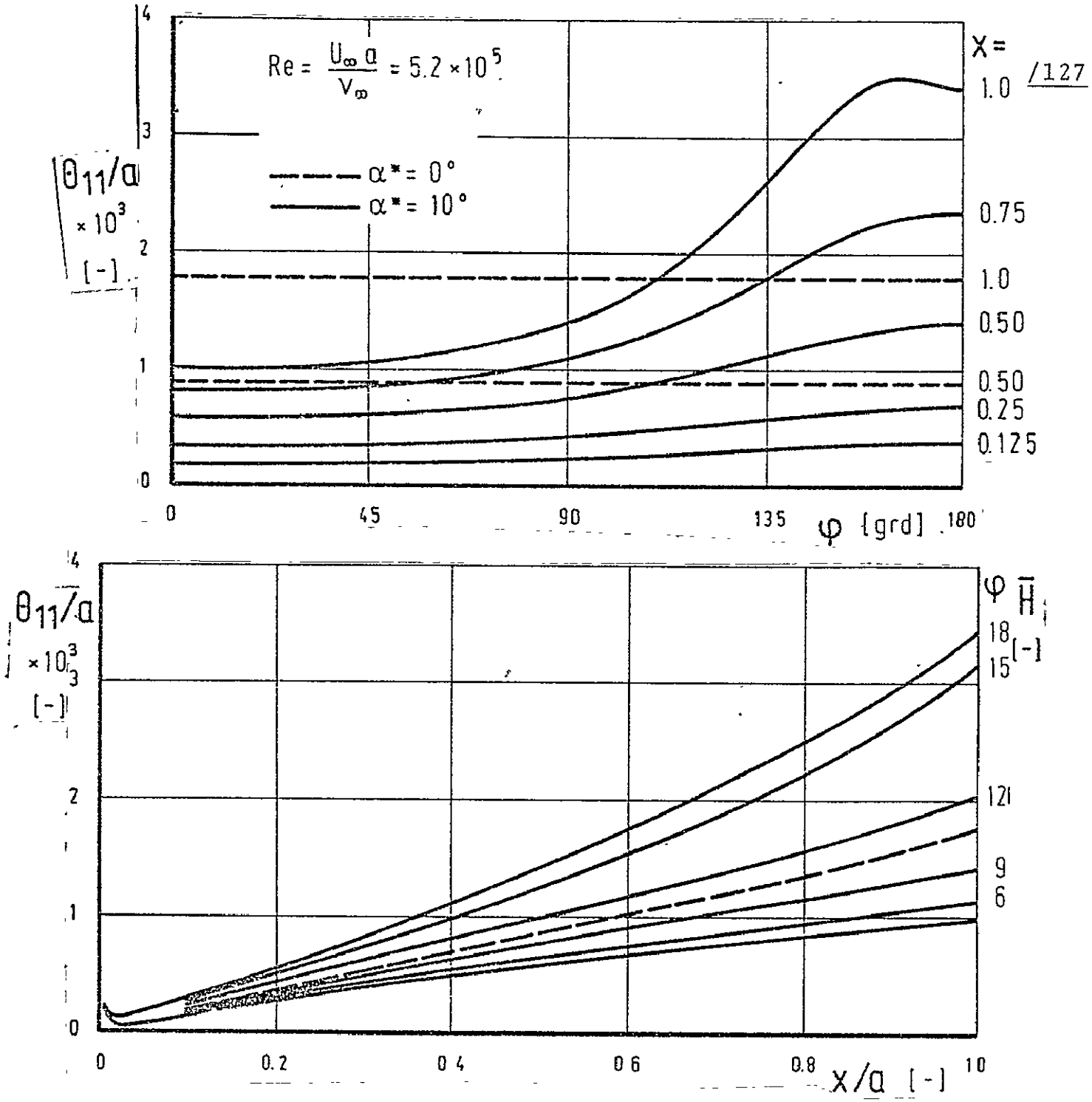

Fig. 39. Distribution of the moment loss thickness θ_{11} for the incident and nonincident revolution ellipsoid (turbulent boundary layer).

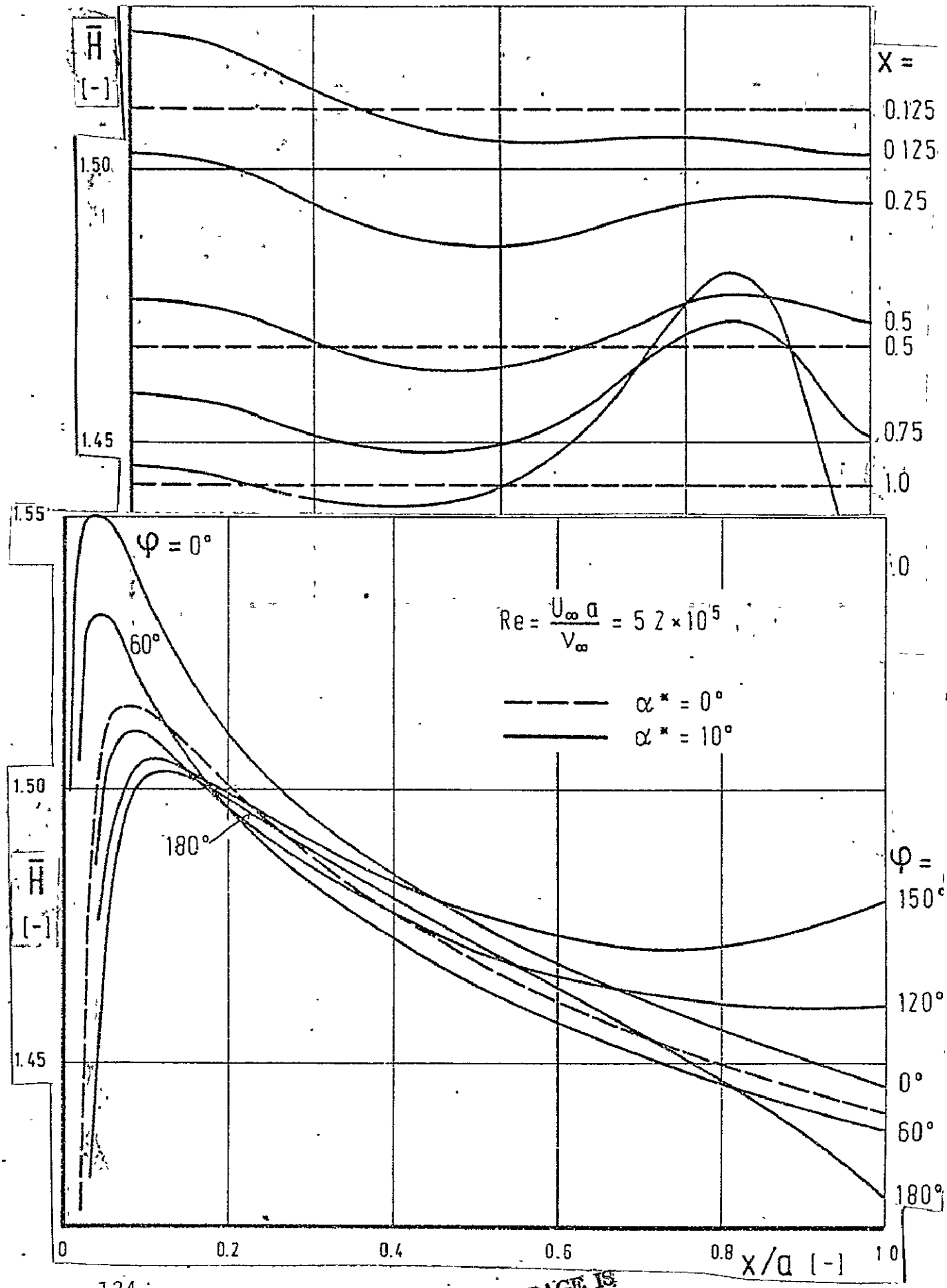

Fig. 40. Trace of the form parameter $\bar{H}$ for the incident and nonincident revolution ellipsoid (turbulent boundary layer)

/128

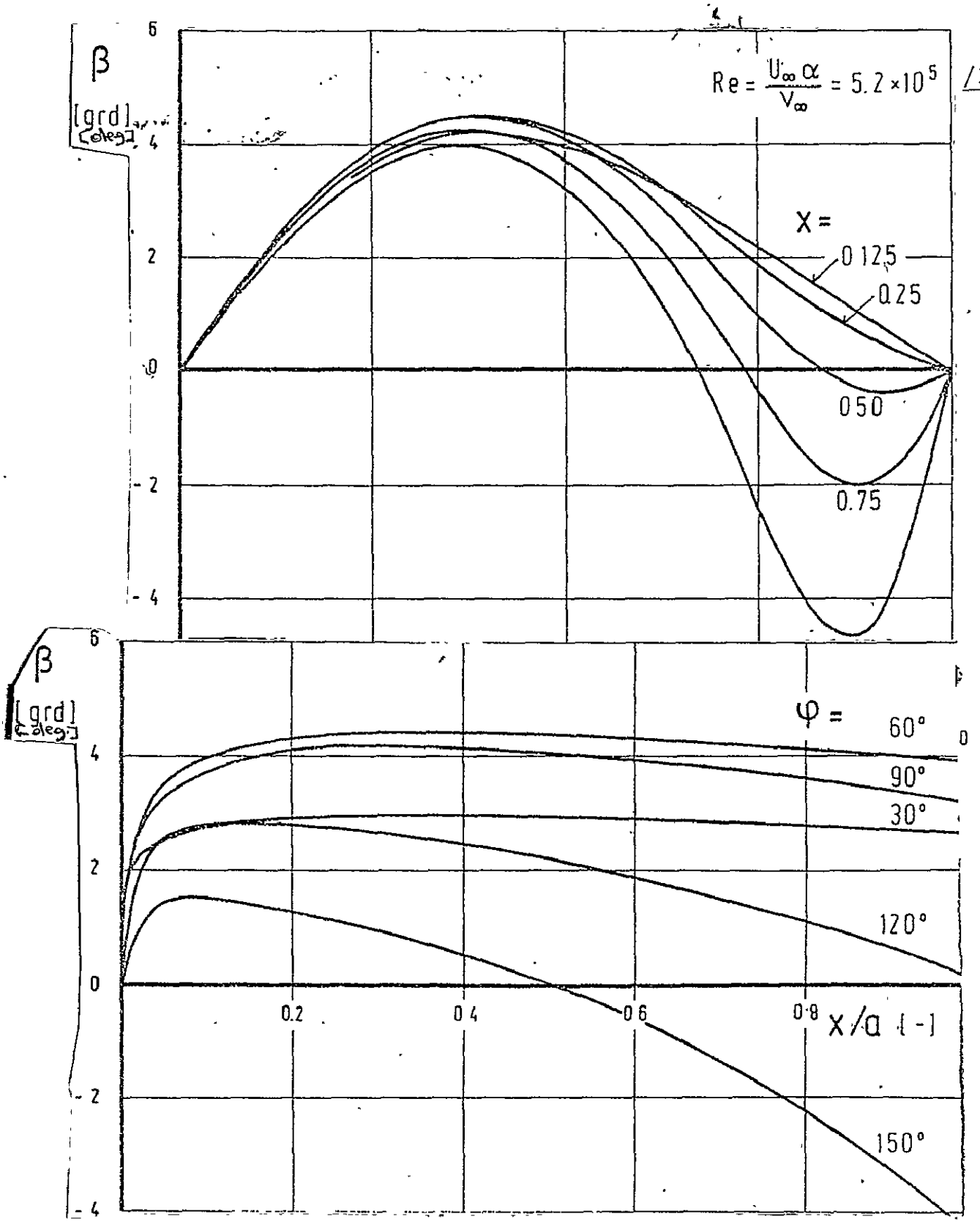

Fig. 41. Trace of the wallflow line angle β for the incident revolution ellipsoid (turbulent boundary layer)